Zr AND SILICOTUNGSTIC ACID INCORPORATED SILICATE STRUCTURED MESOPOROUS CATALYSTS FOR DIMETHYL ETHER SYNTHESIS

A THESIS SUBMITTED TO
THE GRADUATE SCHOOL OF NATURAL AND APPLIED SCIENCES
OF
MIDDLE EAST TECHNICAL UNIVERSITY

BY

SULTAN ORMAN

IN PARTIAL FULFILLMENT OF THE REQUIREMENTS
FOR
THE DEGREE OF MASTER OF SCIENCE
IN
CHEMICAL ENGINEERING

AUGUST 2011

Approval of the thesis:

Zr AND SILICOTUNGSTIC ACID INCORPORATED SILICATE STRUCTURED MESOPOROUS CATALYSTS FOR DIMETHYL ETHER SYNTHESIS

submitted by **SULTAN ORMAN** in partial fullfillment of the requirements for the degree of Master of Science in **Chemical Engineering Department, Middle East Technical University** by,

Prof. Dr. Canan Özgen _____
Dean, Graduate School of **Natural and Applied Sciences**

Prof. Dr. Deniz Üner _____
Head of Department, **Chemical Engineering**

Prof. Dr. Timur Doğu _____
Supervisor, **Chemical Engineering Dept., METU**

Examining Committee Members:

Prof. Dr. Pınar Çalık
Chemical Engineering Dept., METU _____

Prof. Dr. Timur Doğu
Chemical Engineering Dept., METU _____

Prof. Dr. İrfan Ar
Chemical Engineering Dept., Gazi University _____

Assoc. Prof. Dr. Naime A. Sezgi
Chemical Engineering Dept., METU _____

Assist. Prof. Dr. Dilek Varışlı
Advanced Technologies, Gazi University _____

Date: **19.08.2011**

I hereby declare that all information in this document has been obtained and presented in accordance with academic rules and ethical conduct. I also declare that, as required by these rules and conduct, I have fully cited and referenced all material and results that are not original to this work.

Name, Last name: Sultan ORMAN

Signature :

ABSTRACT

Zr AND SILICOTUNGSTIC ACID INCORPORATED SILICATE STRUCTURED MESOPOROUS CATALYSTS FOR DIMETHYL ETHER SYNTHESIS

Orman, Sultan
M.Sc., Department of Chemical Engineering
Supervisor: Prof. Dr. Timur Doğu

August, 2011, 142 pages

Due to high consumption rates of petroleum derived fuels and environmental regulations, significant search has been initiated for the development of environmental friendly and efficient fuels, which were derived from more abundant feedstocks. Dimethyl ether (DME), as having a good combustion quality and high cetane number, is an efficient alternative for diesel fuel. With improved combustion quality, the emissions from DME used engines are greatly decreased. DME synthesis can be carried out via two different methods; methanol dehydration on acidic catalysis and syn-gas conversion on bifunctional catalysis.

In this study, the aim is to synthesize acidic catalysts using direct hydrothermal synthesis method for DME synthesis as using methanol as feed stock via dehydration and to characterize these materials.

The support of the synthesized materials comprises of MCM-41 structure and silicotungstic acid (STA) and metals (Zr / Ni / Cu) were incorporated into the MCM-41 structure during synthesis. Two different techniques were used to extract the

surfactant (CTMABr) from catalyst matrix. First one is the conventional calcination technique (at 350°C) and the second is supercritical fluid extraction (at various operating conditions) with methanol modified CO_2. The effect of metal loading on extraction performance is analyzed through characterizations of Ni and Cu incorporated materials. In addition, The effect of operation parameters on catalyst properties are also investigated with performing extraction at different pressures for different durations. By changing the type of metal incorporated into the catalyst, the extraction performance is also monitored. The characterization results indicated that, SFE process is also a promising method for surfactant removal.

The activities of zirconium added catalysts are tested in methanol dehydration reaction towards DME. It is concluded that the conversion of methanol and selectivity of DME in presence of extracted samples are lower (maximum yield -0.54- obtained at 450°C with sceSZ1) compared to the calcined materials (maximum yield -0.80- obtained at 300°C with cSZ6). This result can also be foreseen by DRIFTS analysis of pyridine adsorbed samples. The acid sites of extracted materials are not as strong as in the calcined catalysts.

Keywords; Dimethyl ether, methanol dehydration, supercritical fluid extraction, heteropolyacid, mesoporous catalysts

ÖZ

DİMETİL-ETER SENTEZİNDE Zr VE SİLİKOTUNGSTİK ASİT İÇEREN SİLİKA YAPILI MEZOGÖZNEKLİ KATALİZÖRLER

Orman, Sultan
Yüksek Lisans, Kimya Mühendisliği
Tez Yöneticisi: Prof. Dr. Timur Doğu

Ağustos, 2011, 142 sayfa

Petrol kaynaklı yakıtların tüketiminin artması ve çevresel yönetmeliklerden dolayı, hammadde kaynağı bol olan çevre dostu ve verimli yakıtlarla ilgili olarak önemli çalışmalar başlatılmıştır. Dimetil eter (DME), yanma kalitesinin iyi olması ve yüksek setan sayısıyla beraber dizel yakıtına alternatif olarak görülmektedir. Yanma kalitesinin iyileştirilmesiyle, DME kullanılan motorlarda emisyonlar oldukça düşürülmektedir. DME sentezi iki farklı yolla gerçekleştirilebilir; asit katalizörler üzerinde metanol dehidrasyonu ve bifonksiyonel katalizörler üzerinde sentez gazı dönüşümü yoluyla.

Bu çalışmada amaç, DME sentezini methanol dehidrasyonu ile gerçekleştirmektir. Çalışma kapsamında, asidik katalizörler doğrudan hidrotermal sentez metoduyla sentezlenmiş ve karakterize edilmiştir.

Sentezlenen katalizörlerin destek maddesi MCM-41'dir ve silikotungstik asid (STA) ve metaller (Zr / Ni / Cu) MCM-41 üzerine sentez süresince eklenmiştir. Yüzey aktif maddenin (CTMABr) katalizör yapısından uzaklaştırılmasında iki farklı metot kullanılmıştır. Bunlardan ilki, kalsinasyon (350°C'de) ve ikinci ise metanol ile

modifiye edilmiş CO_2 ile süperkritik akışkan ekstraksiyondur (farklı çalışma koşullarında). Farklı metal türlerinin ekstraksiyon performansı üzerindeki etkisi, Ni ve Cu kullanılarak hazırlanmış katalizörlerin karakterizasyonları ile incelenmiştir. Buna ek olarak çalışma koşullarının katalizör özellikleri üzerindeki etkisi ekstraksiyonu farklı basınç ve periyotlarda gerçekleştirerek araştırılmıştır. Buna ek olarak, metal tipinin de değiştirilmesiyle ekstraksiyon verimliliği gözlenmiştir. Karakterizasyon sonuçları, ekstraksiyonun da yüzey aktif madde uzaklaştırmada umut verici bir yöntem olduğunu göstermektedir.

Zr eklenmiş katalizörlerin aktiviteleri metanol dehidrasyonu reaksiyonunda test edilmiştir. Sonuç olarak, metanol dönüşümü ve DME seçiciliği kalsine edilmiş numunelerde (maksimum verim -0.80- 300°C'de cSZ6 ile) ekstraksiyon yapılmış numunelere (maksimum verim -0.54- 450°C'de sceSZ1 ile) kıyasla daha fazladır. Bu sonuç, DRIFTS analizi ile de öngörülebilir. Ekstraksiyon yapılmış numunelerin asit bölgeleri kalsine edilen numuneler kadar güçlü değildir.

Anahtar kelimeler: Dimetil eter, metanol dehidrasyonu, süperkritik akışkan ekstraksiyon, heteropoliasit, mezogözenekli katalizör

To my little brothers and sister

ACKNOWLEDGEMENTS

First of all, I would like to express my sincere gratitude to my supervisor Prof. Dr. Timur Doğu for his support and guidance throughout my studies. His motivation, enthusiasm and immense knowledge inspired me in not only my thesis work but also my future career as a chemical engineer. I could not have imagined having a better mentor for my M.Sc. study.

I would like to express my special thanks to Prof. Dr. Gülşen Doğu and her research group in Gazi University Chemical Engineering Department for their support in this work. I would like to thank Assoc. Prof. Dr. Naime A. Sezgi and Assist. Prof. Dr. Dilek Varışlı for their positive attitude and help in this study.

I thank METU Central Laboratory, Metallurgical and Materials Engineering and Chemical Engineering staff for the characterization analyses and the technical assistance.

I thank to my fellow labmates in our research group at Kinetic Lab; Dr. Zeynep Obalı, Canan Martı, Kenan Cem Tokay, Ayça Arınan, Ayşegül Çiftçi, Caner Hocaoğlu and Seval Gündüz for stimulating discussions and all the nice memories we had in these two years. My special thanks go to Zeynep Obalı and Ayça Arınan for helping in technical issues and being so patient in answering all my questions.

Furthermore, I thank my friends Merve Şahin (u) and Merve Şahin (k) for their invaluable friendship and support through years and of course to my homemate, Elif Yavuz for her friendship from the age of 12. Ebru Pelvan and Ahad Kargı are also two of the most important people both in METU and in my personal life. I would like to thank also to the families of Dinçer, Işık and Şahin's (both two) – including all members- for their valuable support to make my life easier in Ankara.

Finally, a special thank goes to my family; my parents; for making me feel a lucky and privileged person and my brothers, Mehmet Ali and Furkan; and sister, Kübra for encouraging me and supporting me to do my best.

This support is received by Türkiye Bilimsel ve Teknolojik Araştırma Kurumu (TÜBİTAK) through BİDEB scholarship that I would like to thank.

TABLE OF CONTENTS

LIST OF TABLES

TABLES

LIST OF FIGURES

FIGURES

NOMENCLATURE

ATR: Autothermal reformer

DME: Dimethyl Ether

EDS: Energy Dispersive Spectroscopy

IUPAC: International Union of Pure and Applied Chemistry

MW: Molecular weight (g/mol)

MCM: Mobil Composition of Matter

MeOH: Methanol

P: Pressure (bar)

P_c : Pressure at Critical Point (bar)

SCF: Supercritical Fluid

SEM: Scanning Electron Microscopy

SFE: Supercritical Fluid Extraction

STA: Silicotungstic Acid

SC: Cu-STA/Silica

SN: Ni-STA/Silica

SZ: Zr-STA/Silica

T: Temperature (°C)

T_c : Absolute Temperature at Critical point (K)

TGA: Thermogravimetric Analysis

XRD: X-Ray Diffraction

CHAPTER 1

INTRODUCTION

Higher consumption rates in fuel reserves in the world make the researchers to look for the newer sources of energy. Dimethyl ether (DME) is considered to be a clean-burning alternative to liquefied petroleum gas, liquefied natural gas and diesel fuel due to its promising fuel properties (like high cetane number). Besides, having higher oxygen content compared to conventional diesel fuels, use of DME decreases the amount of air needed to activate the engine. High quality fuel behavior, suppresses the emission of CO, NOx, hydrocarbons and smoke. Due to its clean burning properties, DME is considered as a green fuel candidate. The details regarding to the properties and usage areas of DME are described in Chapter 2. The production routes, both conventional method and the direct synthesis, are explained in detail at the end of the same chapter.

This work is mainly related to the synthesis and characterization of calcined and supercritically extracted heteropolyacid (HPA) and metal (Zr, Ni and Cu) supported on silicate structured mesoporous materials. These materials were designed to show activity in dimethyl ether (DME) and dimethyl carbonate (DMC) production from methanol. The activity tests of the catalysts were performed in a flow reactor for DME synthesis by methanol dehydration.

In Chapter 3, the general properties of mesoporous materials, namely M41S family members, are summarized. Each member is analyzed in terms of its specific area of properties and particularly, synthesis procedure of MCM-41 is included. In addition, the characteristic properties of MCM-41 are explained with some selected

characterization methods, *e.g.* X-Ray diffraction and Transmission Electron Microscopy.

The details related to the heteropolyacids are explained in four main sections. Considered to approach to behave like a superacid, the acidities of HPAs are analyzed in relation to the whole structural properties. Different types of HPA's affecting the acidity were discussed in the first and second sections of Chapter 4. One other important property of HPAs; their thermal stability, is also discussed in the same chapter, which was concluded with several application areas and reactions utilizing HPAs.

One part of the work done with that study is related to trying different surfactant removal techniques during catalyst synthesis. Calcination is the conventional procedure of surfactant removal, while the second non-conventional procedure is supercritical fluid extraction (SFE). The main aim of SFE application is that to extract the unwanted components of a matrix without destroying it. This matrix can be a foodstuff (coffee, tea etc.) or any material (catalytic, pharmaceutical etc). Uses of SFE in different applications are included in Chapter 5 with general properties of CO_2 as an extracting agent.

In Chapter 6, the details regarding to the experimental studies; including catalyst synthesis (silicotungstic acid and Zr/Ni/Cu incorporated MCM-41) and characterization, surfactant removal steps and activity tests are explained. The experimental set-up of SFE system and methanol dehydration system are also contained in the same chapter. The characterization and activity results of the catalysts are reported in the next chapter; Chapter 7. The synthesized catalysts are compared in terms of characteristic differences formed via different surfactant removal steps. SFE process is also analyzed to determine the effects of operating parameters (extraction period and pressure) on properties of end products. For DME synthesis, only extracted and calcined samples of STA-Zr/MCM-41 catalysts are used. The activity results are analyzed at the end of Chapter 7.

The work is concluded with conclusions and recommendations parts in Chapter 8.

CHAPTER 2

DME AS A DIESEL ALTERNATIVE

One of the main problems of today's world is the global warming and the increase in the level of CO_2, as being the 60% contributor to the situation [1], and other green house gases in the atmosphere, which trigger this problem. To prevent the increase of atmospheric CO_2 level, new ways to produce energy are searched. One option is to decrease the usage of CO_2 emitting sources and find others or produce them environmentally. Dimethyl ether (DME) is an alternative that can be used as a fuel alternate and in petrochemical industry. The usage of DME can contribute to lowering CO_2 both by lowering emissions and by utilization in the synthesis.

DME, also known as methoxymethane, oxybismethane, methyl ether, wood ether; is a colorless gaseous ether with an ethereal odor. Having the formula, CH_3OCH_3 (Figure 1), DME is used as an aerosol spray propellant, and in conjunction with propane to create cryogenic freezing for the removal of common warts found on the human body [2]. One other promising property of DME is that it can also be considered as a clean-burning alternative to liquefied petroleum gas, liquefied natural gas and diesel fuel and has been considered as an ultra clean a multi-purpose fuel which can be used in diesel engines, households, power generation, and for other purposes [3, 4, 5].

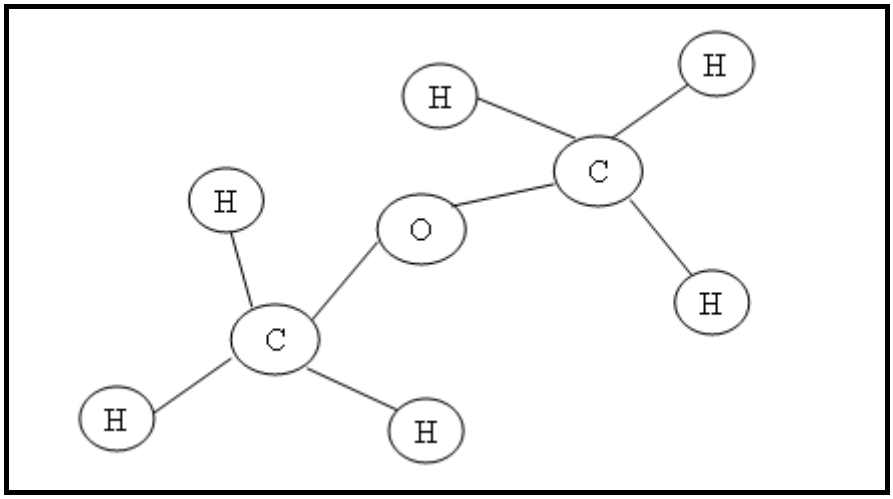

Figure 1: Structure of DME

Due to the huge market potential, the research on dimethyl ether synthesis [6, 7] and its utilization [8, 9] have been attracting more and more interests. Being identified as a potential diesel and cooking fuel, DME has number of excellent characteristics. It has an oxygen concentration of 34.78% and can be burned without soot emission, while for traditional diesel fuels, one cannot expect simultaneous NO_x and soot emission controls.

Conventional DME production uses the methanol dehydration method. The second method is its production directly from synthesis gas, which is composed of CO, CO_2 and hydrogen. This chapter is related to the general properties and application areas of DME and concludes with the synthesis methods.

2.1. Properties of DME

Under standard temperature and pressure, DME exists in gas phase. However, the properties of the liquid and solid phases are also worth researching, such that, the phase may change according to its usage area. Because of that reason, properties of

each phase will be explained separately. In Table 1, these properties are shown [4, 5].

Table 1: Physical properties of DME [4, 5]

Property			Value
Phase	Solid	Melting Point	-141.5 °C
		Heat of Fusion (at 1 atm, melting temperature)	111.34 kJ/kg
	Liquid	Boiling Point	-24.8 °C
		Heat of Vaporization (at 1atm, boiling point)	466.9 kJ/kg
		Vapor pressure (at 20 °C)	5 atm
		Density	734.7 kg/m3
	Gas	Specific Density (air=1) (at 1 atm, 15°C)	1.59
		Specific volume (at 1atm, 21 °C)	0.507 m3/kg
		Density	1.97 kg/m3
Cp (at 1atm, 25 °C)			0.065 kJ/mol.K
Cv (at 1atm, 25 °C)			0.057 kJ/mol.K
Compressibility Factor (at 1atm, 15 °C)			0.9806
Critical temperature			126.9 °C
Critical pressure			53.7 bar

2.2. Application Areas of DME

The promising properties of DME, has opened several application areas for it. Firstly, being a green agent; environmentally benign and non-toxic, DME is considered as safe in ecological aspects.

The application areas of DME can be investigated in two separate sections which consists of firstly the common usages and secondly the fuel alternate behavior of DME.

2.2.1. General Applications

Dimethyl ether (DME) has been increasingly used as a propellant in aerosol formulations to replace chlorofluorocarbons, which are found to destroy the ozone layer of the atmosphere. DME is nontoxic and easily degrades in the troposphere. Although about 90% of the major current U.S. aerosol industry uses hydrocarbon-based propellants (mostly iso-butane and propane), DME could become a more widely used propellant in the next five years.

Several aerosol-based household products include colognes, hair sprays and dyes, personal care mousses, antiperspirants, and room air fresheners. DME is a useful intermediate for the preparation of many important chemicals, including methyl sulfate. Dimethyl sulfate is an important commercial commodity as a solvent and also as an electrolyte in high energy density batteries [10]. Other than these DME can be used as a refrigerant, a (co-)blowing agent for foam, a propellant for aerosol products and as an extracting agent.

2.2.2. Evaluation of Dimethyl Ether as a Fuel

The need to use DME as a fuel mainly arose from the fact that there exists lack in conventional carbon sourced fuels. The way that DME is used depends on the application area; it can be used as an additive to fuel (making a mixture of DME and LPG or diesel) to decrease emissions or increase engine performance with its promising fuel characteristics (high cetane number and low auto-ignition temperature, LPG storage resembling properties), or can be used directly in the diesel engine. The fuel characteristics of DME are given in Table 2 as comparison with diesel and other alternatives [2, 11, 12, 13].

DME has superior qualifications as emphasized in italic form. The strategy in using fuels with developing technology is to decrease the carbon content and increase the remaining (hydrogen or oxygen). In DME case, it is observed that although having the same hydrogen content, DME has high oxygen content. This property decreases the needed air amount during ignition of the engine

Structure of DME, comprises of C-H and C-O bonds but no C-C. Having no C-C bonds, DME provides smokeless operation in compression-ignition (CI) engines. Studies reported in the article of Kowalewicz and Wojtyniak [11], showed that, use of DME as a fuel in CI engine, improved thermal efficiency compared to diesel fuel and also resulted with low emissions of NO_x.

Low auto-ignition temperature of DME decreases the lag time of ignition and enhances the cetane number of DME. This decrease in ignition lag time is again due to the structure of DME. During combustion, fission of C-O bond is easier compared to C-H bond because of smaller bond energy. Therefore the ignition is activated by C-O bond breakage at lower temperatures (low auto-ignition temperature and higher cetane number) which is not the case for diesel fuels [2].

In addition to these superior properties, DME has also some disadvantages as a transportation fuel. Having a lower heating value and lower density, increases the

volume of needed fuel to get the same power. This brings high pumping duties and larger volume of storage tanks.

Table 2: Fuel properties of DME and other fuels [2, 11, 12, 13]

Property	**DME**	**Diesel**	**Propane**	**Methane**	**Methanol**
Chemical formula	CH_3OCH_3	-	C_3H_8	CH_4	CH_3OH
Molar mass (g/mol)	46	170	44	16	32
Carbon content (mass%)	52.2	86	82	75.0	37.5
Hydrogen content (mass%)	13	14	18	25.0	12.5
Oxygen content (mass%)	*34.8*	*0.0*	*0.0*	*0.0*	*50.0*
Carbon/hydrogen ratio	0.337	0.516	0.375	0.25	0.25
Cetane number	*>55*	*40-50*	*5*	*0*	*5*
Auto-ignition temperature (°C)	*350*	*320*	*470*	*532*	*460*
Stoichimetric air/fuel ratio (mass)	*9.0*	*14.6*	-	-	-
Boiling point at 1atm (K)	248.1	450-643	231	111.5	337.6
Vapor pressure (atm)	6.1	-	9.3	-	-
Liquid density (g/cm^3)	0.67	0.84	0.49	-	0.79
Enthalpy of vaporization (kJ/kg)	467.13	300	426	510	1097
Lower heating value (MJ/kg)	28.9	41.86	46.46	50.23	21.10
Ignition limits (vol % in air)	3.4/18.6	0.6/6.5	2.1-9.4	5-15	5.5-36
Kinematic viscosity (at 40°C, mm^2/s)	0.15	2.0-4.5	-	-	-

Studies conducted by Ying *et al* [15] showed that,. increasing the DME content in DME/diesel blends decreases the specific energy consumption up to a point compared with unblended diesel. The reason is higher oxygen content. Further increase of DME, increases the consumed energy in the brake due to the reasons mentioned above (high pumping durations) [2, 14].

Besides, to utilize DME as a fuel, the engine should be modified to overcome the problems arising from different physical properties than diesel (low viscosity, higher vapor pressure etc.). Low viscosity, firstly causes easy leakage in the system, which than brings the need to make extra protection to get rid of this (use of more protective sealing materials). In addition to prevent wearing problems evolving from lower lubricity property, lubricant additives should be used.

Injection of DME into the engine, *i.e.* phase behavior during change from liquid to gas, is different than in diesel. Several studies are performed to analyze and model the flow of DME through the engine cylinder during injection and spraying. In studies conducted by Shu and Lee [16] and Park *et al* [17], spraying characteristics of DME and diesel are compared and it is shown that, DME spray, which is formed in a comparably shorter time, is more evaporative due to its high vapor pressure and has a wider angle showing better atomization characteristics. On the other hand, having a higher viscosity, the spray of diesel arrives earlier to the point of measure [2].

2.3. Production Techniques of DME

The research for the production techniques of DME is a result of discovering the wide usage area of DME which is mentioned in above sections.

DME production can be performed via two different methods. Depending on various feed stocks (coal, biomass, natural gas, methanol, etc.); the synthesis may follow different routes (Reactions present in Table 3 [18]). The first is the indirect conventional method which is by dehydration of methanol that is produced after reactions of CO and H_2, whereas the second is direct method in which syn-gas is

converted directly to DME in a single reactor with simultaneously producing methanol.

In both of the methods, the upstream and downstream flows should be investigated in terms of optimization of the process. The former one comprises of utilization methods of feed stocks.

Table 3: Reaction formulas concerning DME synthesis [18]

Reaction	Reaction Heat (kJ/mol)	Note	Equation
$3CO + 3H_2 \rightarrow CH_3OCH_3 + CO_2$	-246	DME synthesis	(1)
$2CO + 4H_2 \rightarrow CH_3OCH_3 + H_2O$	-205	DME synthesis	(2)
$2CO + 4H_2 \rightarrow 2CH_3OH$	-182	Methanol synthesis	(3)
$2CH_3OH \rightarrow CH_3OCH_3 + H_2O$	-23	Methanol dehydration	(4)
$CO + H_2O \rightarrow CO_2 + H_2$	-41	Water gas shift reaction	(5)
$CO_2 + 3H_2 \leftrightharpoons CH_3OH + H_2O$	-28.7	Methanol synthesis	(6)

The way towards DME passes from firstly syn-gas and then methanol. Therefore being independent from DME synthesis method, the upstream processing is the same. Here, the variable is the feed-stock. Depending on the nature of the

starting feed, the synthesis phenomena varies. Starting from natural gas, also reforming reaction as given in Equation (7) should be considered for formation of syn-gas.#

$$CH_4 + H_2O \rightleftharpoons CO + 3H_2 \quad (7)$$

In Figure 2, the given process flow diagram is referred to a pilot plant developed by JFE and is used to produce DME with a capacity of 5ton/day [12].

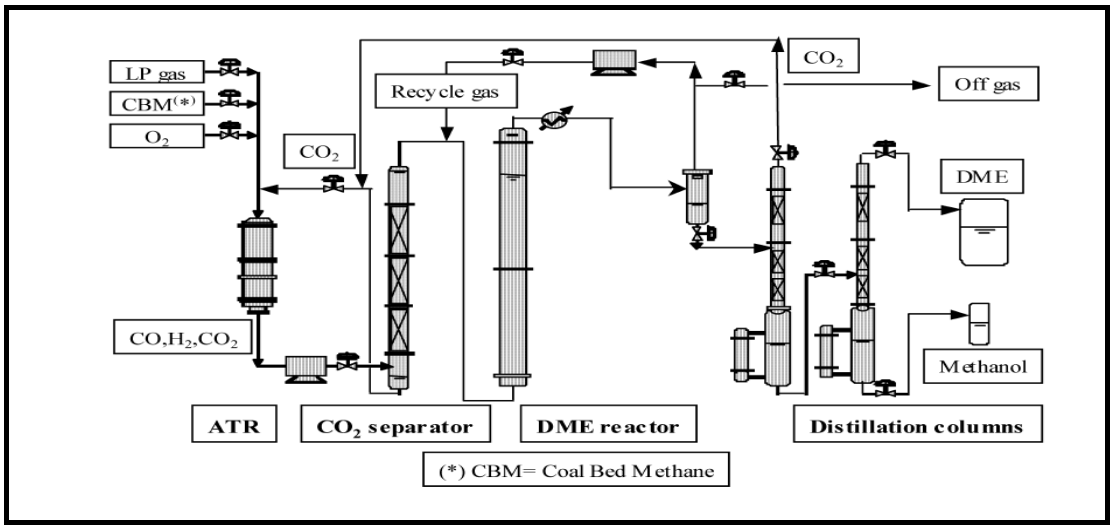

Figure 2: DME synthesis from NG proposed by JFE [12]

In developed technology, after being separated from CO_2, the effluents of auto thermal reformer are sent to a slurry reactor (0.55m in OD and 15m in height) where syngas conversion is performed at 5MPa and 260°C. The downstream of the reactor is sent to two step distillation to purify DME and one part of first distillation column product is recycled back to the reactor to improve yields. With the results obtained with this pilot plant, a large scale DME production facility is established by the same company [12]. The use of slurry reactor provides an efficient transfer of

heat generated from reaction medium which prevents deactivation of the catalyst due to high temperature rise during the reaction.

After formation of syn-gas, the process has two alternatives. Methanol synthesis may be performed in a reactor and DME synthesis can then be carried out in a separate reactor. Or the second alternative is to carry out these two reactions in a single reactor.

After the synthesis, the next step is to treat the downstream components. Again depending on the reaction scheme selected, the resulting product distribution may differ. In methanol dehydration system the major product is DME and water, and there might be the unreacted methanol in the stream. Formation of some formaldehyde is also possible as a side product. The separation can be performed in a distillation column since DME has a higher volatility compared to the others. Or a reactive distillation column can be utilized to distillate water simultaneously during the reaction. This will also enhance the overall reaction performance with shifting the reaction towards the products and will control possible deactivation due to blocking of the catalyst with water.

In a patent by Haldor-Topsoe [19], process flow diagram is created for syn-gas conversion scheme. Although this is the major method, methanol to DME convertor reactor is also included in the process. Figure 3 shows this process scheme.

The process starts with different compositions of syn-gas ($CO/H_2/CO_2$). After conversion to DME and methanol, the unreacted gas and the products are separated into liquid and gas phases in a separator where the former one is sent to a distillation column to recover DME, and the later one is recycled and sent to a purging system with methanol. The unconverted methanol is dehydrated in another reactor after being separated from the system. The overall system performance can be measured with the quality of DME produced. By that way, it is claimed that, 73% (vol/vol), pure DME is produced (where the remaining is water and methanol) [19].

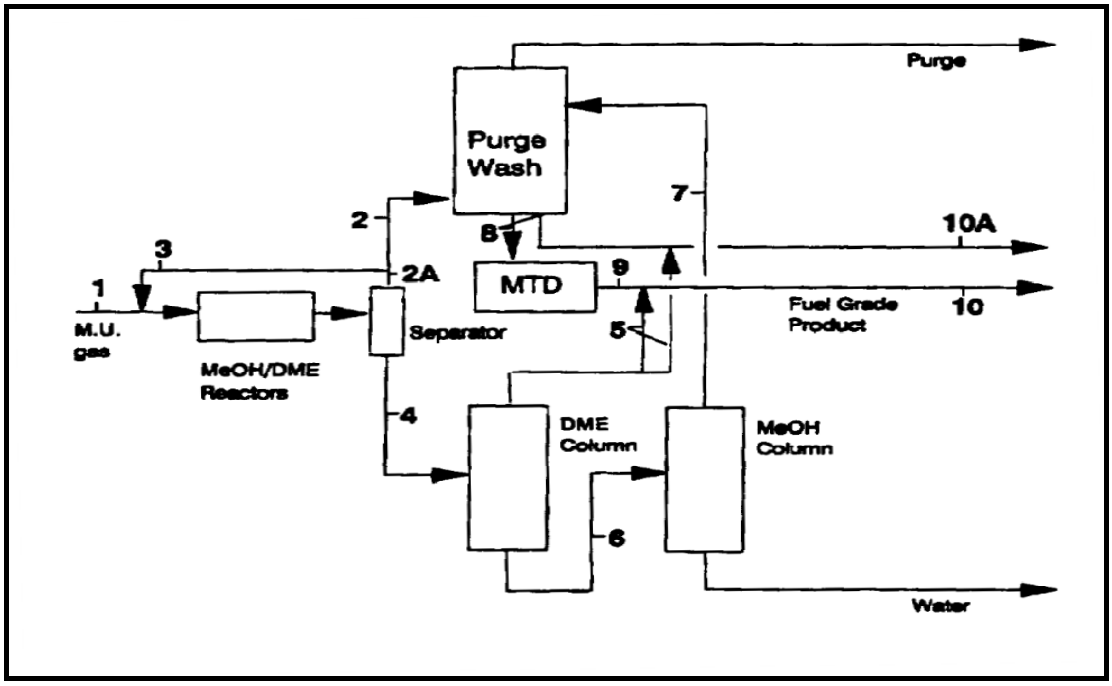

Figure 3: Process flow diagram by Haldor-Topsoe for direct DME production [19]

Both downstream and upstream management operations can be varied. However, to understand the full picture, the details of the process should be investigated. The details regarding to the process conditions, including temperature, pressure and catalysts used, are included in the next sections for both of the methods.

2.3.1. Methanol Dehydration

Methanol dehydration is represented by Equation (4) in Table 3. The reaction is exothermic and total moles of reactants and products are equal. Therefore, the thermodynamics of the system is not expected to be affected by the changes in total pressure, theoretically. In Figure 4, the calculated values of equilibrium conversion of methanol are shown .The details of calculation are given in Appendix A.1.

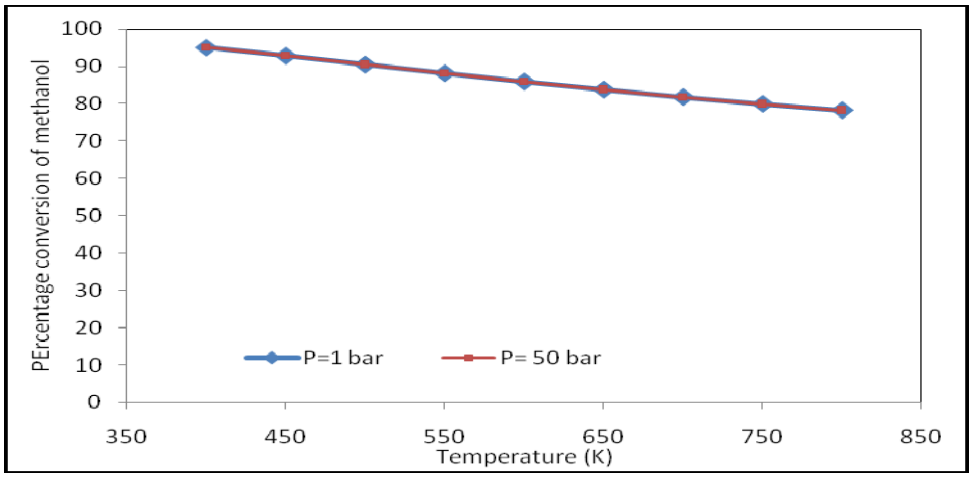

Figure 4: Equilibrium conversion of methanol

Methanol dehydration to DME is carried out at acidic catalysis (γ-Al_2O_3, α-Al_2O_3, HPAs, ion exchange resins, zeolites etc.). Several studies are published on this topic. In studies of Lei *et al* [20], different types of process set-up are utilized. Fixed bed reactors are combined with (catalytic) distillation columns in different configurations. In the processes, final purity is 99.55% meaning that separation is effective. On the other hand, comparing the overall conversion of methanol, that is total amount of DME produced, shows that combination of fixed bed column with catalytic distillation column after it is superior. The reason is the combined conversions in the reactor and the column. Utilization of catalytic distillation column as the extra reaction media, improves the DME yield. In the case of a catalytic distillation column with a fixed bed after it, the conversions are much low compared to the other ones. The main constraint, in this scheme is the pressure drop evolving from high catalyst loadings. To preserve the pressure in the system, catalyst packing should be optimum, which then suppresses higher conversions [20]. A similar reactor and distillation column configuration is used in the studies of Stanislao [21] where Amberlyst 35 is utilized in the fixed bed and the column is packed with separation materials. The operation is adjusted so that, in the case of bypassing the prereactor, the column is operated as a catalytic distillation column where both reaction and separation takes place.

Different SAPO catalysts are examined in methanol dehydration reaction and it is observed that, although SAPO-34 and ASPO-18 have the highest amount of acidic sites (compared to SAPO-5 and SAPO-11) as determined in NH_3-TPD analysis, methanol conversion rapidly decreases at the early stages of reaction. This result is attributed to coke formation with these acid sites and plugging in the smaller pores of the materials [22].

As stated in the above section, formation of water during the reaction suppresses the catalytic activity towards DME through blockage of the active sites in the catalyst. The studies performed by Xu et al [23], showed that the activation energy of the reaction is increased directly with the increase in water content in the feed having a constant molar flow rate of methanol and DME yield is lowered in presence of γ-Al_2O_3. In the same study, the effects of Bronsted and Lewis acid sites are investigated by comparing the activities of γ-Al_2O_3, having only Lewis type acid sites, with H-ZSM-5 having both types of acidic sites. It is revealed that, by addition of water to both of the systems, the decrease in catalytic activity is higher in γ-Al_2O_3 which can be attributed to presence of more Lewis sites which is mainly affected by water addition. By the slight decrease in the zeolite activity, it is concluded that Lewis acid sites are active in methanol dehydration and for the Bronsted acidity, since there exists still DME yield, it is noted that, these sites are active as well.

Heteropolyacids are widely used in alcohol dehydration reactions due to their superior acidic and redox properties. Due to their low specific surface area, the synthesis is commonly carried out by supporting the HPAs into a support. Varisli [24], tested the activities of silicotungstic acid (STA) and tungstophosphoric acid (TPA) supported on mesoporous silica and compared those with that of aluminasilicates. The results indicate that, the selectivity obtained with STA towards DME is more compared to the one obtained in presence of TPA. Conversion of methanol is also higher when STA is used as the catalyst (on the orders of 30%). On the other hand, although the aluminasilicate catalysts are inactive at lower temperatures (200-300°C), with increasing temperature, conversion of methanol reaches to values of 60%. Ethanol dehydration is also performed as well as methanol and similar results are reported.

2.3.2. Syngas Conversion

DME synthesis via syn-gas (mixture containing CO and/or CO_2 and H_2) conversion, is carried out by the reactions given in Table 3. The overall reaction can be summarized in the forms of Equations (1) and (2), depending on the composition of the feed stock. As can be seen, both routes are highly exothermic and pressure dependent (directly). These two are also the major problems associated with that method. The studies regarding to syngas conversion are mainly related to overcome these problems.

Great amount of heat evolved during the reaction may cause deactivation in the catalyst through coke formation or may activate the formation of side products. Figure 5 shows a slurry type used to extract heat generated during the reaction [12].

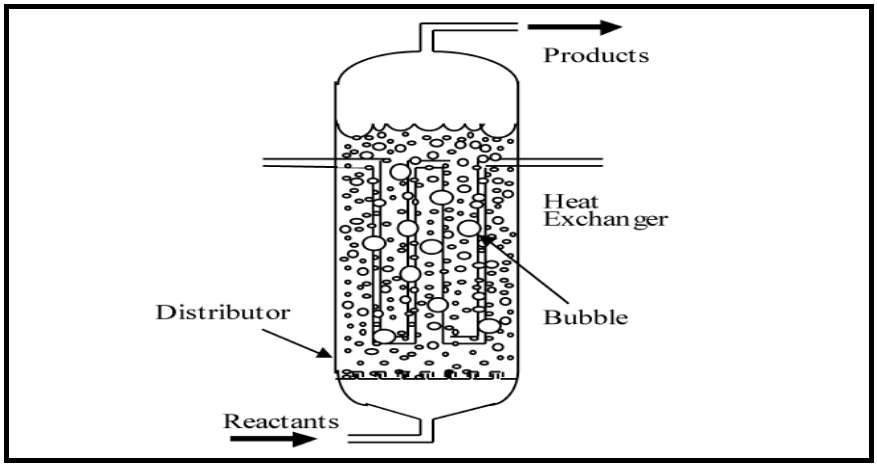

Figure 5: Flow through a slurry reactor [12]

Utilization of slurry bed reactor (Figure 5) where heat of reaction is transferred to some liquid (usually oil) is an option in removal of heat [12]. Here, the

main problem is catalyst loss with the flow of heated liquid. This can be prevented by a filter placed at the outlet of the reactor system.

Vakili *et al* [25], used heat exchanger type reactors to get rid of evolved heat. The reaction is carried out in the tubes of the exchanger (OD=1.5'') which is filled with the catalyst (a hybrid catalyst consisting of $CuO/ZnO/Al_2O_3$ – methanol synthesis – and γ-Al_2O_3 – methanol dehydration –). The generated heat is either removed by water flowing in the shell side or utilized in an endothermic reaction (cyclohexane dehydrogenation). The second configuration couples an exothermic and an endothermic reaction, and no heat is disposed by that way. In addition to formation of extra valuable products with the endothermic reaction, the coupled reactor dimensions are smaller compared to the water utilizing exchanger type reactor and there seems an increase in produced DME.

The second problem is associated with thermodynamic limitations. As can be seen in Figure 6, to reach considerable conversions, the system should be pressurized to high pressures in the orders of 40-50bar. The figure is generated by making mass balance at different inlet conditions (temperature and pressure, details are given in Appendix A.2).

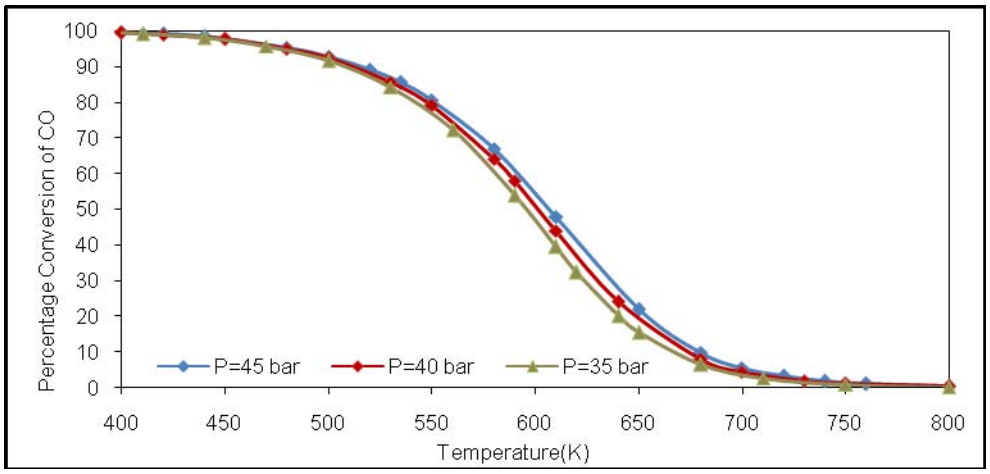

Figure 6: Equilibrium conversion of CO in DME synthesis (CO/H_2=1)

To overcome these limitations, and use the system with the highest efficiency, effective catalyst systems should be created for methanol dehydration at lower temperatures. As both methanol synthesis and methanol dehydration are carried out in the same reactor, the catalyst should possess the properties of both of the systems.

Naik et al [26], investigated DME formation with CO_2 and H_2 with the catalysts CuO-ZnO-Al_2O_3/γ-Al_2O_3 and CuO-ZnO-Al_2O_3/ZSM-5 in fixed bed and slurry bed reactors (at 260°C, 5MPa). It is concluded that, ZSM-5 catalyst is much more efficient in terms of both CO_2 conversion and DME selectivity. The reason of lower conversion of the first catalyst is explained in relation to lower thermal stability and activating reverse water gas shift reaction (Equation 5) through the formation of CO, and therefore decreasing the amount of DME produced. The same methanol synthesis catalyst is also coupled with SAPO in reactions of CO and H_2 (at 260°C, 4.2MPa) by Yoo et al [22]. The results indicate that, the reaction is mainly controlled by methanol synthesis step, but not by the dehydration of methanol. Although the catalysts have drastic differences in methanol dehydration as indicated in previous section, CO conversions are in the same order of magnitude.

In a study conducted by Qi et al [27], it is shown that addition of Mn to the catalyst structure of Cu supported on γ-Al_2O_3, enhances the dispersion of cupper into the support. Syngas conversion is carried out at 2.0 MPa at temperatures between 220-300°C. Enhancement in cupper dispersion is affective in methanol synthesis step which is essentially, the slowest step limiting the overall reaction. The results reveal that, Mn addition to the catalyst matrix improves CuO dispersion and thus increases the metallic cupper amount in the structure. This, at the end, improves the DME yield as well up to a specific amount of loading.

CHAPTER 3

POROUS MATERIALS AND APPLICATIONS

Porous materials are classified according to their pore size by International Union of Pure and Applied Chemistry (IUPAC). The definitions are as follows;

Microporous materials→ with pore size smaller than 2 nm (zeolites)

Mesoporous materials→ with pore size between 2 nm and 50 nm

(M41S family, SBA-15)

Macroporous materials→ with pore size larger than 50 nm

The first discovery of zeolites is made in 1756 by a Swedish mineralogist and the synthesis is developed in 1980s (the name zeo-lithos meaning boiling stone due to high adsorption capacity of water). In addition of synthetic zeolites, there also exists natural zeolites. Zeolites are mainly crystalline aluminosilicate structures (having different Al/Si ratios) in the forms of tetrahedrons with centers of alumina or silicon and tetrahedral oxygens shared. In addition to these, countercations, like sodium, magnesium, potassium, rubidium etc. are found to balance the charge within the structure. In many applications, these cations are replaced by other cations (in ion exchange membranes) [28, 29, 30, 31]

Zeolites exhibit a very narrow pore size distribution due to their crystalline structure. The pore openings and pore size is determined by both the ring structure and nature of cations in zeolite matrix. In characterization of the strucutere X-Ray diffraction is widely used. Being a microporous material, zeolites allow adsorption of

small size molecules that is selective in terms of size as well as shape due to ring structure. These types of microporous materials are mainly used in many processes.

Ion exchange processes are the common industrial applications in which zeolites are used. Water purification is mainly done by use of zeolites showing hydrophilic properties (zeolite 3A, 4A etc). In addition, in hydrocracking process of petroleum industry, zeolites are used to enhance the catalytic activity [31, 32].

3.1. Mesoporous Materials-M41S Family

The family of M41S, which are considered as the first ordered mesoporous materials, has a wide range of applications and consists of three main members which are MCM-41, MCM-48 and MCM-50 (Mobil Composition of Material). Having different characteristic properties, in terms of structure and synthesis conditions, each material has various applications enabling diffusion of higher pore size materials into the pores when compared to microporous ones [33, 34].

The discovery of that family is based in the beginnings of 1990s by the Mobil researchers. The need to derive these kinds of materials arose from the need to convert bulky petroleum products to more useful and valuable fuel [35]. The tunable and uniform pore size distribution within a very narrow range, like that of zeolites, is the most attractive property of this group as well as their high surface area (being larger than 700 m^2g^{-1}). The synthesis steps are mainly the same for each of the M41S family, except the ratio of used surfactant to silica source. Generally the synthesis follows a liquid crystal templating (LCT) mechanism. After the discovery, the researchers aimed to understand the detailed mechanism with developing the synthesis procedure and characterization of the materials. The next step followed by these is to understand the morphology and extend the application areas [36]. In this section MCM-41 will be examined in detail and the other members will be compared in terms of the structures and synthesis mechanism in brief.

3.2. MCM-41

MCM-41 is the most studied member of M41S family, due to its flexible synthesis conditions and reproducible properties. In addition, obtaining changeable pore diameters (ranging from 15°A to larger than 100°A) by applying different synthesis conditions, in a very uniform hexagonal honeycomb like arrays makes MCM-41 suitable for different applications [37]. Having higher surface area and being a thermally stable material (T>1000), MCM-41 is shown as a good candidate as a supporting material in doping of various components like metals or heteropolyacids.

3.2.1 Synthesis Procedure

MCM-41 is synthesized through interactions of negatively charged surfactants and positively charged silicate sources. The most commonly used ones are alkyltrimethylammonium salts and sodium silicate (Na_4O_4Si) or TEOS (tetraethylorthosilicate- $C_4H_{20}O_4Si$) solutions accordingly. The surfactant is used as the template to enable the incorporation of different components into the catalyst structure. The synthesis steps of MCM-41 are optimized as follows:

Step 1→ Addition of surfactant to the solvent (deionized water): The nature and amount of surfactant added to the synthesis mixture is a critical parameter. The tunable property in pore diameters is gained with changing the alkyl chains in the surfactant. It is shown that, increasing the number of alkyl chains, also the pore size of the catalyst increases. Figure 7, shows the XRD pattern of MCM-41 [38]. The major peaks in the patterns shifts right with low alkyl lengths indicating a smaller diameter.

In addition, surfactant amount determines the final structure of the material. Different M41S family members are obtained by varying the surfactant composition.

In Figure 8, these effects can be seen. In the first synthesis performed by Mobil researches, alkyltrimethyl ammonium halides are used as the surfactant [39].

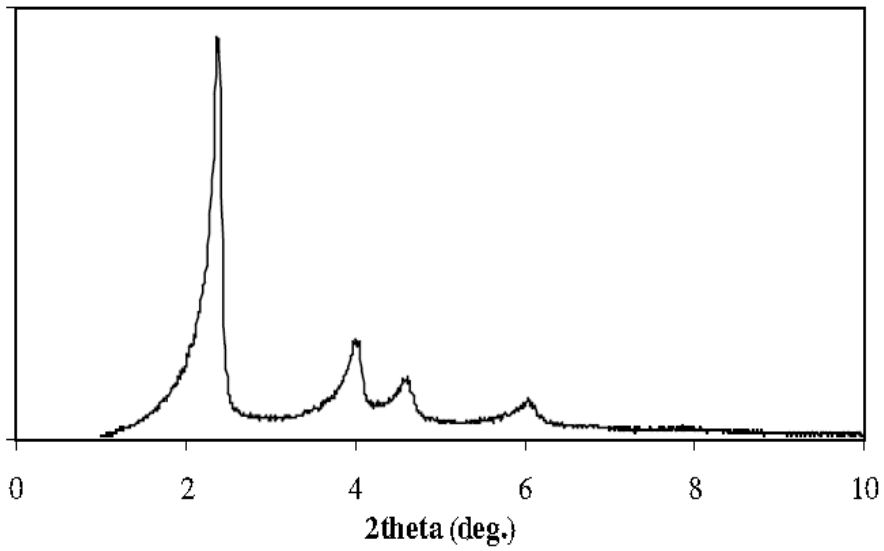

Figure 7: XRD pattern of MCM-41 sample [38]

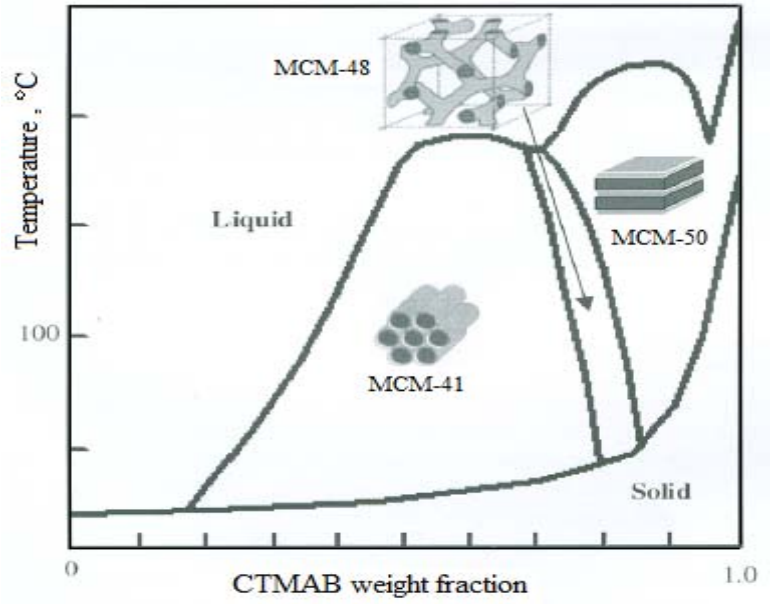

Figure 8: Effect of surfactant amount on catalyst structure [40]

Step 2→ Addition of silica source to the mixture: Different silica sources are used in MCM-41 synthesis like TEOS, sodium silicate, silica gel etc. The synthesis is carried out at acidic or basic conditions depending on the silica source. Temperature during mixing of these agents is also a critical parameter in synthesis when it is considered that main silica network is formed as the silica source is added. [41].

Step 3→ Hydrothermal synthesis: Final gel is placed into a teflon bottle which is then placed to a stainless steel autoclave. The synthesis is carried out at constant temperature. Several temperatures (ranging from 100°C-150°C) are tried in MCM-41 including different periods like 24 hours or 144 hours [39].

Step 4→ Washing and filtering: Synthesized material is washed with deionized water until a constant pH is obtained. In that step, the unbinded structures are removed through washing. Drying is carried out at vacuum and at a constant temperature.

Step 5→Surfactant removal: The surfactant is removed at the end of the synthesis. For that aim, variety of methods is used. The most common one is calcination with air. In addition to calcination supercritical fluid extraction (SFE) is shown as an alternative methods to remove surfactant from catalyst matrix.

- **Calcination** is basically thermal decomposition with air at decomposition temperature. For MCM-41, calcination is generally carried out at about 550°C under atmospheric pressure to remove the surfactant CTMABr.
- **Supercritical Fluid Extraction** with CO_2 is considered to be a new and promising method for surfactant removal. The supercritical behavior of CO_2 under conditions higher than critical properties (T_c=30.4°C, P_c=7.3MPa) is an advantageous property when inertness and high solvating power is taken into account. The detailed information is given in Chapter 5 for SFE. In addition to these methods, also the catalysts are washed (refluxed) with different solutions (*e.g* HCl, H_3PO_4) for the removal of surfactant.

During these steps, the formation of MCM-41 is explained by a liquid crystal templating mechanism (LCT). The literature focuses on mainly two different pathways to define that mechanism. In Figure 9, these pathways are shown [42].

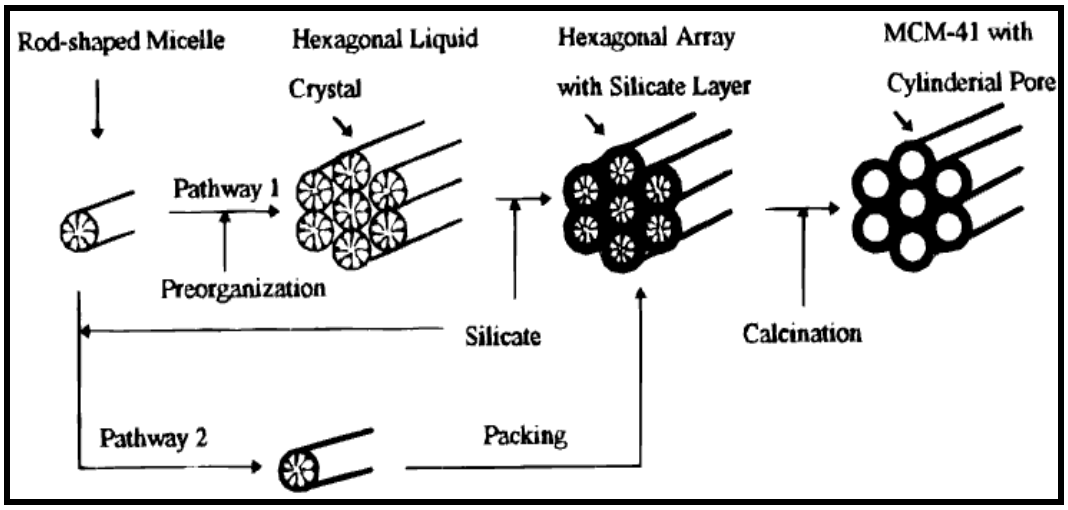

Figure 9: MCM-41 formation via LCT mechanism [42]

As mentioned before, generally synthesis takes place via electrostatic interaction between positively charged surfactants and negatively charged silicate anions. In two different pathways proposed above, the main difference is that the first initiation of formation. In the first one, it is claimed that, the silicate anions diffuse to the preformed liquid crystals forming the silica network, that is the mechanism is initiated with liquid crystals of micelles which are formed before addition of silicates. On the other hand, in the second pathway, the uniform hexagonal liquid crystal formation is activated by silica source addition. The silicate cations form a layer on the surface of micelles which then forms the uniform network by silicate condensation. Further heating to an optimal value improves condensation [40, 42]. Each pathway ends with calcinations where the surfactant network is removed via thermal decomposition.

3.2.2. Characterization of MCM-41

The main techniques used in MCM41 and mesoporous materials' characterizations are X-Ray diffraction (XRD) and nitrogen physisorption. In the first method, the material is analyzed in terms of its structure where in the second one, the textural properties are obtained by adsorption and desorption properties of N_2 on the catalyst surface. Although this section covers MCM-41 characterization, in Chapter 6, material characterization is examined in detail.

3.2.2.1. X-Ray Diffraction

The XRD pattern of MCM-41 is given in Figure 7. The material, has one main peak corresponding to (100) plane (with a d value of 47.3°A) and four reflection peaks for (110), (200), (210) and (300) planes according to intensities of the peaks. The mesoporousity of MCM-41 can also be seen in the peaks between 2θ ranges of 1°-10°. Although there are sharp peaks in its pattern, MCM-41 has amorphous walls.

3.2.2.2. Nitrogen Physisorption

Nitrogen is adsorbed and desorbed on MCM-41 at 77K and Figure 10 is obtained as nitrogen adsorption and desorption isotherm of MCM-41 [41]. Exhibiting a Type IV isotherm, MCM-41 shows the basic property of mesoporous materials. The capillary condensation and pore filling occur at low pressures indicating a smaller pore diameter. MCM-41 has a surface area in the ranges of 1000 m^2g^{-1} and the volume is nearly 75% free. This free volume consists of cylindrical channels (almost 500 nm long) which are arranged in uniform hexagonal shapes [44].

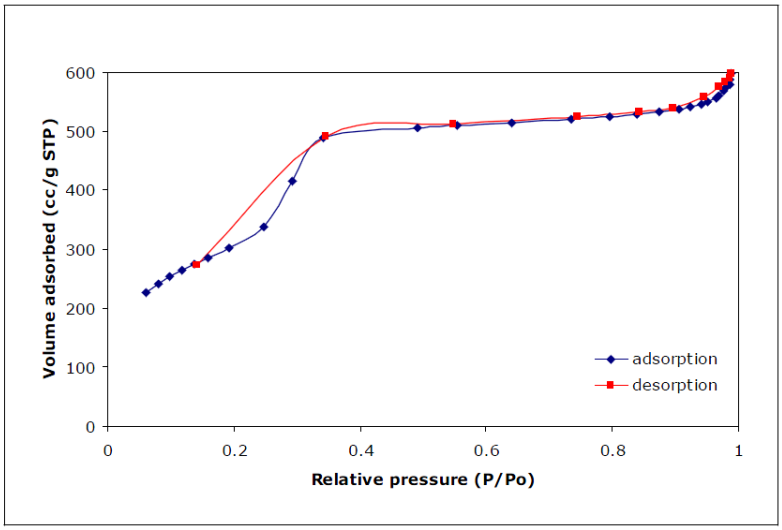

Figure 10: Typical N_2 adsorption-desorption isotherm of MCM-41 [41]

3.2.3. Methods of Modification of MCM-41 Structure: MCM-41 as a Support

Attractive properties and potential use of MCM-41 as a catalyst support material, made researches to search for methods to modify the core catalyst structure to be supported on MCM-41. Having a considerably high surface area and tunable pore structure make MCM-41 a good candidate as a support. The modification can be performed during synthesis, *i.e*, the catalyst is incorporated on MCM-41 during hydrothermal synthesis or after synthesis of MCM-41 is carried out the active component of the catalyst can be implemented into MCM-41 structure by different impregnation techniques.

The most commonly used impregnation method is wet impregnation where both solutions of the support and precursor of the catalyst are mixed and dried. This method is advantageous when chemical reactions taking place on the surface of the catalyst is considered since in the catalyst the active component is distributed mainly on the support surface with that method. In dry impregnation (incipient wetness impregnation), the method is similar to that of wet impregnation. The main

difference is that the added precursor solution does not fill up all the pores of the surfactant resulting dry surfaces. Precipitation (homogeneous deposition precipitation) is another method to prepare catalytic materials. The support material suspended through the precursor solution of the catalyst and by adjusting the solution conditions –pH and temperature- the active component is precipitated on the support surface. The mentioned parameters play an important role in efficiency of precipitation process as the solubility of hydroxyl ions and formation of metal precipitates is directly related to these conditions [45].

Other than these methods, the catalyst can be prepared by using both impregnation and precipitation techniques at the same synthesis or the active material can be incorporated to the catalyst structure during synthesis of MCM-41, for which the method is called co-precipitation. However, with that method, the formation of ordered hexagonal cylindrical tubes-like structure is disturbed. It is slightly possible to have that kind of an ordered mechanism [45].

Both impregnated and directly synthesized materials on MCM-41 find application areas in different reactions. The coming section includes these applications.

3.2.4. Some Application Areas of MCM-41

MCM-41 can be used in various applications with replacing environmentally hazardous materials. Having a large surface area in addition with a regular pore size arrangement makes MCM-41 promising candidate in using support material for catalytic applications in both acidic and basic regions. Good dispersion of the active component in the whole surface enhances the yield of the processes by increasing the accessibility to active sites. Being in mesoporous range with a large pore volume, MCM-41 allows the researchers to study with large molecules, which is not the case with zeolites which are microporous.

Pure MCM-41 has weak acidity and low catalytic property. Thus to imrove catalytic activity, as mentioned in previous section, different methods are used to incorporate the active component to MCM-41 structure. By using different materials, which include acids, bases, metals (both transition and alkaline metals) and oxides of these metals, MCM-41 can be used in acid and base catalyzed reactions as well as in redox reactions. In addition to these, high adsorption capacity towards many molecules, MCM-41 can be used in separation processes in chromatographic or waste treatment applications.

In hydrocracking of large petroleum products that is in hydrodenitrogenation (HDN) mild hydrocracking (MHC) and hydrodesulfurization (HDS) processes, catalysts having nickel and molybdenum as the active components are used (NiMo). The conventional support is USY zeolite. However by the contributions of larger surface area and larger pore size, it is concluded that NiMo incorporated MCM-41 has a higher activity compared to NiMo/USY in terms of removing sulfur and nitrogen [46]. This is also attributed to well-distributed acid sites in the catalyst matrix and easy diffusion of large molecules in uniform and larger pores which is not possible for zeolites.

In addition to HDN, HDS and MHC processes, Friedel-Crafts alkylation and acylation reactions are also carried out in the presence of mesoporous catalysts. Due to pore size restrictions, it is observed that these catalysts are more active compared to HY zeolite which is 7.4°A [46]. Alkylation of 4-tertbutylphenol with isobutene is performed with tungtophosphoric ($H_3PW_{12}O_{40}$- TPA) acid incorporated MCM-41. To obtain acidic characters, it is an active method to use heteropolyacids (HPA) which are in superacid region. It is concluded that, at lower loadings, HPA is finely dispersed and no crystal is formed, that is what is observed is not the original Keggin structure, but the modified one. On the other hand, further loadings makes Keggin structure to dominate in the catalyst [46, 47]

With the large pore diameters accessible for large molecules, MCM-41 allows incorporation of large transition metals into it (Zr, Mo, W). Oxidation of larger molecules is performed in presence of titanium introduced MCM-41. Olefin is oxidized to epoxide with H_2O_2 or THP (tertbutylhydroperoxide) with Ti/MCM-41.

Compared to Ti-β-zeolite, which is the conventionally used one, Ti/MCM-41 dominates in terms of oxidation yield of larger molecules. By using the same catalyst, oxidation of amines, bulky sulfides can also be performed Here it is observed that, there exists an optimum value for Ti loading (2 wt %) into the structure when the yield of oxidation process is considered. To prevent this, it is proposed to develop alternative methods to introduce Ti into MCM-41 [46].

The sorption capacity of MCM-41 can be adjusted depending on the nature of the component used and by modification of catalyst morphology. Removal of both organic and inorganic chemicals in waste treatment, like mercury and other heavy metals, is also possible by using MCM-41. In HPLC applications, MCM-41 is considered as capable of separating both acidic, basic and neutral components [46, 47].

3.3. Other M41S Family Members

Other than MCM-41, there exist two main members of M41S materials which are studied by researchers; namely MCM-48 and MCM-50.

MCM-48 has a cubic structure exhibiting a three dimensional pore system whereas MCM-50 is in (unstable) lamellar form. As the reproducibility in the synthesis of these materials is low, these materials are not studied as much as MCM-41. The main difference in preparing between M41S family members is the surfactant added during synthesis. As can be seen in Figure 8, further addition of surfactant to the mixture causes the formation of MCM-48 and MCM-50 accordingly.

The XRD pattern of MCM-48 shows the reflections of all planes. MCM-48; has similar properties as MCM-41 like thermal stability and porosity. The main difference between the two is that the structures. One dimensional long cylindrical channel system in MCM-41 enables the materials to pass through it and improves the

adsorption on the surface. Although, the cubic structure in MCM-48, provides a three way diffusion, this also may cause easy choking in shorter channels.

MCM-50 has an unstable structure exhibiting a lamellar phase. After calcination, the material becomes microporous and a second treatment with a silica source can be used to stabilize and decrease the pore size to mesoporous region. In addition to increased surfactant amount, heating MCM-48 solutions for longer times also leads the formation of MCM-50 [40].

CHAPTER 4

HETEROPOLYACIDS AND APPLICATIONS

Heteropolyacids (HPAs) get attention in various reactions due to their strong and uniform Brönsted acidities (superacid behavior) and extensive redox properties. The discovery depends on nearly 1970s. HPAs are considered to be green and economical agents when compared with other liquid acids like H_2SO_4. In this chapter, HPAs are examined in terms of their structure and the factors affecting the applications (both pure HPAs and supported ones) are discussed with advantageous and disadvantageous sites.

4.1. Structure of Heteropolyacids

The structure of HPAs mainly consists of a central atom (P, Si, As, Ge, B, etc.) surrounded by polyoxometalate (POM) anions in metal-oxygen octahedra forms. HPA structure can be formed in two different configurations of anions; [48, 49]

→Keggin structure: $XM_{12}O_{40}^{(8-x)-}$

→Wells-Dawson structure: $X_2M_{18}O_{62}^{(16-2x)-}$

→Anderson structure: $XM_6O_{24}^{(12-x)-}$

→Waugh structure: $XM_9O_{32}^{(10-x)-}$

→Silverton structure: $XM_{12}O_{42}^{(12-x)-}$

In these structures, X is the central atom (heteroatom with an oxidation state of x) and M is the metal (Mo^{6+}, W^{6+}, V^{5+}, Co^{2+}, Zn^{6+} etc.) (addenda atoms). Each oxygen forming the tetrahedron is bonded to M_3O_{13} units. The structure is in the form of MO_6 octahedra around tetrahedral XO_4 where the corner and edge oxygens, the ones in octahedral sites of addenda atom, are shared. The atoms in Keggin structure form a spherical shape whereas for the Dawson type, an ellipsoidal structure consisting of two XM_9O_{31} units connected by six oxygen atoms are formed [48, 50]. In addition to these structures, there are also, Linquist, Silverton and Anderson type HPAs [51].

This structure defined above is called as the primary one which is in the form of polyanions. In addition, the three dimensional forms (combination of anions with various cations) are called as secondary structures and tertiary structure is used for different textural properties (like pore size distribution, surface area etc.) of HPAs and defines how the structure is incorporated into other ones [52]. Among the two structures, Keggin is the best known and first characterized owing to its higher thermal stability compared to Dawson structure and its easy availability [48]

4.2. Acidity of Heteropolyacids

HPAs exhibit a higher Brönsted acidity, approaching a superacid behavior. In addition, being soluble in polar solvents, the protons gain a higher mobile property which brings the pseudo-liquid phase in solutions. This mobility property is the distinctive property of HPAs from zeolites. When compared with other liquid and solid acidic materials, it is shown that, HPAs are superior to HX or HY zeolites and SiO_2-Al_2O_3. In Table 4, the dissociation constants are shown for various HPAs and some strong acids in acetone [48].

Table 4: First three dissociation constants for acidic materials in acetone at 25°C [48]

Acid	pK_1	pK_2	pK_3
$H_3PW_{12}O_{40}$ (TPA)	1.6	3.0	4.0
$H_4PW_{11}O_{40}$	1.8	3.2	4.4
$H_4SiW_{12}O_{40}$ (STA)	2.0	3.6	5.3
H_2SO_4	6.6	-	-
HCl	4.3	-	-
HNO_3	9.4	-	-

In an ammonia absorption study conducted by Lefebvre *et al* [50], the heats of absorption of $H_3PW_{12}O_{40}$, $H_4SiW_{12}O_{40}$, $H_6P_2W_{21}O_{71}(H_2O)_3$ and $H_6P_2W_{18}O_{62}$ are found as 196, 185, 164 and 156 kJ mol^{-1} accordingly showing the acidities of the samples in the same order. Therefore, the strength of acidities is in the order of as follows;

$$H_3PW_{12}O_{40} > H_4SiW_{12}O_{40} > H_6P_2W_{21}O_{71}(H_2O)_3 > H_6P_2W_{18}O_{62}$$

By that way, it is proved that the acidity of Keggin HPAs' are higher than those of Dawson HPAs. Comparing the acidity of TPA with H-ZSM-5 zeolite shows the dominating acidic properties of it. The corresponding NH_3 adsorption studies indicate that the values of heats of adsorption for H-ZSM-5 and γ-Al_2O_3 are 150 kJ/mol and 140 kJ/mol accordingly proving the superior acidity capacity of HPAs.

On the other hand, it is stated that SO_4^{2-}/ZrO_2 is more acidic compared to the HPA. Similarly, the acidity of salts of HPAs are also comparable to those of the intact HPA. The NH_3 adsorption studies show that the heat of adsorption for $Cs_{2.5}H_{0.5}PW_{21}O_{40}$ is 165 kJ/mol [53].

For the supported HPAs, the acidity is mainly dependent on two factors which are namely the amount of loading and nature of support. Silica supported HPAs govern the properties of pure HPA (the crystalline Keggin structure) at low loadings where fine dispersion is observed. On the other hand, the Keggin structure becomes dominant at higher loadings [54].

Tunable behavior of acidity, thus the redox properties, is a critical advantage for HPAs. This enables to design different HPAs for various kinds of reactions bringing a selective reaction field for the material. Control of the structure of various HPAs (at molecular level) enables to select the appropriate catalyst for each type of reaction [55].

4.3. Thermal Stabilities of Heteropolyacids

HPAs are used in several industrial processes which are investigated in Section 4.4. in detail. However, despite their acidic behavior, thermal instability brings a limitation to the operating conditions of these processes due to coke formation beginning at lower temperatures (catalyst deactivation) and thus resulting difficulties in regeneration of the catalysis. To remove the coke formed on the surface of the material, that is to decoke it, a combustion process at high temperatures is used (calcinations). However, this is not appropriate for HPAs which are not thermally stable up to these higher levels. The upper level of temperature can be put as the limit where all the acidic properties are lost and in Table 5, these temperatures can be seen for various HPAs [56].

Table 5: Thermal stability limits of selected HPAs [56]

Material	Temperature (°C)
$H_3PW_{12}O_{40}$	465
$H_4SiW_{12}O_{40}$	445
$H_3PMo_{12}O_{40}$	375
$H_3SiMo_{12}O_{40}$	350

Following the TGA curve of hydrated TPA ($H_3PW_{12}O_{40}.nH_2O$), Kozhevnikov [57] proposed a mechanism related to losses during heating. The process consists of three steps of which the first is vaporization of water at 100°C. At 200°C and 450-470°C, water molecules bonded to the acidic protons and the remaining protons are removed respectively. At temperatures higher than 600°C, the component is totally converted to P_2O_5 and WO_3 which shows no acidic property.

Several solutions are proposed to overcome that thermal instability problem. It is shown that, doping HPA with Nb (V), Zr (IV), Ti (IV), Pd or Pt and calcining at temperatures of 500-700°C, improves thermal stability of the catalysis suppressing coke formation. Regeneration of the catalyst can also be performed by supercritical fluids [57].

4.4. Applications of Heteropolyacids

HPAs are used in industrial applications both in pure structure and supported ones. In addition to the advantages as a catalyst (as acidic and redox properties, structure control at atomic and molecular level), using HPAs in industry also meets

the necessities of green chemistry in an economical and sustainable way. Usage of HPAs in catalytic reactions eliminates corrosion of reactors, generation of toxic materials as in the case of usual inorganic acids.

The main drawback related to HPAs in applications is that these acidic materials are considered to be non-porous with a surface area of 1-10 m^2g^{-1} based on nitrogen adsorption results. To overcome that situation, formation of large cation salts (group B salts, with Cs^+, Rb^+, etc.) are proposed. This may lead to formation of catalyst with surface areas on the orders of 150 m^2g^{-1} [58]. These flexible changes in textural properties (pore dimensions) make HPA salts suitable for each type of characteristic pore sizes. Another solution is to incorporate HPAs into porous materials like mesoporous silica (MCM-41, SBA-15), activated carbon, zirconia, etc [58]. This can improve the dispersion of material on the surface and depending on the loading of HPA; the catalyst can possess both the properties of an HPA and the support.

Both supported HPAs and salts of HPAs find their places in industrial applications. In addition, the catalysts with noble metals (Pt, Pd) and transition metals (Ni, Cu, etc) are used widely. These applications include homogenous and heterogeneous processes as well as biphasic reactions where two immiscible liquids are involved. Applications of these materials can be examined in three sections; namely, acid catalyzed reactions, oxidation reactions and reactions involving bifunctional catalysis.

4.4.1. Acid Catalyzed Reactions by HPAs

Due to their highly acidic behavior, HPAs are offered as good candidates for acid-catalyzed reactions. Depending on mainly to the structure of the heteropolyanion, acidity is also affected by the counter cation in the structure and by the support used [59].

Supporting HPAs on materials, by providing a distribution of the active material on a more porous surface, enhances the interaction of the catalyst and the reactants. Ethanol dehydration reaction is performed with $H_3[PMo_{12}O_{40}].xH_2O$ and $H_3[PMo_{11}VO_{40}].xH_2O$ supported on Al/Fe-MCM41 at different temperatures by Popa *et al* [60]. Compared with the bulk catalyst, the supported ones have lower activation energies for acetaldehyde formation than those for the former ones showing the efficiency of supporting process.

Xia *et al* [61], conducted MTBE (methyl-tert-butyl-ether) formation from gas phase methanol and butyl alcohol on TPA supported at MCM-41. The activity results in MTBE formation show slightly higher conversions (~98.6%) with the commercially used ion-exchange resin Amberlyst-15 (.~98.0%) at optimum temperatures (which is 80°C-100°C and 100°C for HPA/MCM41 and Amb-15 respectively).

4.4.2. Oxidation Reactions with HPAs and Bifunctional Catalysis of HPAs

Oxidation properties of HPAs are mainly related to redox characteristics dependent to the addenda atom present in the structure. Formation of mixed addenda HPA salts (V and Mo addenda atoms on Cs salts) to improve thermal stability and redox properties of the catalysts [59, 62].

Commercial synthesis of acetone from propylene and acetaldehyde from ethylene (so called Wacker process), are performed with O_2 as oxidant in presence of Pd impregnated heteropolyanions which disabled formation of chlorine in the system as compared to the conventional system, where $PdCl_2$ and $CuCl_2$ are used [48].

Having both acidic and oxidizing character, HPAs can be used in two step reactions involving mentioned characteristics. Production of acetic acid from ethylene is industrialized by use of Pd impregnated Keggin type HPAs where oxidation step is carried out in HPA site and next step is in Pd sites [50].

CHAPTER 5

SUPERCRITICAL FLUID EXTRACTION

In this chapter, the details regarding to the application of supercritical fluid extraction (SFE) are given. These details include the extraction phenomena and the applications in different industries. The extraction processes of mesoporous materials are analyzed in the latter section.

SFE is considered as a green process in different processes such as separation, organic reactions or material synthesis since environmentally friendly agents are used rather than toxic organic solvents in the operations. The main application areas of SFE are in pharmaceutical and food industry as well as in environmental fields and particle engineering.

The reason of wide use of SFE technique in processes has arised from the need to decrease to use of organic solvents in extraction due to environmental restrictions. In 1879, Hannay and Hoganth examined the properties of SCFs and showed presence of new type solvents in science. However, the commercial use of SCFs are started in nearly 1960s [63].

Supercritical phase of a compound is defined as the phase above its critical temperature and pressure which are characteristic for it. In that state, increasing the pressure does not liquefy the substance, but the density approaches to that of the liquid state. Thus, it has properties between a gas and liquid.

The attractive properties of SCFs in uses of several applications are lowered viscosity and improved mass and heat transfer rates. Thus the energy required with those improved properties is reduced. In addition, adjustment of process conditions

(temperature and pressure) offers adjustable solvating power, which is much more when compared with those of liquids, for the agent acting selectively [64]. This selective behavior is advantageous in selective chemical reactions, in particle sizing processes (control of morphology) [31]. With these gained advantages, the time required to obtain a pure compound is decreased and by the use of inert SCF agents, the corresponding separation cost is also lowered. Simple depressurization technique is enough to remove the extraction agent from the whole matrix. The inertness of the agent simplifies the removal and by that way, purity of the material is improved [65]

5.1. CO_2 as an SFE agent

In applications of SFE, several solvents are used. The commonly used ones and the corresponding critical properties are given in Table 6 [31].

Table 6: Critical properties of common SFE solvents [31, 66]

Solvent	Critical Temperature (K)	Critical Pressure (MPa)
CO_2	304.21	7.38
Methanol	512.6	8.096
Water	647.13	21.94
n-Hexane	507.6	3.04

Among these three, CO_2 is the most used one. In Figure 11, the details of CO_2 phase behavior is shown [67].

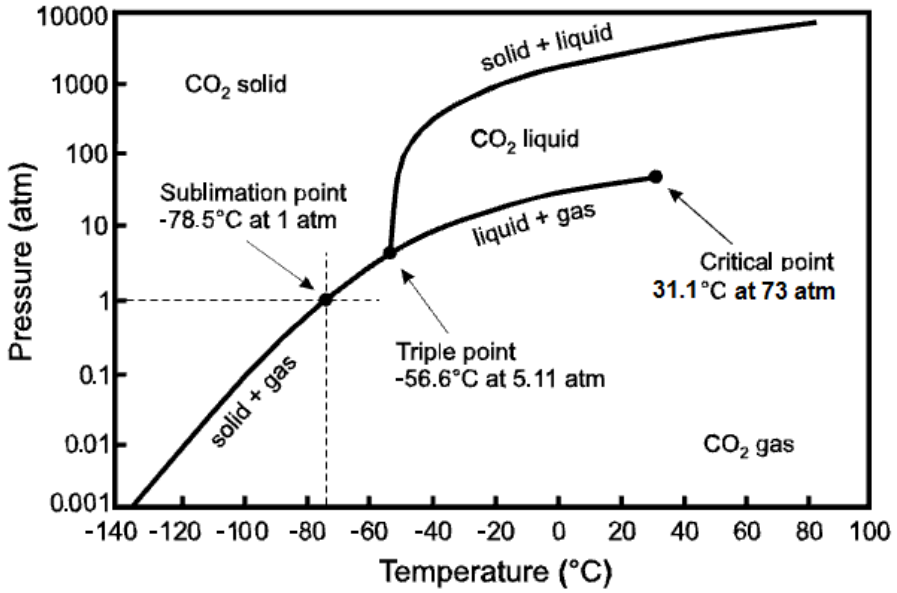

Figure 11: Phase diagram of CO_2 [67]

At supercritical conditions, the improvement on transport properties of CO_2 is well observed. Viscosity of scf CO_2 approaches to that of gaseous one (10^{-4} $gcm^{-1}s^{-1}$ for gaseous CO_2 at 1 bar, same as scf CO_2 [31]) with density approaching to that of liquid phase (0.3 gcm^{-3} for scf CO_2 which is 1 gcm^{-3} for liquid [31]). In addition the diffusivity is closed to that of gaseous CO_2 further improving the diffusion properties.

The improved mass transfer coefficient (self diffusivity) compared to the liquid one, is a result of high density and lower viscosity [31].

The attractive properties regarding to the use of CO_2 as an SFE agent can be summarized as follows; [31, 63]

- Environmentally benign and cheap
- Nonflammable, non-toxic (green solvent behavior)
- Chemically inert: Easy removal from matrix by depressurization
- Moderate critical properties: Advantageous in terms of operating at moderate conditions for those being thermally instable.

On the other hand, low polarity of CO_2 limits the use in extractions of specific polar compounds. To get rid of this problem, several polar modifiers are used to enhance the efficiency of the process by increasing the solvating power of CO_2 towards the component in consideration. Most commonly used ones are methanol and ethanol.

5.2. Applications of SFE

Most common industries using extractions as a method for removal of components are the food and pharmaceutical industries. In addition, in material preparation, SFE is seen as a promising technology in adjustment of material properties to the desired conditions.

High operational cost faced with SFE is mainly due to higher pressures in the process. Although, at the end, the efficiency of recovery (of extracts) and obtained product is higher compared to the conventional extraction processes, SFE conditions need an optimization to minimize the operational costs. This optimization, where the main parameters are temperature and pressure of solvent, duration of process, nature of solvent/modifier, composition of extracting medium, can be achieved by clear understanding of phase equilibrium between the solvent and extract as well as the modifier used [63].

The commercialized SFE processes are decaffeination of coffee and tea, hops extraction, extraction of spices, flavours and aromas and denicotinization of tobacco. Within the scope of this study, SFE is examined in catalyst preparation.

5.3. SFE in Catalyst Preparation

Use of SFE in catalyst preparation is similar to the one in pharmaceutical industry and is mentioned in several points; in design of catalysts (particle sizing,

particle coating, supercritical fluid deposition) or in template removal. Common application of the method is in batch mode. In other words, the process starts with charging the SCF and/or modifier to the vessel containing sample in it. Second step is to pressurize the system and after maintaining for the desired period at the desired conditions, SCF is discharged with depressurizing the system. The process can be performed in continuous mode where, make up SCF and/or modifier are supplied to the system continuously.

The critical advantage of this technique over the conventional ones such as impregnation is that, control of end-product properties and improved mass transfer rates. In addition to tuning in physical properties of the material, catalyst nature (namely coating distribution, concentration, morphology etc.) can also be controlled by SCF application with adjustment of operating parameters.

Formation of different type of structure is mainly affected by solvent nature. CO_2, known as the most common extracting agent, is inert and does not have chemical interaction with the materials. On the other hand, use of water or ammonia, facilitate the formation of oxides and nitrides accordingly. In addition, the crystal structure of the catalysis can be tuned by using different types of solvents. The alumina particles show various characteristic XRD patterns in presence of CO_2/water and ethanol mixtures [68].

Material coating, which then be used for various applications like catalytic or microelectronic, is performed by supercritical fluid deposition (SCFD). Incorporation of metals to polymer matrices and design of nanostructured materials are two examples of SCFD applications. Other than, incorporation, SCF applications are also used in formation of nanorods/wires such as carbon nanotubes (CNTs). Use of supercritical CO_2 rather than gaseous one improves the yield of process without utilizing a catalyst [68, 69].

The three steps mentioned above are all affect the SCFD process by having different mechanisms. Dissolution of the metal precursor in the SCF solution is explained by solubility. As the first step, solubility phenomena and the regarding rates are investigated to develop a model defining the mass transfer rates. To enhance

the solubility rates, co-solvents are utilized. The second adsorption step is generally defined as mass transfer of supercritical solution (containing active component in it) to the external surface and into the pores of the support. Depending on the natures of support and metal, and the operating conditions the model describing the adsorption mechanism can have several expressions. The reduction step is also similar to the previous one. Investigation of the mechanism indicates that, the nature of the reducing agent and the type of support used, critically affect the incorporation [69].

Other than formation of finely and uniformly dispersed materials for incorporation to the support materials on the surface and/or into the pores, supercritical applications are used in template removal in catalyst synthesis as well. As in other processes, nature of extracting agent and the material to be extracted are the main factors affecting the supercritical application as well as the operating conditions and whether a co-solvent is present or not. The studies regarding to develop a newer technique for template removal is primarily due to operating conditions of calcination. Being performed at higher temperatures to get considerable efficiencies, calcination brings the risk in distortion of original catalyst matrix.

Several studies are published in this area. Chatterjee et. al. [70], reported the importance of using a co-solvent in surfactant removal from titanosilicates synthesized with different Ti/Si ratio. In addition, the results of carrying out the extraction at different temperatures (at a fixed pressure, 35 MPa) reveal that, there exists an optimum temperature (353 K) to remove the template with the highest efficiency (defined with the results associated with TGA analysis).

Huang et al [71], reported extraction efficiencies for different catalytic materials; MFI and beta zeolites and MCM-48. The results indicate that template removal in mesoporous MCM-48 is much more compared to that of zeolites due to differing pore sizes. Average pore diameter of zeolites, being smaller to MCM-48, does not allow CO_2 and the modifier solvent to get into the pores and extract the template from the matrix. The extraction is on the orders of 1-10% for zeolites whereas for MCM-48, this value reaches up to 95% depending on the extraction pressure, temperature and duration.

One other advantage of extraction over calcination is that recovery of organic template, thus reduction in synthesis cost (which is nearly 77% of total MCM-41 synthesis cost), becomes possible with extraction. The burning process in calcination causes the surfactant to go off [71, 72].

Investigating the effects of operating parameters; Huang et al [72], with the experiments conducted with MCM-48, concluded that the extraction efficiency is dependent to both temperature and pressure with an optimum value. Increasing the pressure (between 80-140 bar), while keeping the other parameters fixed, improves template removal up to a pressure and after that optimum value, due to approaching critical point where CO_2 and methanol reach an homogenous phase, extraction efficiency starts to decrease. During extraction of organic templates, the modifier liquid is used to take off the material while CO_2 is mainly the transporting media. Higher pressures, thus presence of homogenous phase, therefore decrease the amount of liquid methanol phase in the mixture resulting a decrease in final removal efficiency. After the supercritical phase is achieved for methanol and CO_2 (at 141 bar, 85°C), extraction is controlled mainly by solvating power of the whole mixture. Further pressurizing the system enhanced the extraction process with increased solvating capabilities in the studies conducted by Huang et al [72]. The temperature dependency is similar to this issue such that at higher temperatures composition of liquid methanol may decrease leading to the same result as stated. In addition, the density of final solution decreases as well which then lowers the solvating power of the extracting agent. The reduction in residence time with increased temperature and thus the volumetric flow rate, may also limit the amount of extracted template from the system.

CHAPTER 6

EXPERIMENTAL STUDIES

This chapter comprises of three subsections which mainly includes the detailed steps in catalyst preparation and the methods used in catalyst characterization, in addition with the experimental set up used in DME synthesis.

6.1. Catalyst Preparation

In this section, the preparation steps of the catalysts used are explained in detail. These include direct hydrothermal synthesis, namely incorporation of HPA and metal (Zr, Ni, Cu) into the MCM-41 structure with different synthesis conditions.

6.1.1. One Pot Hydrothermal Synthesis of STA-Zr/Silica (SZ Group) Catalysts

6.1.1.1. Chemicals Used

In synthesis of SZ group catalysts, the following reagents are used.

- Silica source: Tetraethylorthosilicate (TEOS), $C_4H_{20}O_4Si$ (Merck)
- Surfactant source: N-Cetyl-N,N,N trimethylammonium bromide (CTMABr) $C_{16}H_{33}(CH_3)_3NBr$, (Molecular weight: 364.46 g/mol, powder, 99% pure, Merck)

- Silicotungstic Acid (STA) (Sigma Aldrich)
- Zirconium source: $Zr(NO_3)_2.H_2O$, zirconly nitrate monohydrate (Sigma Aldrich)
- Solvent source: Deionized water (Millipore Ulta-Pure Water System, Milli-QPlus)
- Base source: Sodium hydroxide (NaOH, 1M) (Merck)

6.1.1.2. Synthesis Procedure

- 13.2 g of surfactant CTMABr added to 87ml deionized water and the mixture is mixed with 500rpm rate at 30°C until a clear solution is obtained.
- 15.64 ml TEOS is added to the clear solution dropwise and mixed to reach adsorption equilibrium (pH of the solution: 4.6). The synthesis is perfomed at acidic conditions to prevent formation of any aggregates after addition of STA.
- STA and Zr source, for which the amounts are adjusted according to the tungsten to silica and zirconium to silica ratios as given in Table 7, are mixed with 5ml and 10 ml of deionized water accordingly. Addition of STA and Zr source is performed with two different procedures

  →Procedure 1 (P1): The prepared solutions are mixed and added to the solution prepared in the first step together dropwise and mixed with the same rate for 1 hour.

  →Procedure 2 (P2): STA solution is added first and then Zr source is added to the whole mixture. After addition of each solution, the mixture is mixed continuously for 30 minutes.

- The pH of the solution is adjusted by adding NaOH (final pH of the solution; 6-6.5)

- After addition of raw materials, the resulting gel solution is transferred to a Teflon bottle which is then placed into a stainless steel autoclave for hydrothermal synthesis at 120°C for 96 hours.
- The obtained solid is then washed with 300 ml of deionized water and filtered until a constant pH (5-6) is obtained and dried at 40°C for 24 hours at vacuum.
- Finally the dried material is treated with two different techniques for surfactant removal.

  ➔ **Calcination:** The dried sample is placed in a quartz tube and treated with 1dm^3/min air flow at atmospheric pressure and 350°C for 8 hours with a heating rate of 1°C/min. The calcined samples are named with a "c" before the catalyst name as cSZ1, which refers to the calcined sample of catalyst SZ1 (Table 7).

  ➔ **Supercritical fluid extraction:** The dried samples are treated with methanol modified supercritical CO_2 at 85°C and at different pressures (Table 8) as described in Kawi *et al* [73]. CO_2 flow rate is measured as 2.5 L/min whereas the methanol is fed with an HPLC pump with 0.45 ml/min rate at STP resulting a molar ratio of 10:1 for CO_2:Methanol. Detailed conditions related to the extractions are given in Table 8. In addition to regular extraction of the samples, SZ3 and SZ4 are extracted at different pressures and for different time intervals to test the effect of these parameters on the catalyst properties. Supercritically extracted samples are named with a "sce" before the catalyst name such as sceSZ1, which refers to the extracted sample of catalyst SZ1.

Table 7: Synthesis Conditions for STA-Zr/Silica Catalysts

Catalyst name	Synthesis Procedure	pH of the solution	Amount of STA used (g)	Amount of Zr source used (g)	Atomic ratios	
					W/Si	Zr/Si
SZ1	P2	0-0.5	6.77	4	0.4	0.24
SZ2	P2	6-6.5	6.77	3	0.4	0.18
SZ3	P1	6-6.5	6.77	2	0.4	0.12
SZ4	P2	6-6.5	6.77	1	0.4	0.06
SZ5	P2	6-6.5	5.08	1	0.3	0.06
SZ6	P2	6-6.5	8.46	1	0.5	0.06

Table 8: Extractions Conditions for STA-Zr/Silica Catalysts

Catalyst name	Pressure (bar)	Temperature (°C)	Period (hour)	Resulting Catalyst
SZ1	450	85	3	sceSZ1
SZ2	450	85	3	sceSZ2
SZ3	450	85	3	sceSZ3
SZ3	300	85	3	sceSZ3-300
SZ3	600	85	3	sceSZ3-600
SZ4	350	85	6	sceSZ4
SZ4	350	85	3	3SZ4
SZ5	350	85	6	sceSZ5
SZ6	350	85	6	sceSZ6

6.1.2. One Pot Hydrothermal Synthesis of STA-Ni/Silica and STA-Cu/Silica Catalysis

6.1.2.1. Chemicals Used

Similar to SZ Group catalysts, STA-Ni/Silica and STA-Cu/Silica Catalysis are synthesized via direct hydrothermal synthesis route and the following chemicals are the components of the synthesized catalysts.

- Silica source: Tetraethylorthosilicate (TEOS), $C_4H_{20}O_4Si$ (Merck)
- Surfactant source: N-Cetyl-N,N,N trimethylammonium bromide (CTMABr) $C_{16}H_{33}(CH_3)_3NBr$, (Molecular weight: 364.46 g/mol, powder, 99% pure, Merck)
- Silicotungstic Acid (STA) (Sigma Aldrich)
- Nickel source: $Ni(NO_3)_2.6H_2O$, nickel (III) nitrate hexahydrate (Merck, molecular weight 290.8 g/mol)
- Copper source: $Cu(NO_3)_2.3H_2O$, Copper nitrate trihydrate (Merck)
- Solvent source: Deionized water (Millipore Ulta-Pure Water System, Milli-QPlus)
- Base source: Sodium hydroxide (NaOH, 1M) (Merck)

6.1.2.2. Synthesis Procedure

- 13.2 g of surfactant CTMABr added to 87 ml deionized water and the mixture is mixed with 500rpm rate at 30°C until a clear solution is obtained.
- 15.64 ml TEOS is added to the clear solution dropwise and mixed to reach adsorption equilibrium (pH of the solution: 4.6).
- 6.77 g of STA mixed with 5 ml of deionized water is added to the solution to achieve a W/Si ratio of 0.4 and stirred for 30 minutes (pH of the solution 0-0.5).
- Metal source is added to get a metal/Si ratio of 0.06 as given in Table 9 after mixed with 10 ml of solvent. The resulted solution is mixed for 30 minutes.

- The pH of the solution is adjusted to 6-6.5 by adding NaOH.
- The resulted gel is treated as the same way described in the previous section; hydrothermally synthesized in Teflon, washed and dried. The surfactant removal steps are calcination and extraction. Notations for the samples are similar to SZ group catalysts. Details regarding to the extraction conditions are given in Table 10.

Table 9: Synthesis Conditions for STA-Ni/Silica and STA-Cu/Silica Catalysts

Catalyst name	Metal used	pH of the solution	Amount of STA used (g)	Amount of metal source used (g)	Atomic ratios	
					W/Si	Metal/Si
SN1	Ni	6-6.5	6.77	1.25	0.4	0.06
SC1	Cu	6-6.5	6.77	1.04	0.4	0.06

Table 10: Extractions Conditions for STA-Ni/Silica and STA-Cu/Silica Catalysts

Catalyst name	Pressure (bar)	Temperature (°C)	Period (hour)	Resulting Catalyst
SN1	350	85	6	sceSN1
SC1	450	85	3	sceSC1

6.2. Characterization of Catalysts

Characterization of catalytic materials involve examination of structural mechanism including crystal structure, elemental composition or molecular bonding, and physical properties such as pore size distribution, surface area etc. There are several methods to characterize such materials. However, this section includes the methods used in the present study.

6.2.1. X-Ray Diffraction (XRD)

X-Ray diffraction is used to define the structure of the sample by utilization of diffraction patterns obtained at different incident angles. The sample is treated with two incident rays, applied at different angles and the diffraction occurs in where the atomic layers are placed in the structure.

By that way, the spacing between the layers are obtained. A sample with a crystallographic structure, gives peaks corresponding to different atomic spacing (d) at each angle present in the sample structure. This relation between atomic spacing and incident angle is defined by Bragg's Law stated below [74];

$$\text{Bragg's Law: } n\lambda = 2d\sin\theta \tag{8}$$

Where

n: a constant

λ: wavelength of incident ray; fixed with X-Ray instrument (0.154 °A when Cu is used as metal target)

d: atomic layer spacing in the structure

θ: angle of incident ray

On the other hand, a sample with amorphous structure, *i.e*, form of arrangement in a random way, gives no peaks in its XRD pattern which is a characteristic property for the sample itself [74].

XRD characterizations of the catalysts used in this study are performed in METU Metallurgical and Materials Engineering Department using the Rigaku D/MAX2200 diffractometer associated with CuK metal target in a 2θ range of 1°-50° with a scanning step of 0.02°.

In XRD analysis, the pattern is examined with the peaks corresponding to each d-value spacings predefined with the sample's properties.

6.2.2. Nitrogen Physisorption

Nitrogen physisorption is one of the widely used adsorption methods used to characterize catalytic materials. Nitrogen at 77K is physically adsorbed and then desorbed on the surface of the sample and the corresponding isotherms are obtained. Depending on the pore structure (including both size and distribution) different types of isotherms and associated hysteresis classified by IUPAC.

The gas is adsorbed in the sample surface and the specific amount of gas adsorbed on the surface is reported as the partial pressure of the gas (p/p^0) increases in the sample. The isotherm is analyzed with steepness of the curve and where that steepness occurs. For instance for Type I, the curve becomes sharp at a very low p/p^0 such that the pores are filled with a small amount of adsorbed gas indicating a micropore structure [75].

Uniform mesoporous structures exhibit Type IV isotherms as stated before. Different than the first three types, Type IV shows also a hysteresis loop (H2) which is associated with capillary condensation of the gas during adsorption. H2 type of hysteresis is commonly seen in narrow distributed mesopores like in MCM-41 structure [74, 76].

The physisorption analysis is carried out in METU Central Laboratory with nitrogen. The degassing is done at 100°C for 16 hours. With that method, pore size distribution and pore volume of the sample are obtained as well as the surface area.

6.2.3. Energy Dispersive Spectroscopy (EDS)

EDS characterization provides the user to identify the sample in terms of its constituents both quantitatively and qualitatively. When electron beams are subjected to the sample, electrons are extracted from the molecule and another molecule in an outer shell replaces the extracted one emitting an X-ray. That emitted X-ray at different intensities of electron beam corresponds to a different atom. With the obtained spectra, the elemental composition of the sample is well-defined. However since the beam hits the sample in the bulk, what is found with the analysis is that the bulk composition [77].

The EDS characterizations of the samples are performed in METU Metallurgical and Materials Engineering Department by a JSM-6400 (JEOL) instrument equipped with NORAN System Six. Depending on the sample and the used materials during synthesis, the sample is coated with either gold or carbon.

6.2.4. Thermogravimetric Analysis (TGA/DTA)

TGA provides the analyzer to obtain data on weight change (rate) during a uniform temperature rise in a defined range. The causes of that change (both loss and gain depending on the purge gas used) may be due to decomposition, oxidation or else. By that way, thermal stability, oxidative capability or moisture content of the sample can be determined. The weight of the sample is recorded simultaneously during temperature change. The most commonly used purge gas is with its inert behavior N_2; then helium and also air.

In thermogravimetric analysis of the samples in this study are carried out by METU Chemical Engineering Department by utilizing air as the gas and a temperature raise of 10K/min is applied during analysis. The effectiveness of the SFE applications are tested with that method for some selected samples.

6.2.5. Scanning Electron Microscopy (SEM)

Scanning electron microscopy is used to make a look at the catalyst with much bigger magnifications and resolutions compared with that obtained with naked-eye.

In the analysis, the sample is treated with a focused electron beam with a very short wavelength created in vacuum. These beams are absorbed on the sample and scattered. The resulting signal is used to generate an image reflected as a magnified picture of the sample. Topographical, morphological and crystallographic information can be obtained with that picture as well as the compositional details regarding to the sample if the SEM instrument is equipped with an EDS analyzer also [77, 78].

SEM pictures of the samples of this study are obtained in Scanning Electron Microscopy (SEM) analyses were done in METU Metallurgical and Materials Engineering Department by using JSM-6400 (JEOL) equipped with NORAN system Six. Samples.

6.2.6. Fourier Transform Infrared Spectroscopy (FT-IR) and Diffuse Reflectance Fourier Transform Infrared Spectroscopy (DRIFTS)

FT-IR is used to characterize the sample in terms of the present molecular bonds in the structure. Mathematical fourier transformation is utilized in the method. Sample, on which an IR radiation is passed through, absorbs some amount of the

radiation whereas the rest is transmitted. That transmitted and absorbed radiation due to vibrations between molecular bonds, are processed with fourier transformation and the results are monitored as a spectrum. This spectrum can be used as a fingerprint for the material such that no other sample can have the same spectrum. The advantages of FT-IR over conventional dispersive IR techniques are primarily increased sensitivity and simultaneous recording, *i.e* increased speed [79, 80].

Fourier Transform Infrared Spectroscopy analyses of the samples are performed in METU Central Laboratory by a Bruker FTIR-IFS66/S instrument with dilution with KBr.

Diffuse Reflectance FT-IR (DRIFTS) spectroscopy with adsorbed pyridine is used to characterize the acidic sites (including both Brönsted and Lewis) present in the catalytic structure. The method used is similar to that used in FT-IR. As a dilution material KBr is used with a concentration of 5% (wt/wt). A baseline is obtained with KBr itself. After mixed with KBr (two sets of samples are prepared), the samples are dried to remove volatile components in the structure and pyridine is adsorbed on one set of samples. DRIFTS analysis is done both by pyridine adsorbed and non-adsorbed samples of the same catalyst and the difference between these two forms the final spectra.

DRIFTS analyses are performed in METU Chemical Engineering Department in the Kinetic Laboratory by using a Perkin Elmer Spectrum One instrument.

In both DRIFTS and FT-IR, the spectrum is analyzed with peaks corresponding to each molecular vibration (like C-H strechings etc).

6.3. Experimental Set Up

The experiments conducted in the scope of this study, is performed in two sections. Firstly, the catalyst synthesis, where different types of metals are incorporated to MCM-41 structure together with the STA, is performed. Other than synthesis of catalysis with different metals, two different surfactant removal

mechanisms are investigated to create the final structure of the catalyst. In the first part of this section, the experimental set-up for supercritical fluid extraction system is given. In addition to catalyst synthesis, the synthesized catalysts are tested in methanol dehydration system. The details related to the experimental conditions and the set-up is given in the second section.

6.3.1 Supercritical Fluid Extraction System

Surfactant removal with supercritical fluid extraction method is carried out in and SFE system consisting of a stainless steel vessel with an inner volume of 24 ml and outer diameter of 1". The vessel is connected to a supercritical fluid extraction system (Applied Separations, Spe-ed SFE model 7070) that can be pressurized up to 690 bar (10000 psi) with an oven temperature of maximum 240°C. In addition to CO_2 inlet, the system is connected to a liquid inlet for modifiers that can be used in extraction.

As shown in Figure 12 [79], CO_2 is fed to the system and pressurized to predefined values by an air compressor (Atlas Copco) whereas methanol feeding is achieved by an HPLC pump after an input of flow rate value. On the other hand, CO_2 flow rate is measured by a rotameter (having two ranges measurement property with dual ball system -carbon and steel-) which is placed at the exit of the system and calibrated for CO_2 flow. The temperatures of oven, the extraction vessel and the outlet valve of species are controlled by SFE itself. While the former two are set according to the operating conditions of extraction, the valve temperature is set to 40°C to avoid evaporation of methanol at the outlet.

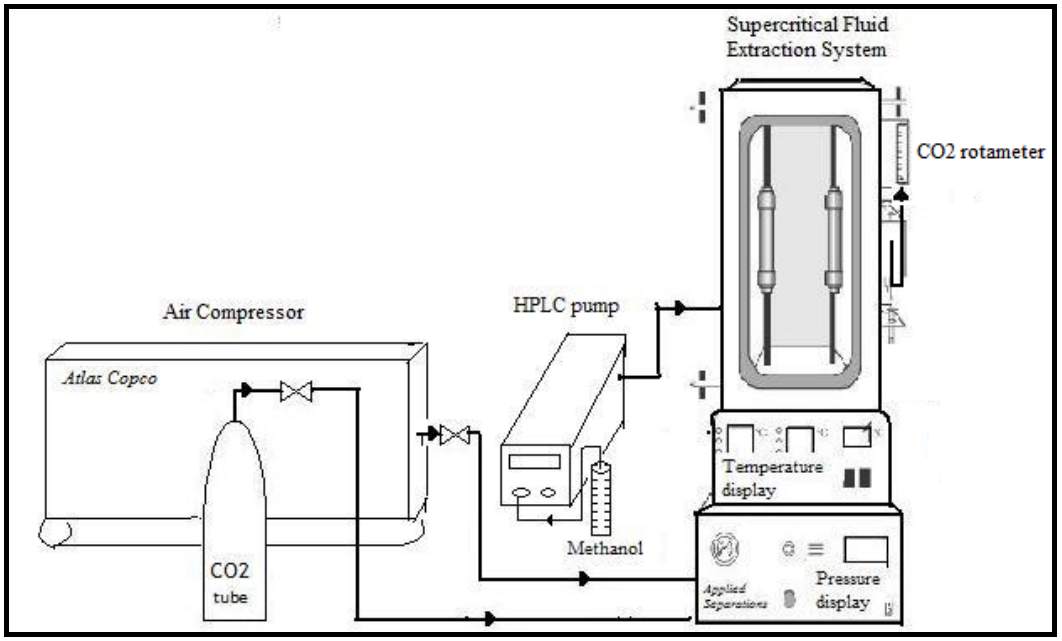

Figure 12: Supercritical fluid extraction system [modified from 81]

The exiting species from the system are mainly CO_2, methanol and the extracted surfactant. At 40°C valve temperature, CO_2 is directly sent to the flow meter where surfactant dissolved in methanol is collected in the bottle connected to the valve. The extraction conditions applied to each catalyst are given in Table 8 and Table 10. All catalysts are treated with SFE. The effects of operating conditions, pressure and period, are tested with SZ group catalysts and with the SC and SN catalysts, effect of metal type is investigated.

6.3.2 Methanol Dehydration System

The synthesized catalysts are tested in methanol dehydration reaction which is carried out in a tubular reactor that is placed into a tubular furnace to keep the temperature constant during the reaction. 0.2 g of each catalyst is fixed in the middle of the reactor (1/4" OD) by the use of glass wool, which does not have any

interaction with neither the reactant nor the products. As can be seen in Figure 13, gas chromatograph (GC) is connected to the reactor outlet (online) to make qualitative and quantitative analysis of the exiting species from the reactor. 150°C) Methanol is fed with a syringe pump into the system after being evaporated (at with a flow rate of 2.1ml/hr.

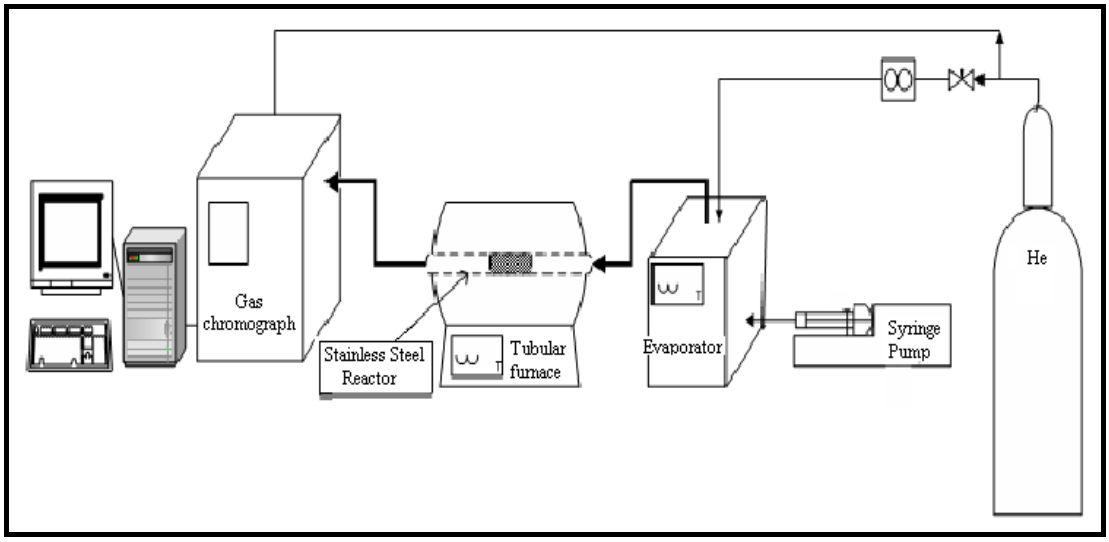

Figure 13: Methanol dehydration system [24]

The detector in the GC (Varian CP 3800 GC) is a thermal conductivity detector (TCD) and Propak T column was used. As a carrier gas and reference gas in GC, helium is utilized. The flow rate of methanol and helium (23.1 ml/min measured at room temperature and pressure) is adjusted so that, the rates are equimolar. With 0.2g of material placed in the reactor and with that gaseous flow rate, the space time is 0.27 s.g.cm^{-3}. The additional conditions regarding to the operation of GC is given in Table 11.

Table 11: Conditions of GC

Position	Temperature (°C)
Sample delivery	200
Column	75
	170 (10°C/min)
Detector	225

To prevent condensation of the effluent components from the reactor to the GC, the connecting lines are heated up to 150°C**.** The analysis in TCD detector is carried out at 225°C. The separation in the column is firstly performed at 75°C and then the column temperature is raised to 170°C with a rate of 10°C/min to increase the rate of separation and decrease the elution times of the constituents with high values of retention times.

The analysis in GC is resulted with individual retention times and calibration factors of the species. A sample calculation regarding to the conversion and selectivity is given in Appendix B.

The activity tests are performed with calcined and extracted samples of STA-Zr/silica at atmospheric pressure with varying temperature. The experimental conditions are summarized in the Table 12. The main parameter in the tests is the temperature and with that analysis, the activities of extracted and calcined samples are compared. The extracted catalysts are scanned in the range of 300-500°C, while this is 250-450°C for the calcined ones.

Table 12: Summary of experimental conditions

Catalyst	Temperature (°C)	Amount used
Calcined STA-Zr/Silica samples	250	0.2 g catalyst, 0.27 s.g/cm^3 space time
	300	
	350	
	400	
	450	
Extracted STA-Zr/Silica samples	350	
	400	
	450	
	500	

CHAPTER 7

RESULTS

7.1. Characterization Results

In this section, the results regarding to the characterization of the catalysts are given. These characterizations include XRD, EDS, N_2 physisorption, FTIR and SEM results. The section comprises of two subsections which are classified according to the type of metal incorporated to the catalyst structure.

7.1.1. Characterization Results of STA-Zr/Silica (SZ Group) Catalysts

Characterization results of Zr and STA incorporated on MCM-41 support are presented and discussed in this section. These results are in two sections; the first part consists of the results of calcined group, where the second includes the results of exracted SZ catalysts.

7.1.1.1. Characterization Results of Calcined SZ Group Catalysts

The calcination process is one of the two methods used to extract the surfactant from catalyst matrix. This section comprises of the results of calcined SZ catalysts.

7.1.1.1.1. XRD Results

X-Ray diffraction analyses are used to see the crystal structure of the materials. In Figure 14 and Figure 15, the XRD patterns of calcined SZ catalysts are shown.

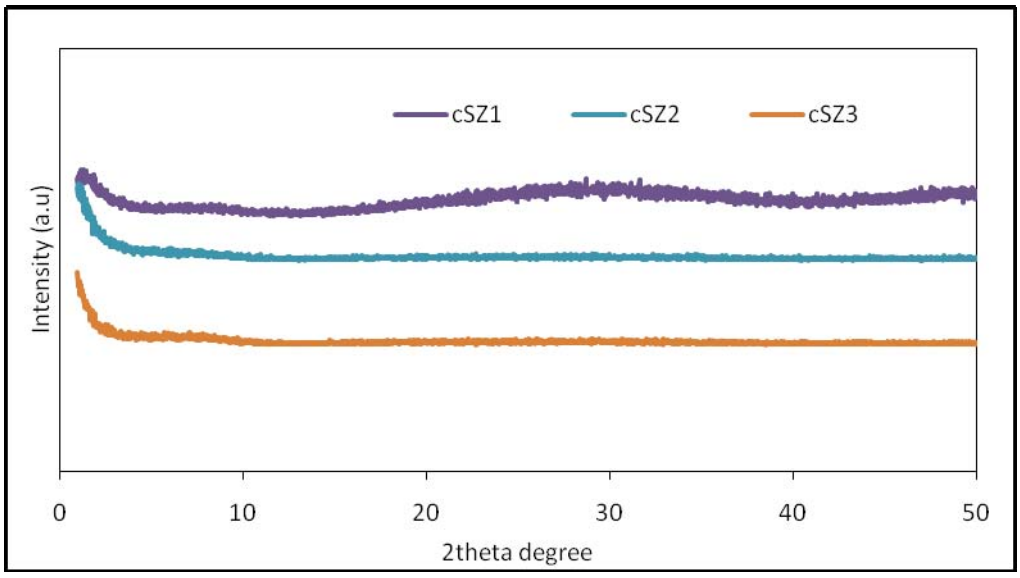

Figure 14: XRD pattern of calcined SZ group catalysts (1 to 3)

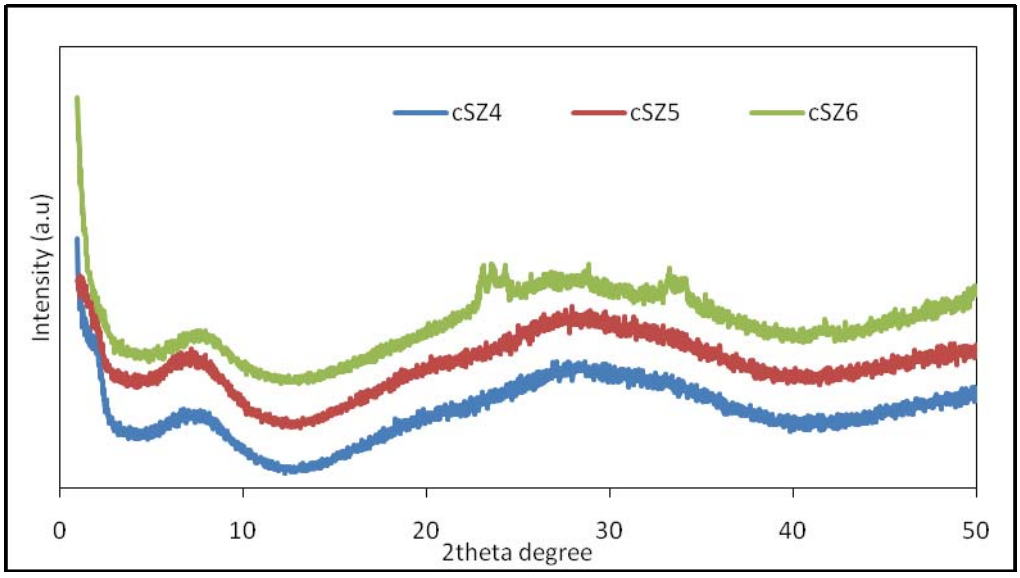

Figure 15: XRD pattern of calcined SZ group catalysts (4 to 6)

The patterns shown in Figure 14 and Figure 15, indicate well dispersed highly amorphous structures. The catalysts from SZ1 to SZ3 show no reflection peaks when compared with the ones SZ4 to SZ6. The main difference between these two groups is the Zr/Si ratio. Increasing Zr content of the catalyst matrix enables the materials to be well-dispersed in the structure. Having the least Zr/Si ratio, cSZ6 catalyst shows peaks corresponding to the STA structure ($W_{20}O_{58}$) at 2θ degrees 23.2° and 32° [82]. The broad peak between 1° and 10° indicates the presence of amorphous silica structure of the synthesized mesoporous material.

Compared with the original MCM-41 structure, as shown in Figure 7, there exists distortions in the core pattern during incorporation. The (100) peak of MCM-41 (first reflection peak) is rather dispersed at a wider range. The other reflection peaks at 2θ of 3.2°, 3.8° and 5.0° cannot be observed in these patterns.

7.1.1.1.2. EDS Results

EDS analysis, gives the bulk composition (both atomic and weight) of the sample. EDS results of the catalysts are given in Table 13. It is clear from the results that metals are successfully incorporated to the catalyst structure.

In all of the catalysts, the prepared Zr/Si ratio is less than the result indicated by EDS analysis. The integration of Zr is much better compared with the other constituents, silica and tungsten. Excluding cSZ4 and cSZ5, W/Si ratios in EDS results are also higher than the prepared ratios. During synthesis, silica is not very well incorporated into the structure and thus, lost during washing step. In addition to the incorporation issues of the materials, the difference between the experimentally prepared ratios and EDS results can be attributed to the fact that EDS characterization analyses the bulk of the catalyst to a limited deep and thus, the real metal contents may not be observed during analysis. Furthermore, there might be unhomogeneities during sampling part of characterization.

Table 13: Prepared atomic ratios in SZ catalysts compared with EDS results

Catalyst	W/Si		Zr/Si	
	Prepared	**EDS**	**Prepared**	**EDS**
cSZ1	0.40	0.42	0.24	0.31
cSZ2	0.40	0.44	0.18	0.25
cSZ3	0.40	0.43	0.12	0.19
cSZ4	0.40	0.34	0.06	0.11
cSZ5	0.30	0.24	0.06	0.11
cSZ6	0.50	0.57	0.06	0.14

7.1.1.1.3. Nitrogen Physisorption

Physisorption of nitrogen on the catalyst surface characterize it in terms of the surface area, pore size distribution, and pore volume as well as how nitrogen is adsorbed or desorbed on the surface. Table 14 summarizes these properties of the calcined samples of SZ group catalysts.

The surface areas of the catalysts are in the range of 200-350 m^2g^{-1} which are within the same order of magnitude. Increasing the Zr content of the catalyst, does not have a major effect to the physical properties. On the other hand, STA, as being a bulk molecule, when decreased in content, the catalyst becomes more porous resulting as a much higher pore volume (cSZ5, with the least W/Si=0.3). The desorption pore diameters are calculated manually as shown in Appendix C by excluding and including the last data of nitrogen isotherms.

Table 14: Physical Properties of the calcined catalysts

Catalyst	BET area (m^2/g)	BJH Ads. pore volume (cm^3/g)	BJH Des. pore volume (cm^3/g)	BJH Des. pore diameter (nm)		Micropore volume (cm^3/g)
				*	**	
cSZ1	278.2	0.32	0.33	8.2	5.1	0.14
cSZ2	263.1	0.26	0.26	9.2	4.4	0.13
cSZ3	280.4	0.31	0.31	9.7	6.4	0.14
cSZ4	246.9	0.77	0.77	57.6	12.5	0.12
cSZ5	345.4	0.93	0.93	73.2	12.8	0.17
cSZ6	211.3	0.67	0.67	32.4	12.8	0.11

*: Last data included
**: Last data excluded

The adsorption-desorption isotherms of the calcined SZ catalysts (cSZ1, cSZ2, and cSZ3) are given in Figure 16.

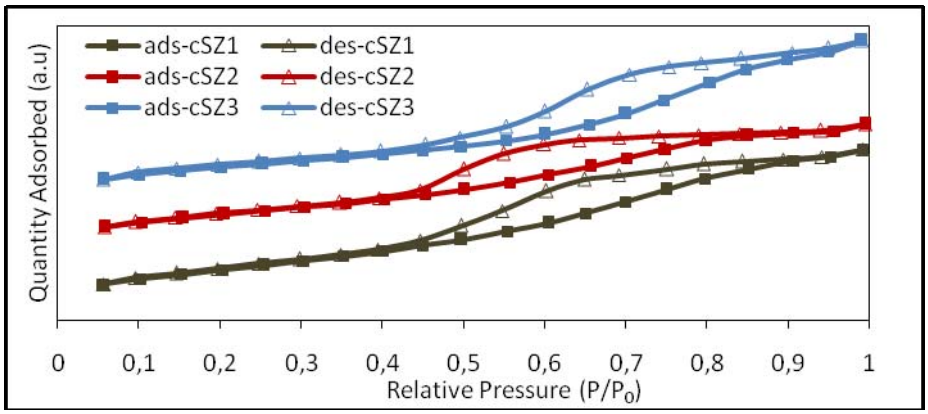

Figure 16: Nitrogen adsorption-desorption isotherm of calcined SZ catalysts (1-3)

As can be seen in Figure 16, cSZ1, cSZ2 and cSZ3 have similar behaviors towards N_2 adsorption. They show Type IV isotherm as defined in IUPAC classification with exhibiting a hysteresis loop type H2 showing the presence of interconnectivity between the pore network [75]. However, the hysteresis loops are not as sharp and parallel as it would be expected for mesoporous materials with ordered pore structures. Also, the closure of the adsorption and desorption branches is at a quite high relative pressure of nitrogen (about 0.9). These results clearly indicated that the mesoporous structure of the synthesized materials do not contain pores with long range order. Instead, a more complex and interconnected pore structure was formed.

The adsorption-desorption isotherms of the rest of calcined SZ catalysts (cSZ4, cSZ5, and cSZ6) are given in Figure 17.

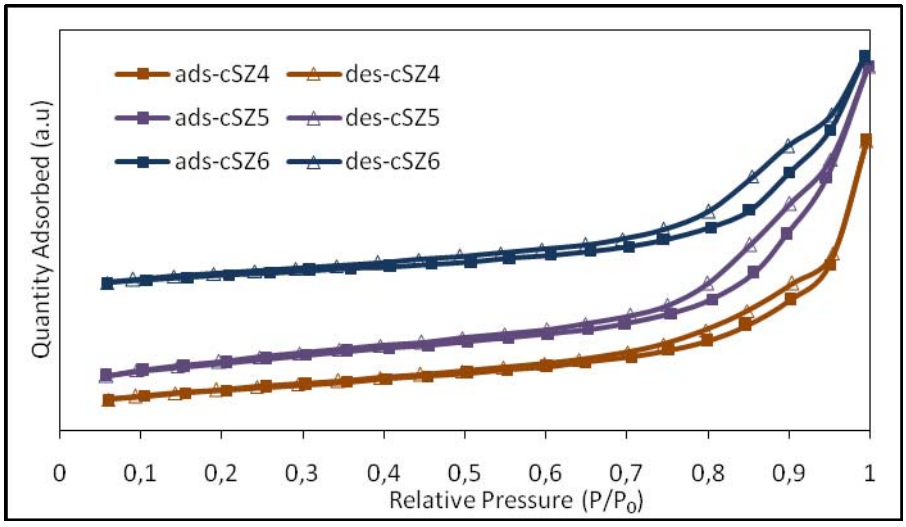

Figure 17: Nitrogen adsorption-desorption isotherm of calcined SZ catalysts (4-6)

The N_2 isotherms of the calcined catalysts of SZ1, SZ2 and SZ3 show the properties of mesoporous structure. On the contrary, in the isotherms of SZ4, SZ5

and SZ6 catalysts there exists a distortion in the mesoporous structure compared to the first group (SZ1, SZ2 and SZ3). These have a nitrogen isotherm between Type III and Type IV with a hysteresis loop of type H3. The main difference between these two groups is that, Zr/Si ratio is smaller in the latter ones. This destruction can be explained by dispersing property of Zr within the mesoporous materials. Addition of Zr to the structure improves the dispersion of materials in the catalyst. Thus the mesoporous structure cannot be observed in these catalysts.

The corresponding pore size distributions obtained with nitrogen adsorption are shown in Figure 18. The pore size diameters are consistent with the distributions. In addition depending on whether last data of BJH desorption isotherm is included or not, there exists deviations in the results. But for these materials, macroporous region should be considered due to nitrogen isotherms.

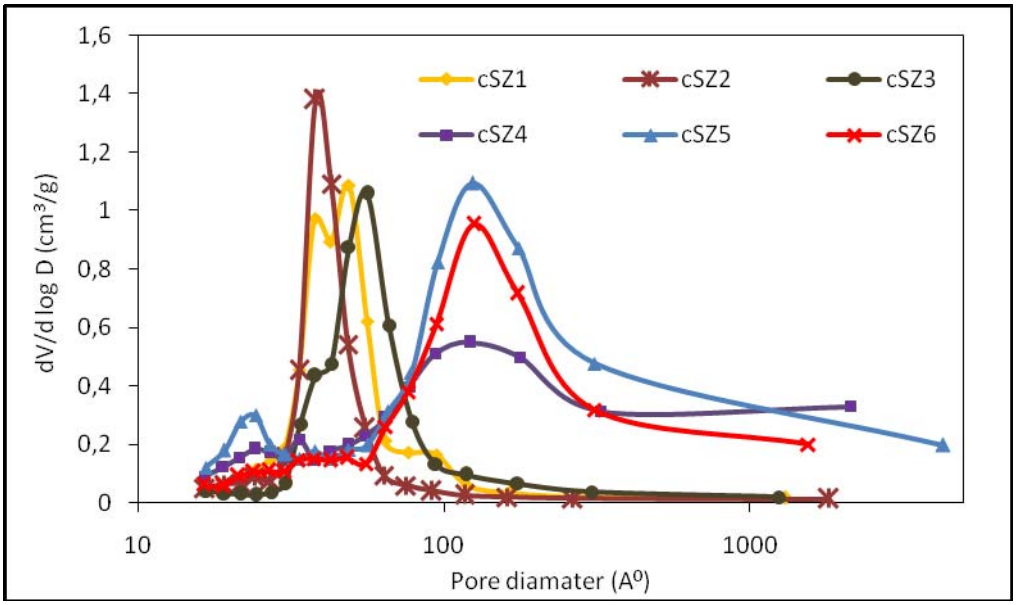

Figure 18: Pore size distributions of cSZ catalysts

As can be seen in Figure 18, the calcined samples have rather broad pore size distributions especially for cSZ4, cSZ5 and cSZ6. The pore size distributions are narrower for cSZ1-3. These results are consistent with the N_2 isotherms such that, increasing the STA content of the material, caused choking, and thus decrease in the surface area as a result of increase in pore diameter (for instance for SZ4-6 catalyst).

7.1.1.1.4. FT-IR Results

FT-IR analyses of the samples are conducted to see the bond structures. In Figure 19, the finger-print region (550-1450 cm^{-1}) of the results is given for each catalyst.

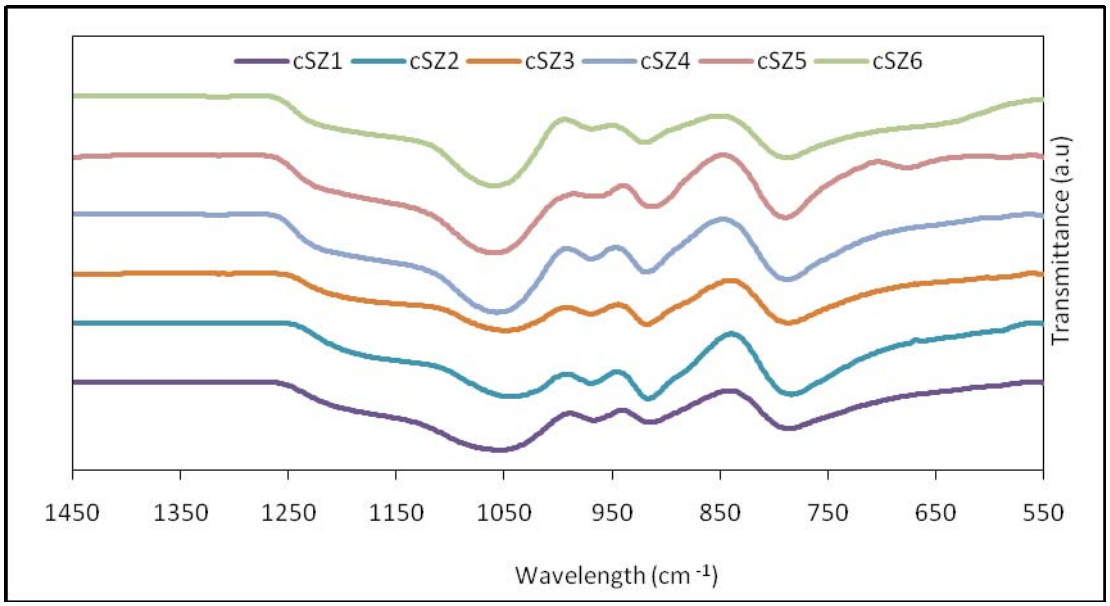

Figure 19: FT-IR results of calcined samples

As the bond characteristics are given in Table 15, when the FT-IR spectra of the synthesized materials are compared with that of untreated pure STA, there exists distortions in STA structure as well as similarities with it.

Table 15: Comparison of calcined materials with untreated STA

Bond Character (cm^{-1}) / **Catalyst**	**W-O-W**	**W=O**	**W-O_{corner}-W**	**Si-O-Si**	**Si-O**
Untreated STA [82]	796	970	876	1090	920
cSZ1	786	967	-	1055	915
cSZ2	784	969	-	1043	917
cSZ3	786	970	-	1048	918
cSZ4	788	970	-	1056	918
cSZ5	789	966	-	1059	913
cSZ6	787	969	-	1059	920

As shown in Table 15, the catalysts show, W-O-W, W=O, Si-O-Si and Si-O stretching as in pure silicatungstic acid. On the other hand, W-O_{corner}-W bond cannot be observed in the structure. The synthesized calcined materials have most characteristic bonds of pure STA, as well show some indications of distortions.

7.1.1.1.5. DRIFTS Results

Drifts analysis of the pyridine adsorbed calcined samples are shown in Figure 20. The pyridine adsorbed samples show peaks corresponding to both Brönsted and Lewis acid sites. Relatively broad peak between 1460-1480 cm^{-1} shows the presence of Lewis acid sites whereas the peak at 1540 cm^{-1} is a sign of Brönsted acid sites. The sharper peak at 1490 cm^{-1} is the combined sign of both types of acid sites [82].

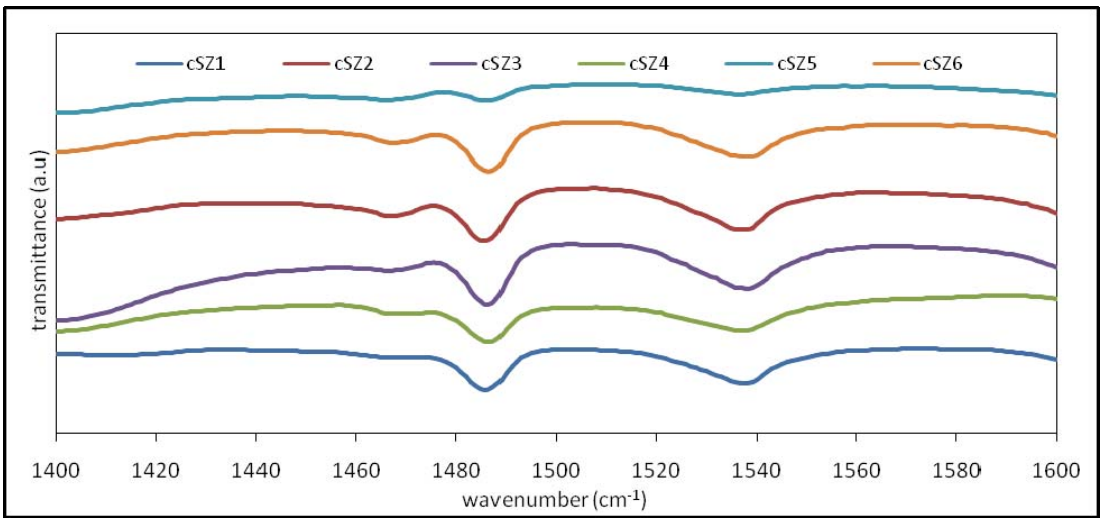

Figure 20: Drifts analysis of calcined SZ catalysts

Among the synthesized calcined catalysis, cSZ5 has the least acidity compared to the others and do not show considerable peaks of Brönsted and Lewis acid sites. The main reason is the lowest W/Si ratio of 0.3. Analyzing the effect of W/Si ratio in the synthesized materials show that, increasing the W/Si ratio (addition of higher amounts of STA), enhances the acidity of catalyst. cSZ6 has the highest STA content and the pyridine adsorbed analysis shows the highest acidity.

cSZ4 also has a rather broad peaks in DRIFTS analysis This result can be attributed to the lowest Zr/Si ratio. Addition of Zr to the structure also enhances the acidity of the material as zirconia itself is acidic [83].

7.1.1.1.6. SEM Results

SEM pictures show the morphologies of the catalysts and give and idea about the inner structures to a limited resolution. In Figure 21 and Figure 22, SEM pictures of selected calcined samples are given with a magnification of 5000 times. The rest of the SEM pictures are in Appendix D.

cSZ1 catalyst consists of particles of rather large compared to cSZ2, cSZ4 and cSZ5. This can be attributed to the higher Zr content in the material.

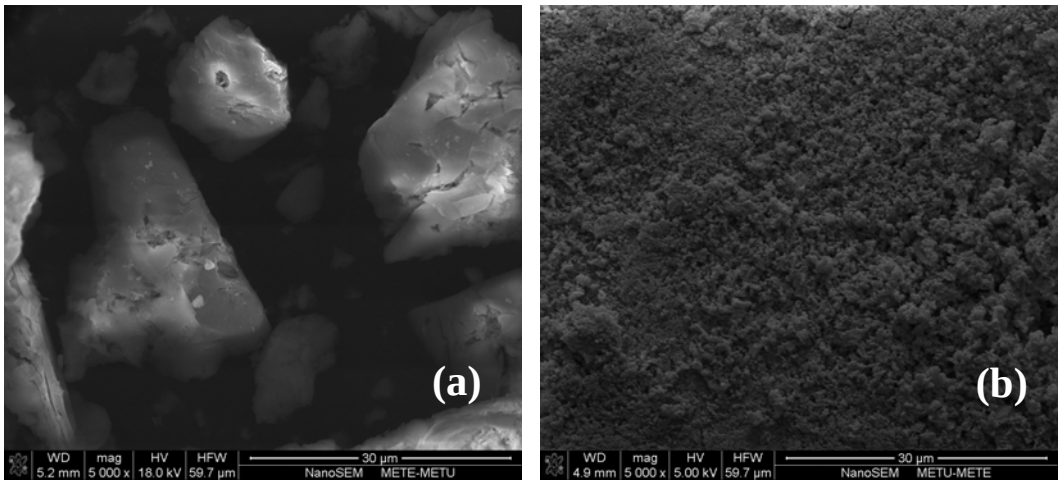

Figure 21: SEM images of (a) cSZ1 (b) cSZ2 (magnification 5000 times)

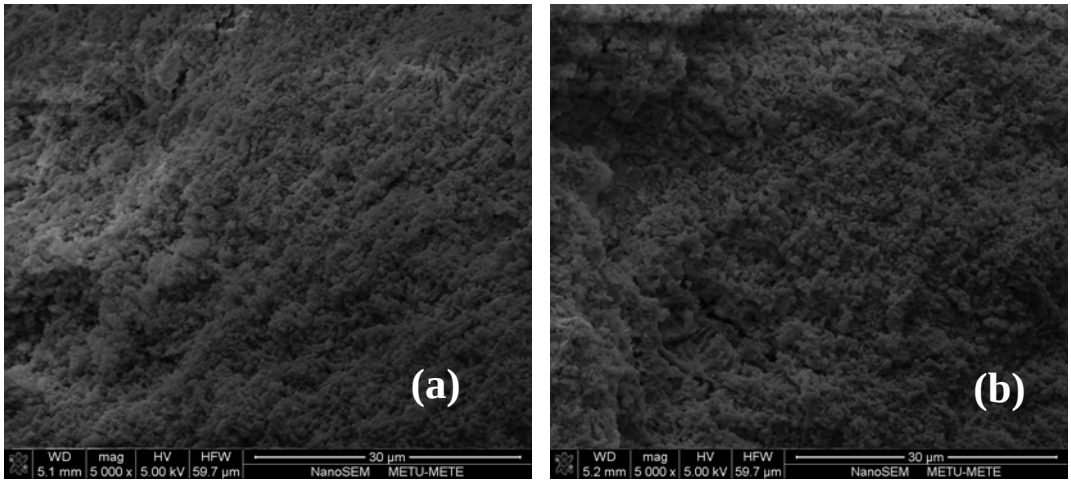

Figure 22: SEM images of (a) cSZ4 (b) cSZ5 (magnification 5000 times)

7.1.1.2. Characterization Results of Extracted SZ Group Catalysis

This section includes the analysis results of extracted samples. The samples are characterized with the same analysis methods as in calcined materials.

7.1.1.2.1. XRD Results

The following results show the XRD patterns of extracted SZ catalysts. Figure 23, Figure 24 and Figure 25 show the XRD graphs of extracted SZ group catalysts. When compared with Figure 14 and Figure 15, there exist major differences between these XRD patterns.

Extracted samples (processed at the conditions given in Table 8) have peaks in 1°-10° region corresponding to the characteristic ordered mesoporous structure. For sceSZ1, sceSZ2 and sceSZ3 (extraction pressure 450 bar, temperature 85°C, 3 hours) (Figure 23) the main peak is observed at 2θ of 4.0°, whereas the reflections are at 7.98° and 8.42°. On the other hand, the material shows characteristic peaks at 2θ of 23.2° and 32°, which corresponds to $W_{20}O_{58}$ structure [82]. At higher Zr/Si ratios, the patterns show peaks of ZrO_2 at 2θ=28° [84].

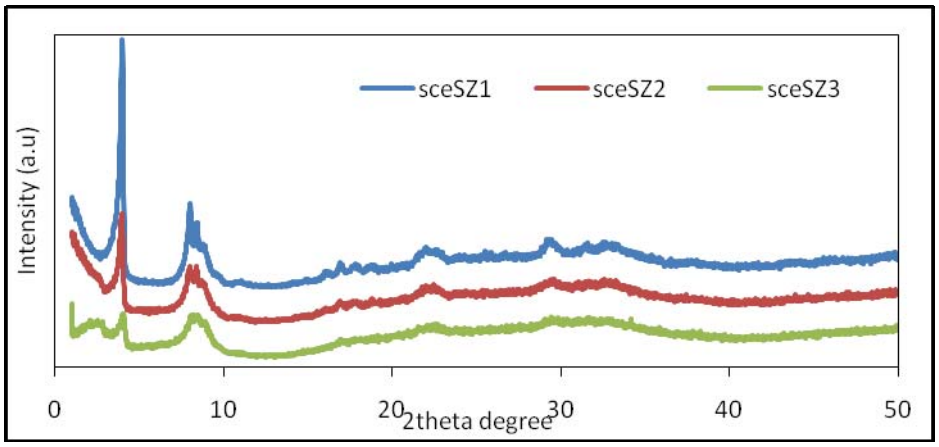

Figure 23: XRD pattern of extracted SZ group catalysts (1-3)

In Figure 24, low angle (1°-10°) region of the XRD patterns are compared with that of calcined MCM-41.

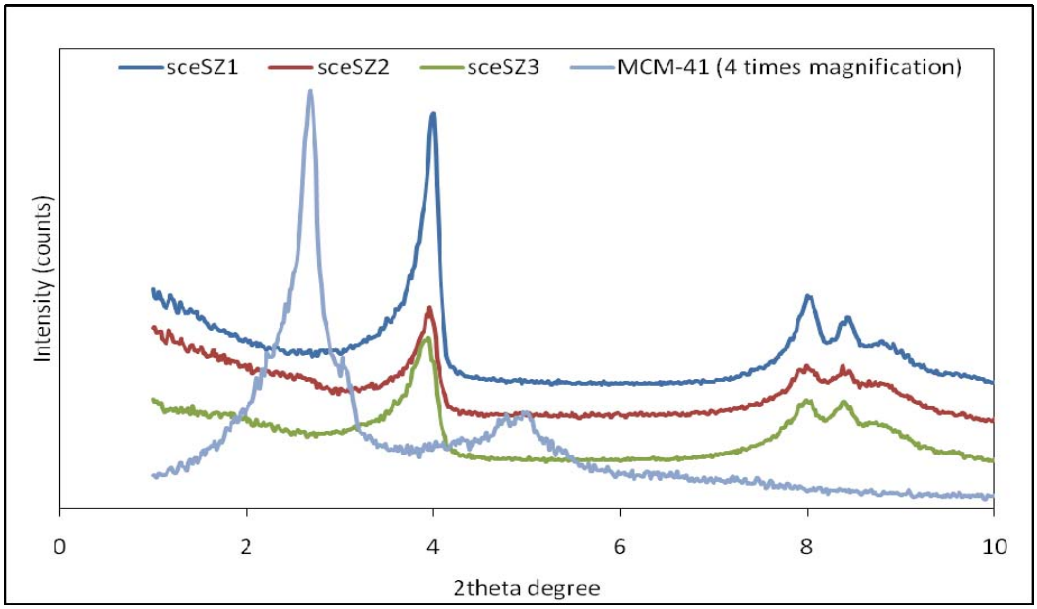

Figure 24: Low angle XRD pattern of SZ (1-3) catalysis compared with MCM-41

Compared with MCM-41, the peaks in the extracted samples are shifted to right. The main peak for MCM-41 is observed at 2.3°, whereas for sceSZ1 sample the value is 3.9°. This is valid for the reflection peaks as well. This indicates a smaller pore diameter for the extracted samples as explained by Bragg's Law. However, by nitrogen isotherms the observed A detailed examination of pore diameters is performed in the next section 7.1.1.2.2.

Carrying out the extraction at lower pressures broadens the peaks in XRD patterns. The results of catalysts sceSZ4, sceSZ5 and sceSZ6 (processed at 350 bar, 85°C for 6 hours) are shown in Figure 25. Although the XRD patterns are similar to each other, the corresponding peaks are not very well observed for these materials. The main peaks at 4.0°, 7.98° and 8.42°, are rather broad and the intensities are rather lower. The presence of $W_{20}O_{58}$ and ZrO_2 structures can be seen in broad peaks observed at 23° and 32°. However as in the main peaks of 1°-10°, the intensities are not comparable to the ones seen in sceSZ1-3.

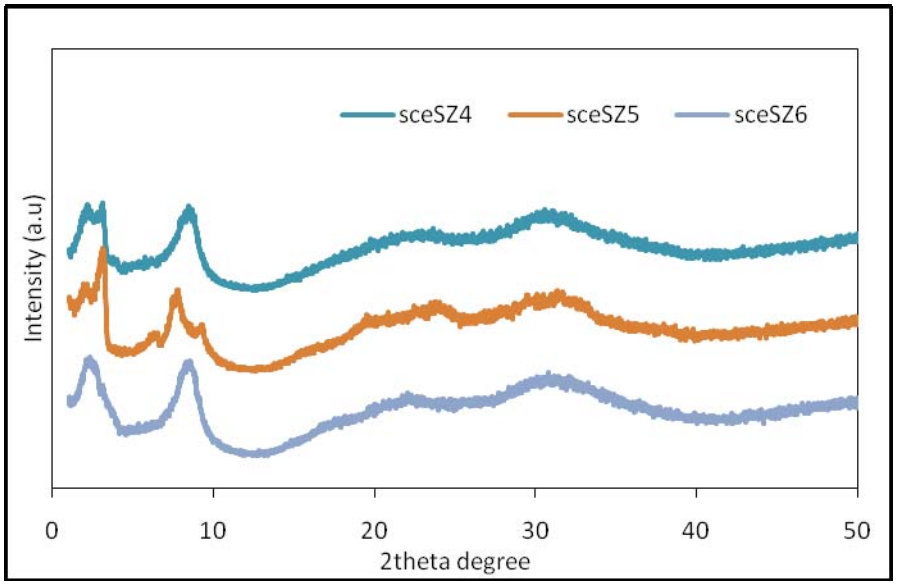

Figure 25: XRD pattern of extracted SZ group catalysts (4-6)

7.1.1.2.2. Nitrogen Physisorption

In Table 16, the results of N_2 physisorption analysis are shown. As in the calcined samples, the surface areas of the extracted catalysts are in 250-300 m^2g^{-1} for the ones extracted at 450 bars indicating a successful process. The catalysts, sceSZ1, sceSZ2 and sceSZ3 have the nearest surface area and higher pore volumes when compared with the calcined samples. This high pore volume shows effectiveness of the extraction process. On the contrary, the group of 350 bar extracted catalysts is considerably less porous. This is merely the effect of extraction pressure and carrying out the process at lower pressures decreased the solvating capability of CO_2 [83]. Although the extraction process is carried out for 6 hours on sceSZ4-5 catalysts, it can be concluded that, the effect of pressure is more dominant than the extraction period in the ranges in consideration.

Table 16: Physical Properties of the extracted catalysts

Catalyst	BET area (m^2/g)	BJH Ads. pore volume (cm^3/g)	BJH Des. pore volume (cm^3/g)	BJH Des. pore diameter (nm)		Micropore volume (cm^3/g)
				*	**	
sceSZ1	240.9	0.51	0.51	14.2	6.3	0.12
sceSZ2	207.5	0.38	0.38	11.9	4.8	0.10
sceSZ3	242.9	0.56	0.56	8.8	6.9	0.12
sceSZ4	167.8	0.61	0.6	37.7	12.1	0.08
sceSZ5	120.1	0.71	0.71	30.1	15.2	0.06

sceSZ6	123.8	1.39	1.38	802	11.4	0.06
MCM41	1250	1.28	1.29	5.2	3.0	0.6

*: Last data included
**: Last data excluded

Comparing the textural properties of extracted samples with those of calcined MCM-41 and coupling these results with the XRD patterns shown in Figure 24, indicate that the supercritically extracted samples have a larger pore diameter. Although the XRD patterns of extracted samples are shifted to right, indicating a smaller diameter, the results reveal that, there exists larger pore materials with thinner wall thickness.

The nitrogen adsorption and desorption curves of the extracted samples are given in Figure 26 and Figure 27.

The extracted catalysts also show similar behaviors as with the calcined ones. Type IV and Type IV and Type III isotherms are prevailing properties for SZ1-3 and SZ4-6 catalysts, respectively.

As shown in Figure 26, for sceSZ1 catalyst, pore filling occurs at relatively high P/Po ratios (at nearly 0.62) when compared with sceSZ2 (of which the corresponding value is nearly 0.46). This result is consistent with higher pore diameter of sceSZ1.

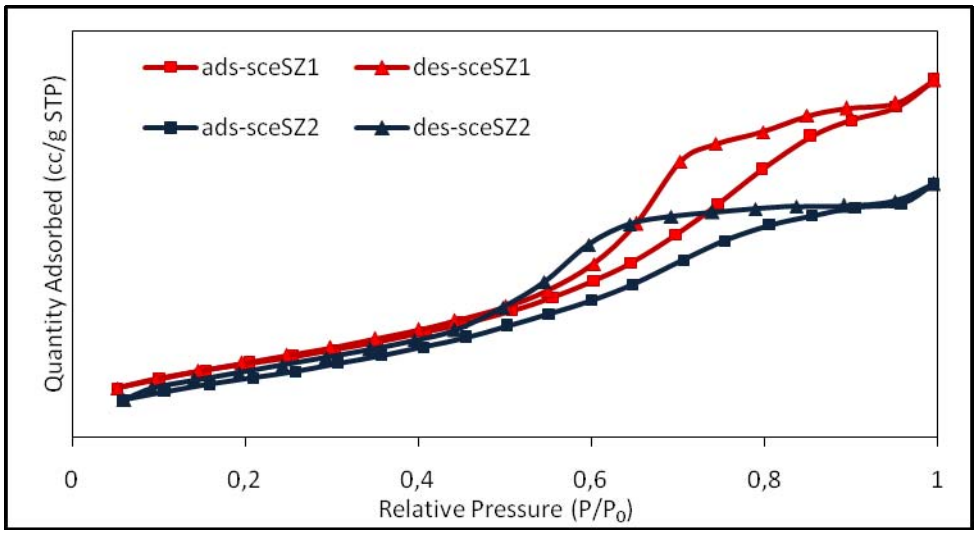

Figure 26: Nitrogen adsorption-desorption isotherm of extracted SZ catalysts (1-2)

The adsorption and desorption pore volume of sceSZ1 is higher than of sceSZ2 as shown in Table 16. This result can be seen in Figure 26 as well; the quantity adsorbed and desorbed for sceSZ1 catalyst much compared to sceSZ2.

Figure 27, shows nitrogen isotherms of sceSZ4 and sceSZ5 catalysts.

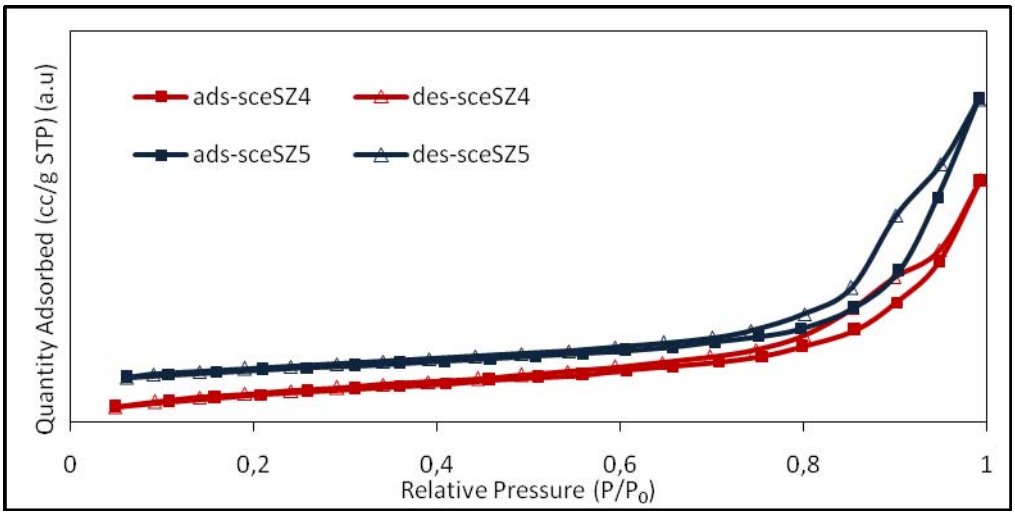

Figure 27: Nitrogen adsorption-desorption isotherm of extracted SZ catalysts (4-5)

The resulting isotherms are different from the ones obtained in sceSZ1-3 catalysts. These ones have isotherms between Type III and Type IV. The effect of carrying out the pressure at lower pressures (350 bar) can also be seen in these isotherms. The distortion in mesoporous structure is obvious from the isotherms. In addition, pore size distributions of the extracted samples are shown in Figure 28.

The distortions in the mesoporous structure are present in low Zr/Si ratios. The extracted samples have a pore size distribution as shown in Figure 28. The ones extracted at lower pressure (SZ4-6 at 350bar), has a larger pore diameter indicating a lower surface area. This result is also a consequence of increased STA content for those catalysts.

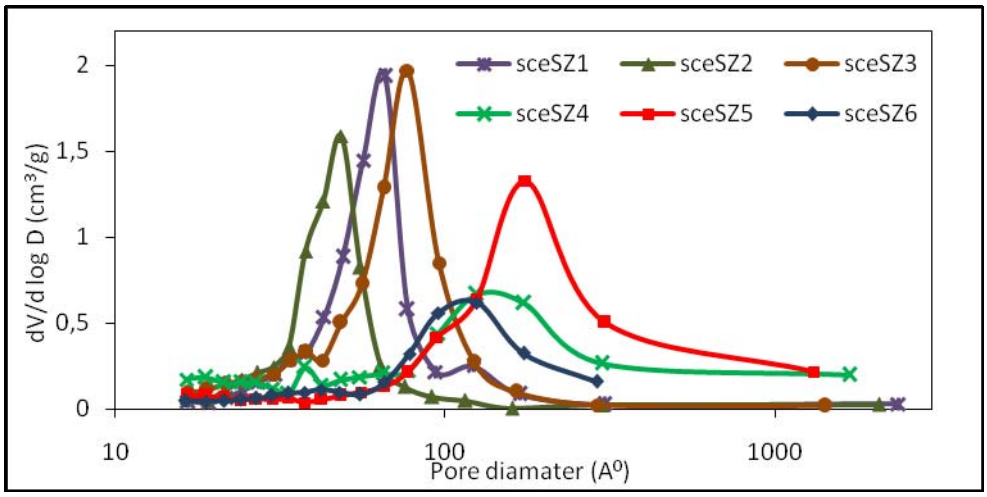

Figure 28: Pore size distributions of sceSZ catalysts

sceSZ4-6 samples have pore size distributions in a wider and larger pore diameters. These results are consistent with the ones tabulated in Table 16. Furthermore, the microporous behavior indicated in nitrogen isotherms of these samples (Figure 27) are also reflected to the calculated pore size distributions in Appendix C.

7.1.1.2.3. FT-IR Results

The FT-IR results of the extracted samples are given for the finger-print region in Figure 29.

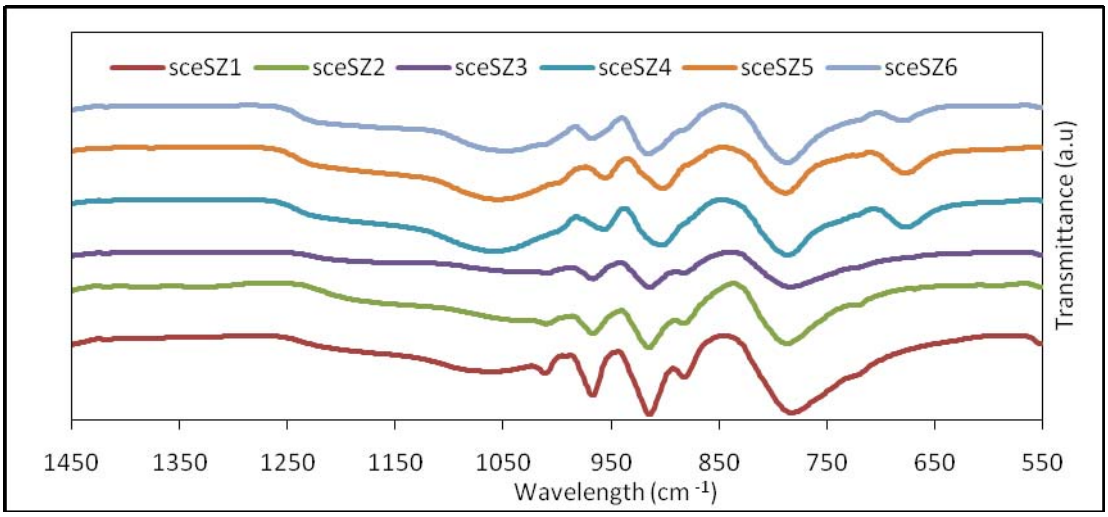

Figure 29: FT-IR results of extracted samples

Compared with the calcined sample, the Keggin structure is much more conserved in the extracted samples of sceSZ1-3. In Table 17, the bond characteristics are shown with a comparison with untreated STA and can be seen that, the specific peaks are totally conserved in extraction process for sceSZ1 sample. The firstly destroyed bond in the extracted samples of low pressure group is the W-O_{corner}-W. This bond was never observed for calcined samples. Thus, it is concluded that, high pressure (450 bar) processing for the catalysts enables the material to conserve its own structure.

7.1.1.2.4. DRIFTS Results

Drifts analysis carried out by comparing the results of pyridine adsorbed samples and the catalysis itself. The results are shown in Figure 30. As shown in this figure, the extracted samples do not show considerable peaks of acidic sites. However, peak corresponding to wave number between 1480-1500 cm^{-1} (for sceSZ1, 3, 4 and 6) is a sign of combined Brönsted and Lewis acid sites.

Table 17: Comparison of extracted materials with untreated STA

Bond Character (cm^{-1}) / Catalyst	W-O-W	W=O	$W-O_{corner}-W$	Si-O-Si	Si-O
Untreated STA [82]	796	970	876	1090	920
sceSZ1	783	967	883	1062	916
sceSZ2	787	967	883	-	915
sceSZ3	784	967	883	-	916
sceSZ4	787	957	-	1058	915
sceSZ5	788	956	-	1054	904
sceSZ6	787	967	-	1048	902

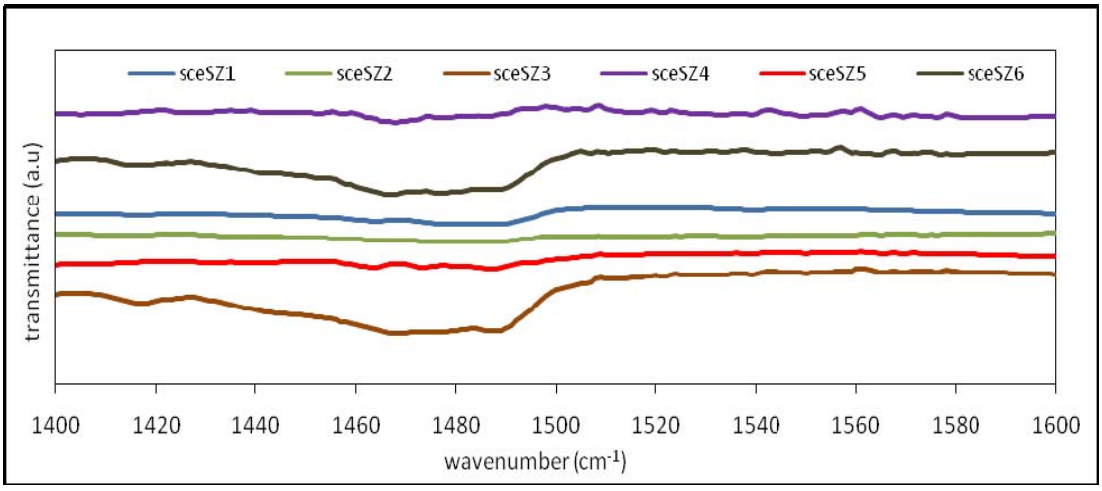

Figure 30: Drifts analysis of extracted SZ group catalys

Compared with the calcined samples, the acidities observed with these samples are rather weaker. With the extraction process, the acidic sites formed in the catalyst matrix during synthesis is distorted and not formed.

7.1.1.2.5. SEM Results

The selected SEM pictures of the extracted samples are given in Figure 31 and Figure 32. The rest of SEM pictures are given in Appendix D.

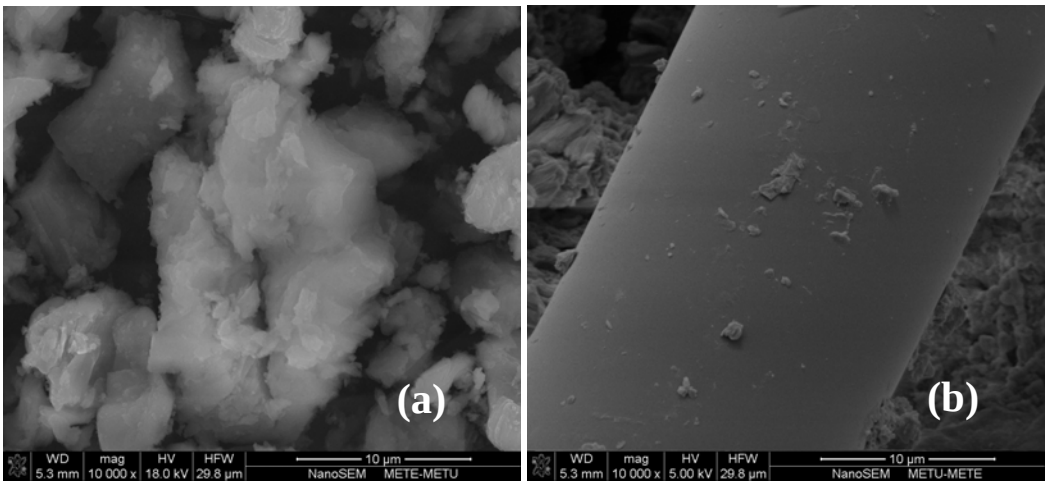

Figure 31: SEM images of (a) sceSZ1 (b) sceSZ2

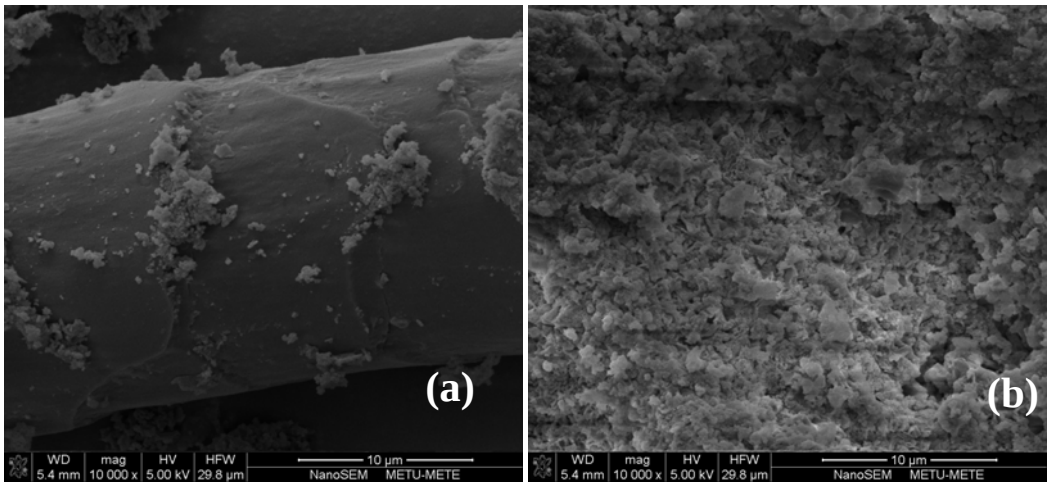

Figure 32: SEM images of (a) sceSZ4 (b) sceSZ5

All the pictures are in magnification of 10000 times. Depending on the extraction conditions applied and W/Si and Zr/Si ratios, the morphologies differ. There exist cylindrical structures in SEM pictures of sceSZ2 and sceSZ4, whereas sceSZ1 and sceSZ5 are well-dispersed.

7.1.1.3. Comparison of Extraction and Calcination Processes through Characterization Results of SZ1 and SZ2 Catalysts

In this section, the effect of extraction process is investigated by comparing the properties of selected catalysts; namely SZ1 and SZ2; with W/Si=0.4 and Zr/Si=0.24 and 0.18 accordingly. In comparison the results of characterizations of X-Ray Diffraction, N_2 Physisorption, EDS, FT-IR and SEM tests are used. The selected ones are compared with characterizations of untreated STA.

7.1.1.3.1. XRD Results

The comparison of XRD results are made for SZ catalysts as well as for untreated STA [24] sample in Figure 33.

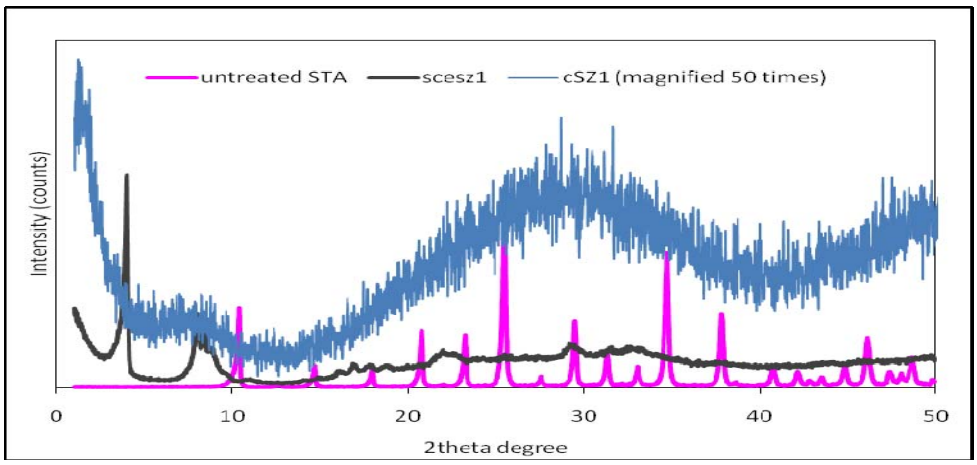

Figure 33: XRD pattern of SZ1 catalysts compared with untreated STA

The results show both similarities and differences. The distortions in crystal STA structure can be seen in XRD patterns compared with the calcined and extracted SZ1 sample. The reason of the distortions arises from the treatments that the sample has. When the sceSZ1 and cSZ1 are compared, it is seen that the latter one has a well-dispersed amorphous structure. On the contrary, sceSZ1 shows the mesoporous range peaks within 2θ ranges of 1°-10°. In addition it shows also characteristic peaks of STA, but not the 100 peak. Therefore it is concluded that, the extraction process preserved STA structure to some extent, and still causes some distortion. However, for the calcined sample, the distortions are more clear with no peaks of pure STA.

7.1.1.3.2. EDS Results

The EDS results of SZ2 catalysts are compared to see the differences of the catalytic properties after surfactant removal process. Table 18, shows the EDS characterization results of SZ2 catalysts; sceSZ2 and cSZ2.

The below EDS results indicate that both the extraction process and calcinations process are successful in terms of incorporation of materials into the MCM-41 structure.

Table 18: Comparison of EDS results of extracted and calcined samples of SZ2

Catalyst	W/Si		Zr/Si	
	Prepared	**EDS**	**Prepared**	**EDS**
cSZ2	0.40	0.44	0.18	0.25
sceSZ2	0.40	0.39	0.18	0.27

7.1.1.3.3. Nitrogen Physisorption

Figure 34 ((a) and (b)) and Table 19 indicate the differences between the properties of extracted and calcined sample of SZ1 catalyst through nitrogen physisorption.

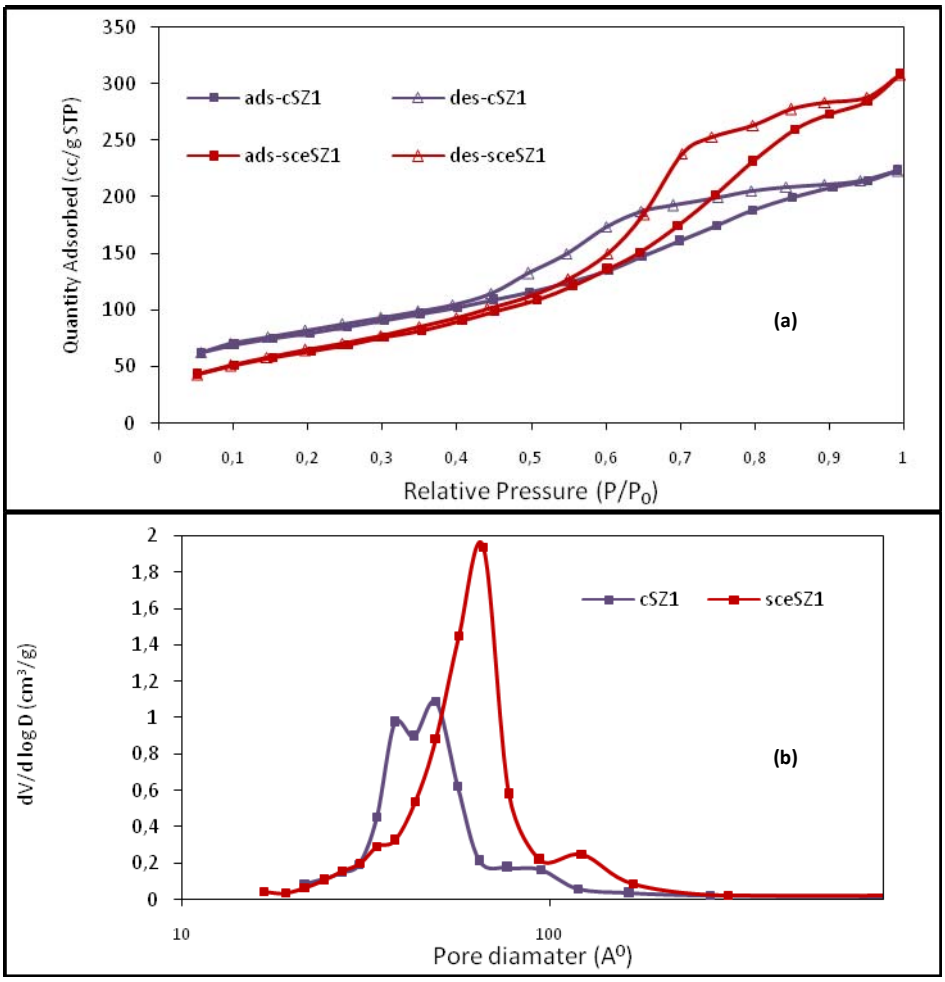

Figure 34: Comparison N_2 physisorption results of SZ1 catalysts; (a) N_2 isotherms (b) Pore size distribution

As can be seen in Figure 34 (a), pore filling occurs at a higher pressure in the extracted sample. For sceSZ1, at P/Po of 0.6, and for cSZ1 at P/Po of 0.45, pore filling starts indicating a difference in the pore diameters. This higher P/Po value results as a higher pore diameter which is also obvious from pore size distribution plots (Figure 34 (b)) and BJH pore diameter as shown in Table 19.

The extraction process caused larger particled materials to be formed. Adsorbing a higher volume of nitrogen, sceSZ1 is more porous and has the higher pore volume. On the other hand, the materials have a comparable surface area.

Table 19: Comparison of physical properties of SZ1 catalysts

Catalyst	**cSZ1**	**sceSZ1**
BET Area (m^2/g)	278.2	240.9
BJH Ads. pore volume (cm^3/g)	0.32	0.51
BJH Ads. pore diameter (nm)	5.1	6.3

7.1.1.3.4. FT-IR Results

The FT-IR results of SZ1 catalysts are given in Figure 35 as compared to that of untreated STA sample [24]. The fingerprint region is also included at the bottom left of the Figure 35. Both of the samples show similarities with STA as mentioned before and also as can be seen in that region. Here it should be emphasized that, the extracted sample has peaks at wavelengths between 2800 cm^{-1}-3000 cm^{-1} and also at 1467 cm^{-1} corresponding to C-H stretchings within the bond structure. These C-H

bonds come from the surfactant CTMABr which has the similar bond characteristics. Showing properties of the surfactant, it is concluded that, the extracted sample has still some surfactant in the structure. Therefore, it is important to enhance the extraction process in terms of removing all of the surfactant from it. These can be done by determination of optimum extraction conditions for the corresponding samples; namely by changing pressure, temperature or extraction period.

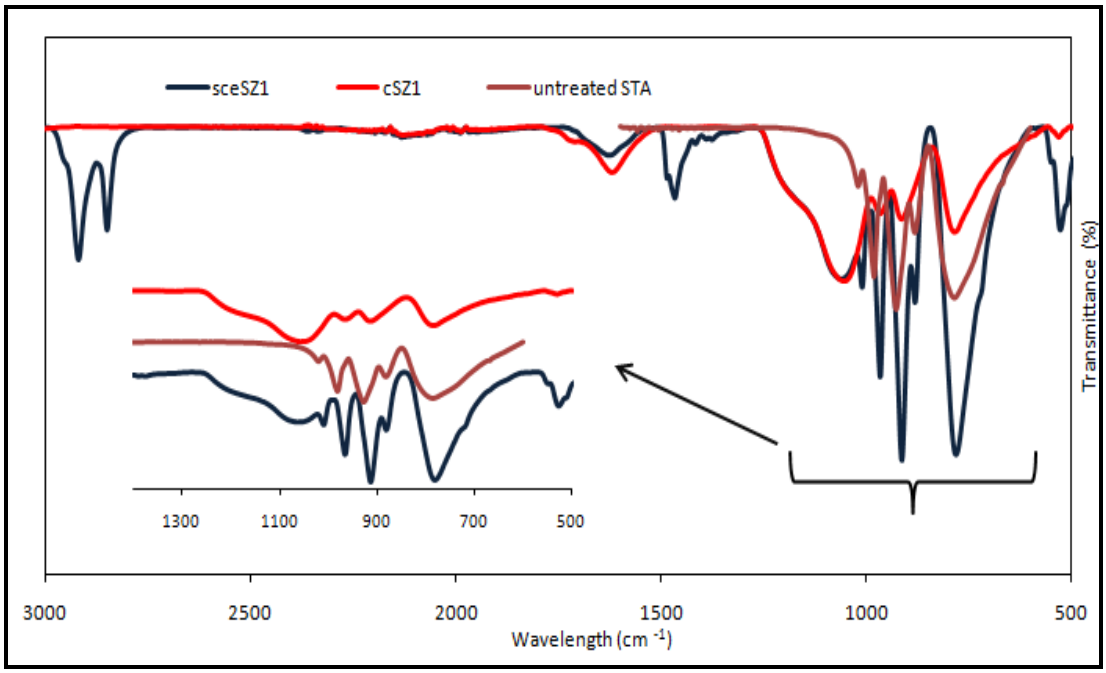

Figure 35: Comparison of FT-IR characteristics of SZ1 catalysis

7.1.1.3.5. SEM Results

SEM pictures of SZ2 catalysts are given in Figure 36. The morphological differences are obvious in the images. There are cylindrical structures within sceSZ2, on the other hand even at higher magnifications; the calcined sample is well-distributed through catalyst matrix.

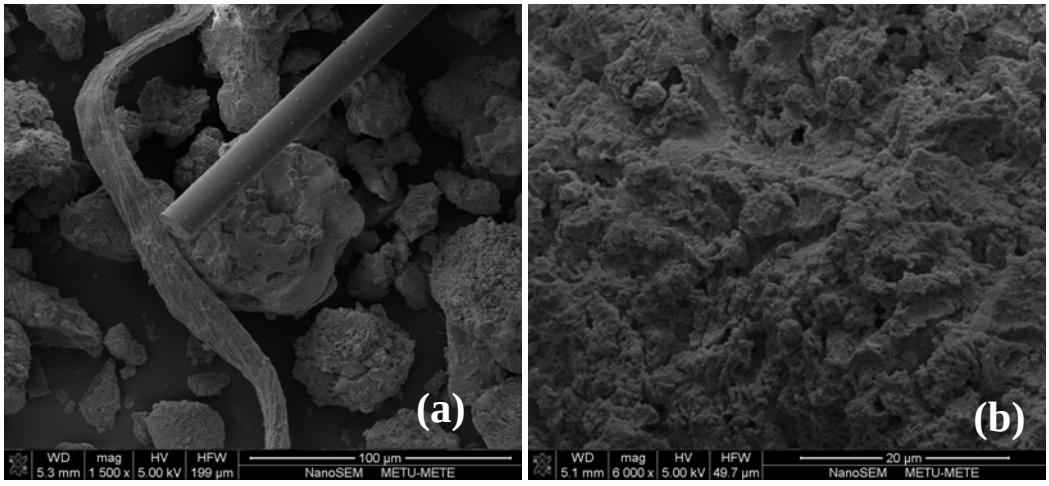

Figure 36: SEM images of SZ2 catalysts (a) sceSZ2 (magnified 1500 times), (b) cSZ2 (magnified 6000 times)

7.1.1.3.6. TGA Results

Thermogravimetric analysis of the cSZ1 and sceSZ2 are given in Figure 37 to get an idea about the efficiencies of the calcined and extraction processes respectively. The tests are carried out from room temperature up to 400°C and 600°C for the extracted and calcined samples respectively with air and the removed amount of mass is measured. Both show a decrease at 100°C corresponding to removal of water. The following Table 20 summarizes the weight losses for each of the sample.

As can be seen in Figure 37and Table 20, the weight losses corresponding to each material have differences. In Appendix A1, the original of TGA curves are included with other curves for cSZ1 and sceSZ1. TGA curve of extracted sample (sceSZ2) has a sharp decrease at temperatures of 380°C, whereas for the calcined sample, the curve has a smooth behavior at the considered temperature range. Therefore, it should be concluded that, there still remains extra surfactant that should be removed within the structure of extracted sample. It is worth saying that to overcome that situation, it is important to optimize the conditions related to extraction process.

Table 20: Weight losses (%) of sceSZ2 and cSZ1 in TGA

Temperature	Weight Loss (%)	
Catalysis	**100°C**	**380°C**
sceSZ2	3.02	16.5
cSZ1	1.07	-

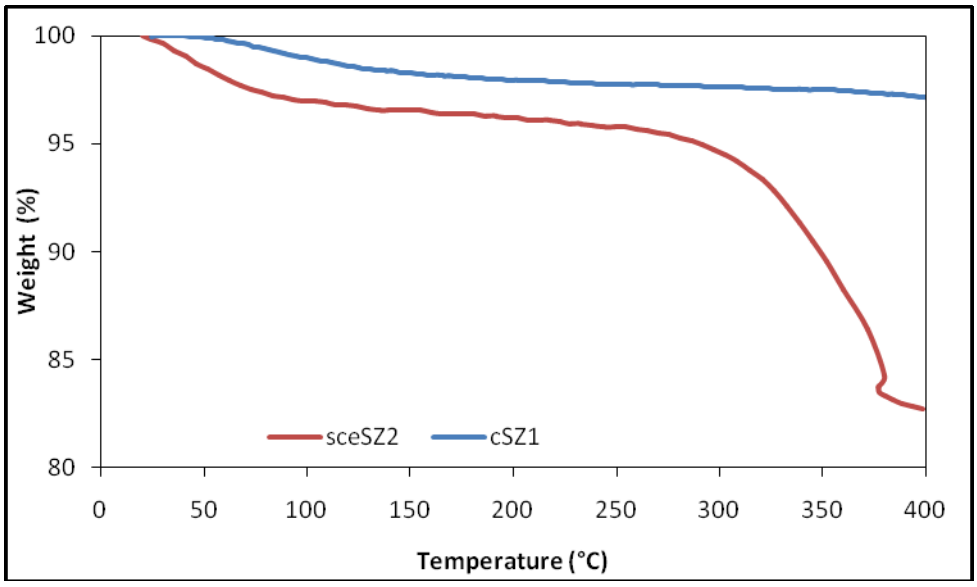

Figure 37: TGA curves of selected catalysis

7.1.1.4. Effect of Extraction Parameters on Catalyst Properties

Extraction process mainly depends on temperature, pressure, extraction period and flow rates of extracting mediums. Within the scope of this study, to see

the effects of pressure and period, SZ4 and SZ3 catalysts are treated at various conditions given in Table 8 and characterized with the methods mentioned above. For temperature and flows, the conditions are constrained as explained in Kawi et al [73]. However it should be noted that, within supercritical region, further increasing the temperature, decreases the efficiency of extraction process due to decrease in fluid density and thus the solvating power of the agent. In addition, the contact time between the surfactant and agent decreases with low residence time with higher flow rates at elevated temperatures [71].

7.1.1.4.1. Extraction Period

Carrying out the extraction for different periods resulted major differences in catalyst properties. While the ones extracted at 450 bar for 3 hours (SZ1, SZ2 and SZ3) has comparable properties such as surface area and pore volume which is actually higher, than the calcined samples; the ones extracted at 350 bar for 6 hours (SZ4, SZ5, SZ6), have much lower surface areas and lower pore volumes which mainly indicates a need for optimization of extraction conditions for these catalysts. It is shown from the results that, increasing period of extraction has less effect than decreasing the operating pressure which can be explained by a result of equilibrium behavior of methanol and CO_2 at 350 bar. Keeping the process at a longer period, does not affect the extraction efficiency since the dissolving capability of methanol and CO_2 mixture has already been reached equilibrium in supercritical region.

As summarized in Table 21, 3sceSZ4, has the lowest pore volume which is an indication of a need to developed process conditions. At 3 hours operation CO_2 and methanol does not reach equilibrium with the surfactant and the extraction process still goes on.

Further increasing the extraction period may increase the porosity and surface area of the material.

Table 21: Effect of extraction period on catalysts' physical properties

Cat.	BET area (m^2/g)	BJH Ads. pore volume (cm^3/g)	BJH Des. pore volume (cm^3/g)	BJH Des. pore diameter (nm)	Micropore volume (cm^3/g)
sceSZ4*	167.8	0.61	0.6	12.1	0.08
3sceSZ4*	117.8	0.11	0.11	11.5	-
cSZ4	246.9	0.77	0.77	12.5	0.12

*Extraction pressure: 350 bar

Figure 38, shows pore size distributions of these catalysis. Three hours extracted sample has considerable amount of pores in micropore region which is an indication of low surface area and pore volume. The pore size distribution is consistent with the calculated pore diameters in Appendix C.

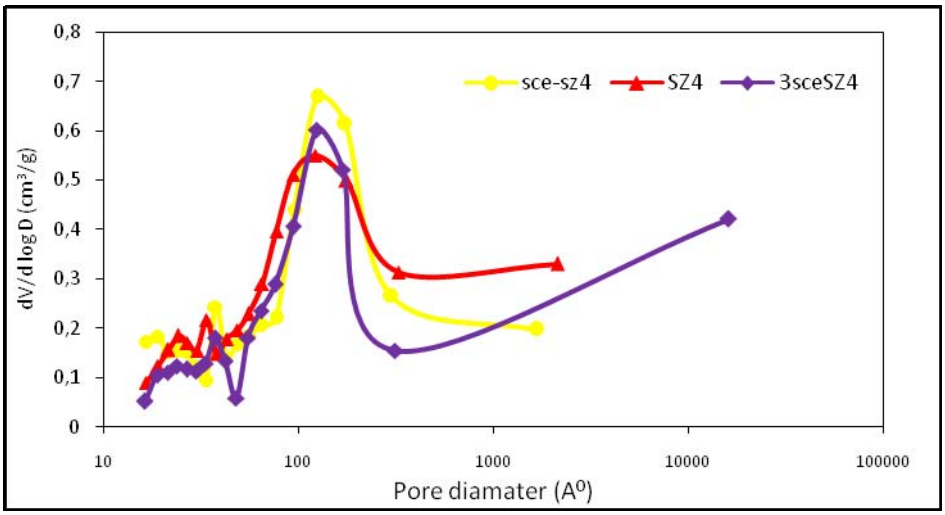

Figure 38: Pore size distributions of SZ3 catalysis

7.1.1.4.2. Extraction Pressure

Pressure is a critical process variable for supercritical extractions. At high pressures, density of CO_2 and liquid methanol ratio increase which also improve dissolution of surfactant in the extraction mixture and solvating ability of CO_2. In extraction processes of organic surfactant material, liquid methanol has an important role in dissolving the surfactant and removing it from the catalyst matrix. This condition results as an increase in extraction efficiency. On the other hand, high pressure causes packing of the catalyst which also blocks contact between materials [86]. These effects are seen at pressures of 300 bar, 450 bar and 600 bar which are also supported by characterization results. Increasing the extraction pressure has a positive effect on the physical properties of the catalysts with an optimum value of pressure. When compared with the calcined sample; at 85°C, SZ3 catalyst has the highest pore volume and nearest surface area at 450 bars. Carrying out the extraction at 600 bar, does not have a major role which is a result of occurrence of blocking due to packing of the material at high pressures. This prevents contact of both methanol and CO_2 with the catalyst matrix [86]. Figure 39 shows that extraction process has optimum operating conditions by which the surfactant removal can be achieved with the most effectiveness.

Therefore to remove the surfactant with the highest effiency, it is important to decide on the operating conditions while considering the nature of the material also. The results given in Figure 39 can also be explained by N_2 isotherms of the catalysts. Within the conditions scanned, carrying out the process at 450 bar, yielded the highest surface area and pore volume of the catalyst sceSZ3 with the highest extraction efficiency.

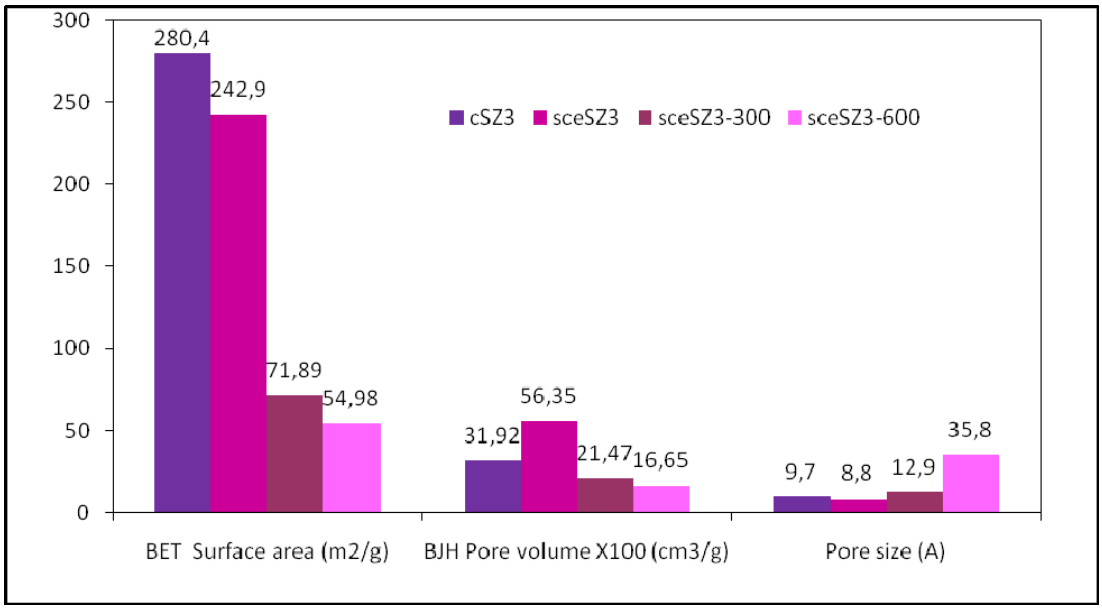

Figure 39: The effect of extraction pressure on catalyst SZ3 physical properties

The efficiency of the processes can be compared with the resultant surface area, in other words with the removed surfactant from the structure. Thus the efficiencies (E) can be ordered as $E_{calcination} > E_{extraction\text{-}450\ bar} > E_{extraction\text{-}300\ bar} > E_{extraction\text{-}600\ bar}$.

Further comparison can be made with the nitrogen isotherms as shown in Figure 40.

All the catalysts have Type IV isotherm and H2 hysteresis loop. The arrangement in terms of pore volumes can be explained by higher adsorbed volumes in adsorption isotherms. The arrangement in comparing the values of pore volumes are sceSZ3 > cSZ3 > sceSZ3-300 > sceSZ3-600. The final reached values of the isotherms indicates the same arrangement also.

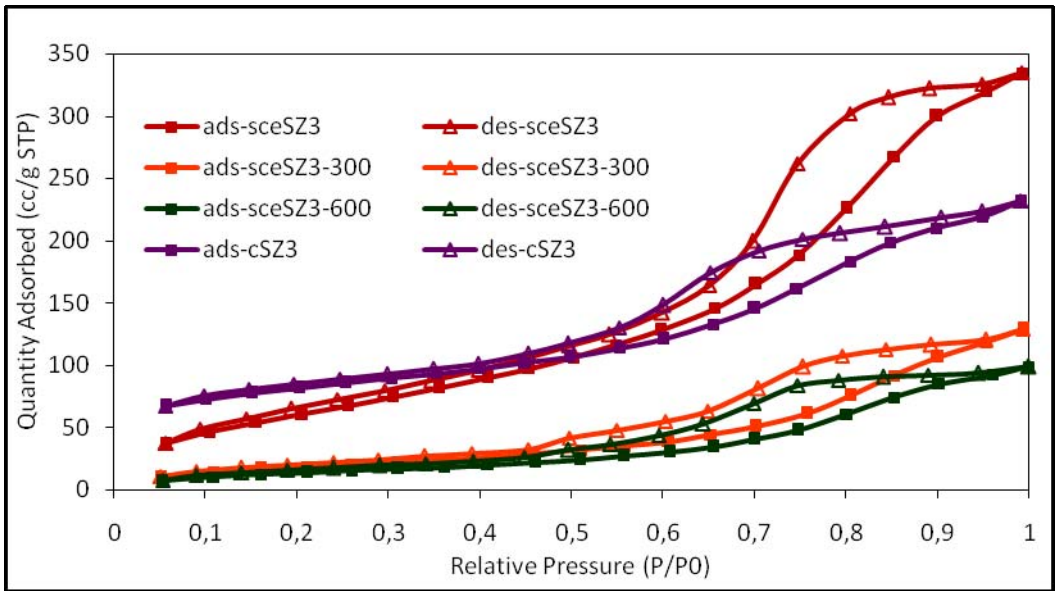

Figure 40: The effect of extraction pressure on catalyst SZ3 N_2 ads-des isotherms

In Figure 41, the XRD patterns of the SZ3 catalysts are shown. As can be seen in Figure 41, the formation of mesoporous structure can also be seen in XRD patterns of the SZ3 catalysis.

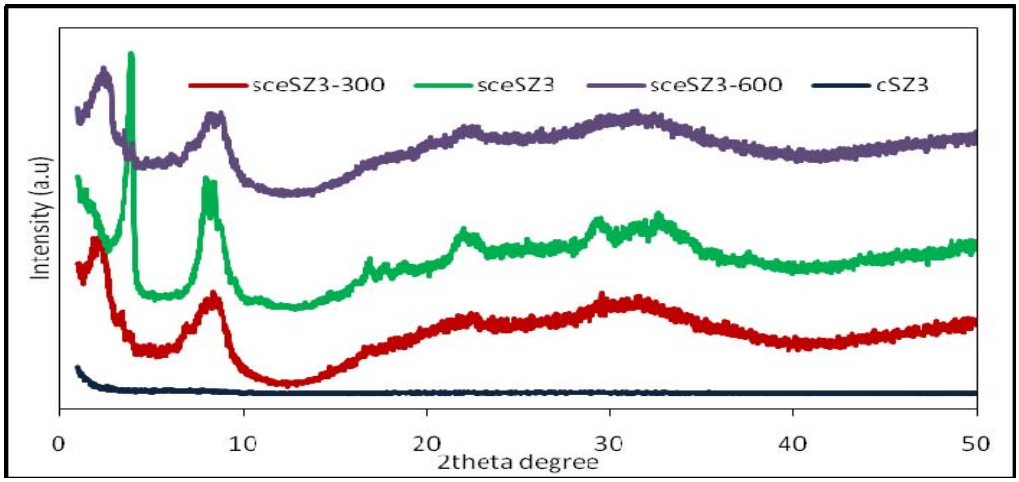

Figure 41: XRD patterns of SZ3 catalysis

The differences between the extracted and calcined samples are mentioned before. These XRD patterns also show the characteristic changes during extraction process at various pressures. The extracted sample has a well-distributed structure and does not show peaks of any structure as crystal. As explained in Section 7.1.1.2, extracted sceSZ3 catalyst, have characteristic peaks of $W_{20}O_{58}$ (at 2θ of 23° and 32°) [82] and ZrO_2 (28°) [83] as well as with the peaks corresponding to the mesoporous structure (at 2θ between 1-10°). However the sharpness of the peaks change with the operating conditions of extraction. For the catalyst extracted at 300 and 600 bar, the peaks corresponding to the $W_{20}O_{58}$ and ZrO_2 structures are rather broad and cannot be distinguished from each other.

To further analyze the, XRD patterns of the samples are drawn in low angle in Figure 42 and compared with calcined MCM-41. As in previous comparison made in Figure 24 for extracted samples of SZ1-3, the effect of carrying out the extraction at different pressures, is mainly shifting the peaks of virtual MCM-41 towards right. However, although it is expected the pore diameters to be smaller with XRD results, the pores of these samples are larger than that of MCM-41 (Figure 39 and Table 16). This can be attributed to differences in pore structures of the materials.

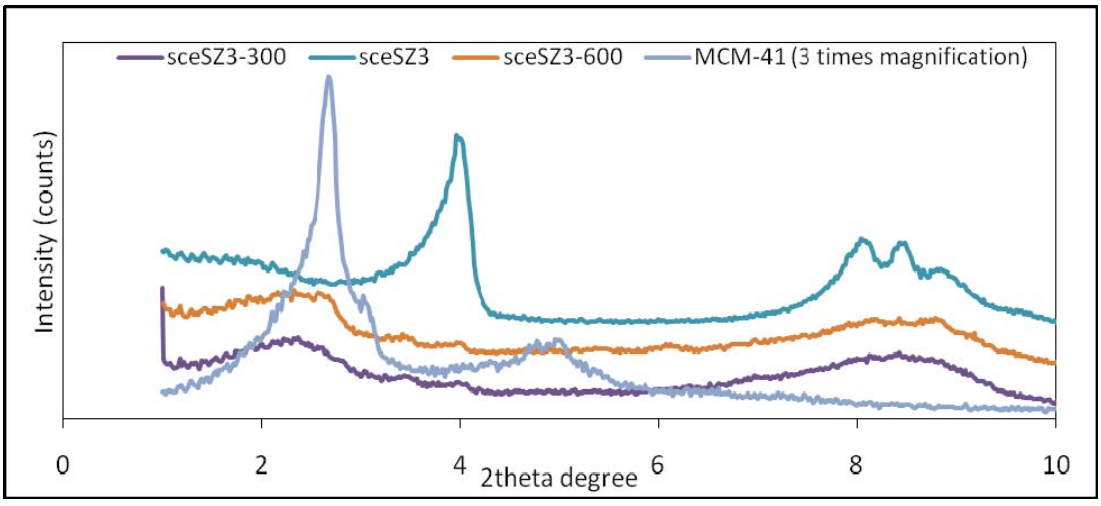

Figure 42: Low angle XRD pattern of SZ3 catalysis compared with MCM-41

In Appendix E, TGA curves of three samples are included with DTA curves. Figure 43 shows only the weight loss percent during thermal treatment.

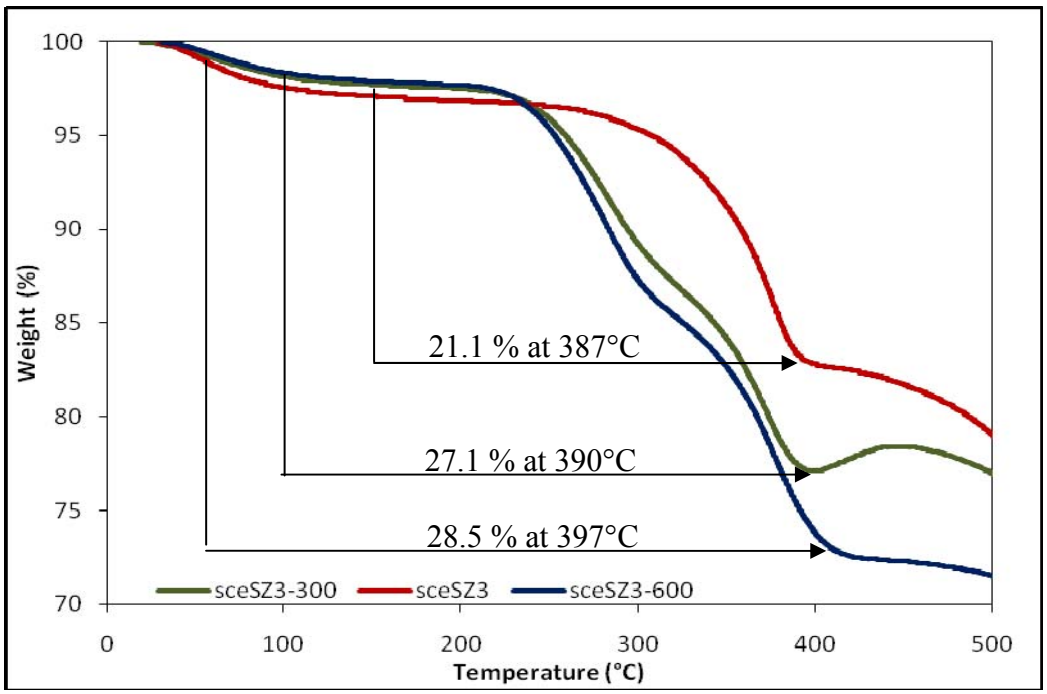

Figure 43: TGA curves of SZ3 catalysis

TGA curves of the catalysts are consistent with the nitrogen adsorption results. All three samples have the highest weight loss at nearly 390°C as shown in Figure 43 with the given values. By thermogravimetric analysis, further loss during thermal treatment is found after surfactant removal step is applied. Higher weight loss indicates the presence of extra surfactant that should be removed within the catalyst matrix. Therefore comparing the losses, during the rise of temperature, sceSZ3-600 lost the 28.5% of its original structure which is the highest value when compared with sceSZ3 and sceSZ3-300. This result can be linked with the efficiency

of the extraction process. Presence of higher amounts of surfactant in the sceSZ3-600 catalyst showed that, the efficiency of carrying out the process at 600 bar is least among others. In addition, sceSZ3-300 and sceSZ3-600 have weight losses at 299°C and 294°C respectively as different from sceSZ3 which has the only loss at 387°C as indicated in DTA curves (Appendix E). Thus it can be concluded that, for the samples other than sceSZ3, weight loss occurs at two steps indicating removal of two different components.

7.1.2. Characterization Results of STA-Ni/Silica (SN) Catalyst

Nickel/copper and STA incorporated MCM-41 catalysts are examined with comparison with the extracted samples. In each characterization, both extracted and calcined samples are included.

7.1.2.1. XRD Results

In Figure 44, the XRD patterns of SN catalysts are shown. In the figure, both extracted and calcined sample are included.

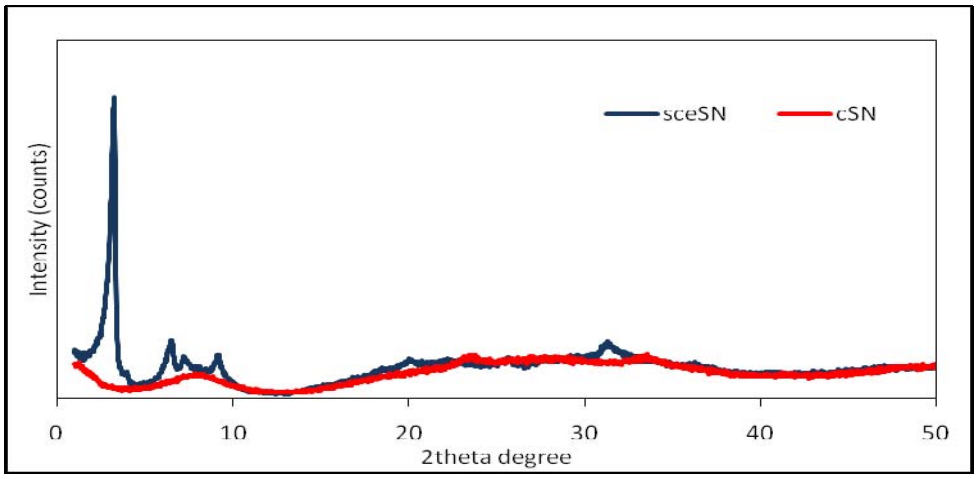

Figure 44: XRD pattern of SN catalysts

The peaks at 2θ degrees of 1°-10° (at 3.18°, 6.26°, 6.18° and 8.96°) are characteristics of extracted samples as in extracted SN. Compared with the extracted SN, calcined sample has a well-distributed amorphous structure showing no presence of crystal structure.

7.1.2.2. EDS Results

The incorporation of the metals into the catalyst matrix can be examined via EDS analysis. The calcined sample is characterized by EDS to see whether incorporation is successful. In Table 22, the preparation conditions are compared with the EDS results carried out with the final catalyst formed.

The results indicate that metal and STA incorporation to the structure is successful. However compared to the cSZ4 catalyst having the same metal/Si and W/Si ratio as cSN catalyst, both STA and the metal ratios are lower. It is concluded that, during synthesis the incorporation of both metal and tungsten is not successful with the synthesis conditions applied

Table 22: Prepared atomic ratios in SN catalysts compared with EDS results

Catalyst	W/Si		Ni/Si	
	Prepared	EDS	Prepared	EDS
cSN	0.40	0.28	0.06	0.03

7.1.2.3. Nitrogen Physisorption

In Table 23, the results of nitrogen physisorption analysis are shown.

Table 23: Physical Properties of the SN catalysts

Catalyst	**BET area (m^2/g)**	**BJH Adsorption pore volume (cm^3/g)**	**BJH Adsorption pore diameter (nm)**
cSN	76.9	0.5	88.5
sceSN	45.8	0.97	811

The surface areas of the samples are in the same order of magnitude (50 m^2g^{-1} - 100 m^2g^{-1}). The reduction in the surface area compared to the SZ group catalysts can be attributed to the presence of nickel. The mesoporous structure is not formed in these materials as observed from nitrogen isotherms (Figure 45) and pore diameters

(Table 23, Appendix C). Although the Ni/Si ratio is equal to the least (0.06) among the values of SZ catalysts, when compared with zirconium, nickel is not. Nitrogen isotherms, shown in Figure 45, are in good agreement with these results.

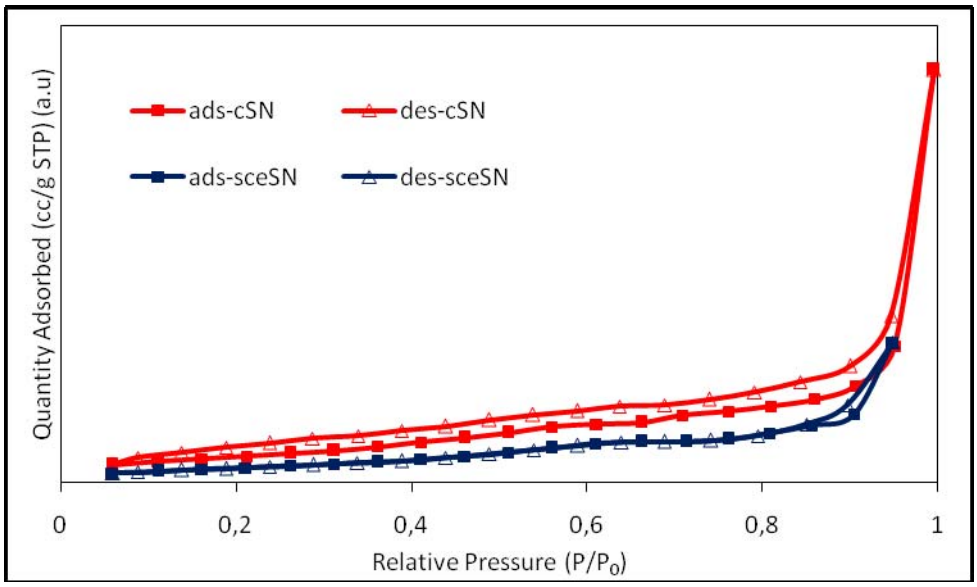

Figure 45: Nitrogen adsorption-desorption isotherm of SN catalysts

The catalysts have both isotherms between Type III and Type IV, having distortions in mesoporous structure. The hysteresis observed is H3 type.

7.1.2.4. FT-IR Results

The FT-IR results of the extracted and calcined sample of SN catalyst are given for the finger-print region in Figure 46.

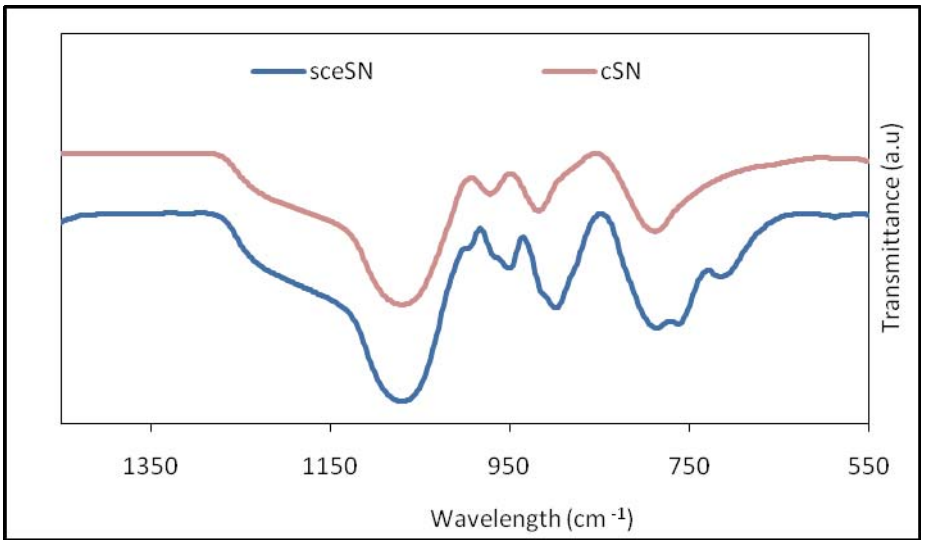

Figure 46: FT-IR results of SN samples

The SN catalysts also show characteristic peaks of STA structure. Compared to the SZ group catalysts, sceSN catalysts have one distinct peak other than other catalysts at wavelength of 716 cm^{-1} which corresponds to symmetric stretchings in the structure of NiO_2 (defined as 745 ±30 cm^{-1}) [87]. In addition to this, the peaks corresponding to asymmetrical stretchings coincide with Si-O bonds at 951 cm^{-1}.

7.1.2.5. SEM Results

The selected SEM pictures of SN samples are given in Figure 47. The differences in the resulting morphologies are clear in the pictures (with magnification of 20000 times). Both samples have spherical structures in the presented pictures. However the diameter of spheres is larger for the extracted sample indicating a larger pores which is consistent with the nitrogen physisorption results given in Table 23.

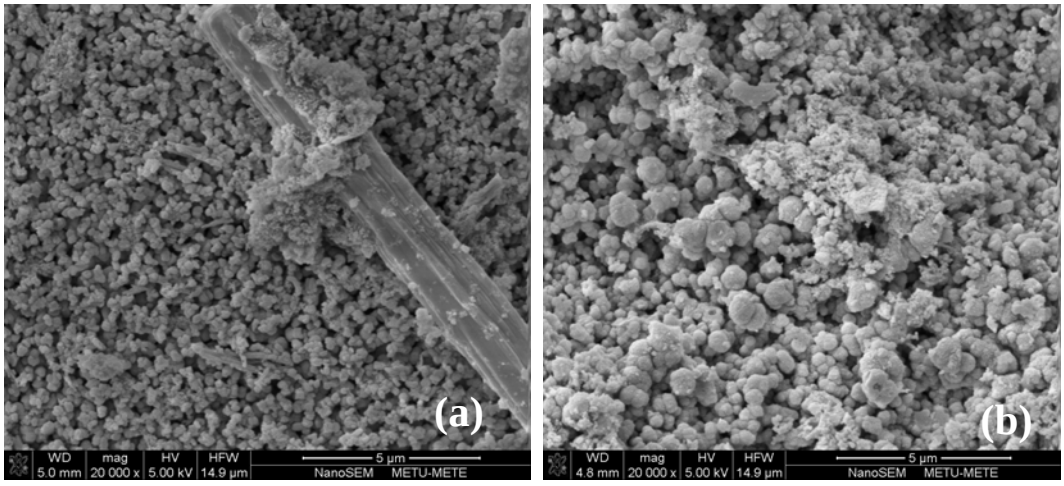

Figure 47: SEM images of SN catalysts (a) cSN (b) sceSN

7.1.3. Characterization Results of STA-Cu/Silica (SC) Catalyst

The characterizations of extracted and calcined SC samples are given in following section. XRD, Nitrogen physisorption, SEM, FT-IR and EDS methods are used to characterize the materials.

7.1.3.1. XRD Results

The XRD patterns of calcined and extracted SN samples are given in Figure 48.

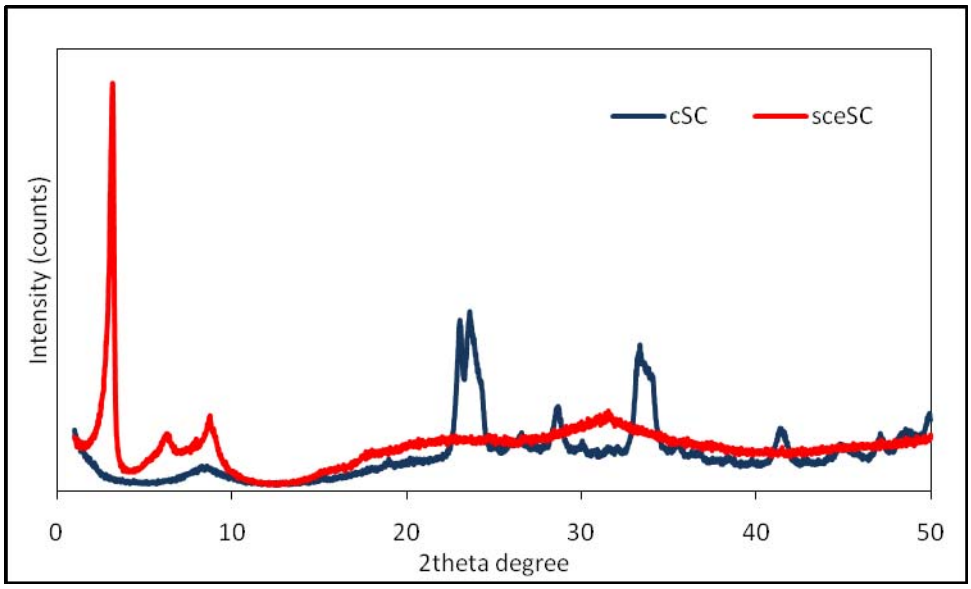

Figure 48: XRD patterns of SC catalysts

X-Ray diffraction patterns of SC catalysts show different behaviors. The extracted sample has peaks at only 1°-10° region (at 3.18°, 5.8° and 8.6°) and also a peak at 33.2° corresponding to $W_{20}O_{58}$. This is similar to the previously mentioned SZ catalysts. However sceSC catalyst does not show any characteristic peak belonging to any cupper structure. For the calcined sample, there exists peaks of $Cu(OH)_2$ at 2θ values of 23.6° and 33.4°. The peak at 1°-10° region is relatively broad.

7.1.3.2. EDS Results

Calcined SC sample (cSC) is characterized with EDS. The incorporation of metal and tungsten to the structure is achieved with direct hydrothermal synthesis of Cu-STA/Silica catalysts which is also supported by EDS characterization results summarized in Table 24.

Table 24: Prepared atomic ratios in SC catalysts compared with EDS results

Catalyst	W/Si		Cu/Si	
	Prepared	EDS	Prepared	EDS
cSC	0.40	0.28	0.06	0.05

Both the cupper and tungsten incorporation is successfully performed during the synthesis as indicated in EDS results. However as in SN samples, tungsten and cupper ratios are lower compared to the prepared ratio values.

7.1.3.3. Nitrogen Physisorption

In Table 25, the results of nitrogen physisorption analysis are shown. The resulting catalysts with copper are less porous and have smaller volume compared to the SZ group catalyst. Addition of Zr improves dispersion of metals to the structure as well as incorporation. On the other hand, metals as copper or nickel cause chocking within the catalyst which actually then results as lower surface areas.

Table 25: Physical Properties of the SC catalysts

Catalyst	**BET area (m^2/g)**	**BJH Adsorption pore volume (cm^3/g)**	**BJH Adsorption pore diameter (nm)**
cSC	94.3	0.47	64.9
sceSC	74.2	0.39	775

In Figure 49, the nitrogen isotherms of SC catalyst are shown with the pore size distribution graph on the right of the figure.

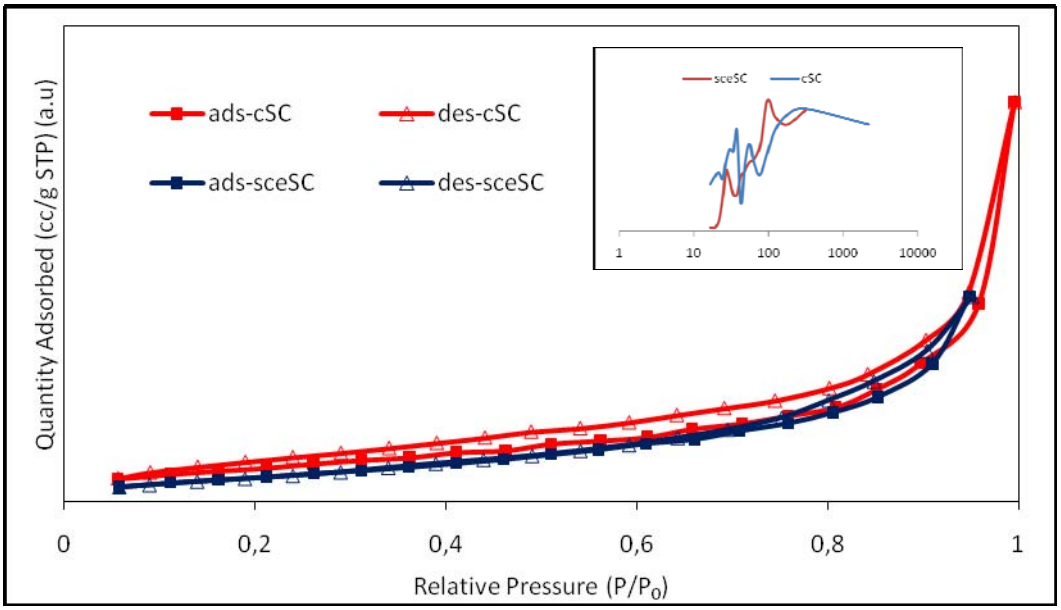

Figure 49: Nitrogen adsorption-desorption isotherm of SC catalysts

The extracted and calcined sample of SC catalyst shows both isotherms between Type III indicating a distortion in mesoporous structure. The synthesized materials are therefore in microporous region as can be seen in pore size distributions and pore diameters (as calculated in Appendix C) given in the same Figure 49.

7.1.3.4. FT-IR Results

The FT-IR results of the extracted samples are given for the finger-print region in Figure 50.

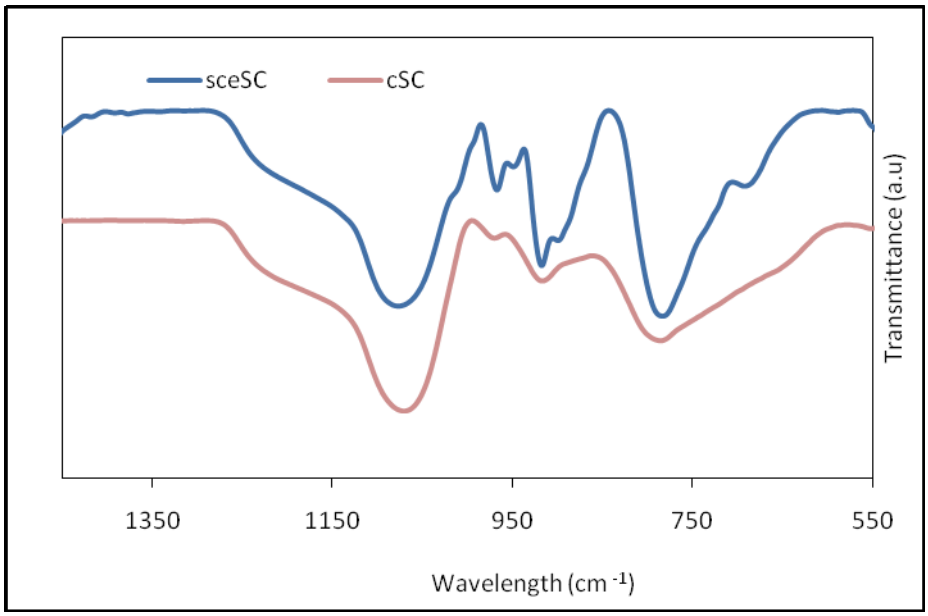

Figure 50: FT-IR curves of SC samples

The dominating bond characteristics in Cu-STA/Silica catalysts are STA structure. The catalysts both show similar properties. However by extending the x-axis, the C-H deformation of surfactant becomes more clear for the extracted sample (at wavelengths of 2800 cm^{-1} -3050 cm^{-1}) [86]. This result show the need for optimization of extraction conditions to remove surfactant with the highest effectiveness.

7.1.3.5. SEM Results

The selected SEM pictures of the extracted samples are given in Figure 51 (magnification 20000 times)

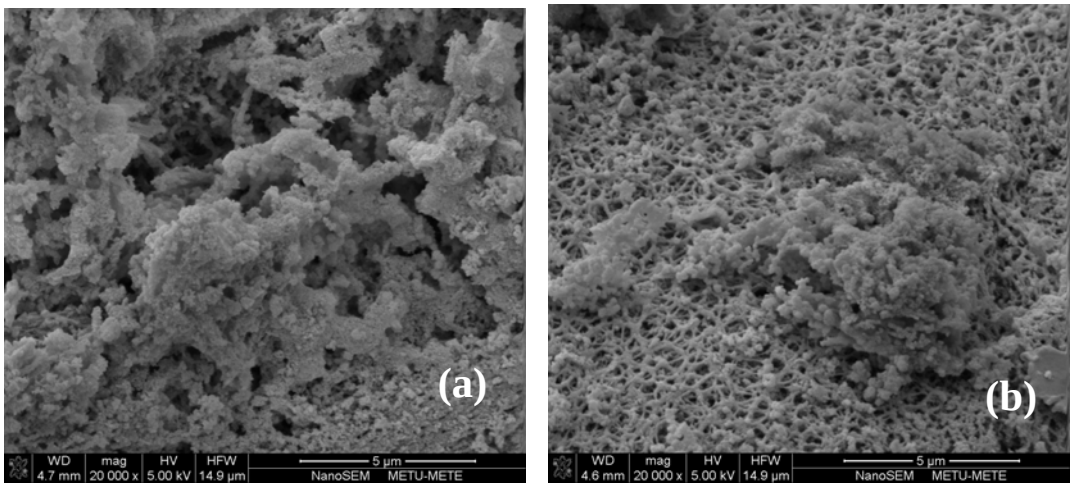

Figure 51: SEM images of SC catalysts (a) cSC (b) sceSC

7.2. Activity Results

This section includes the activity results of the synthesized catalysts in methanol dehydration to produce DME. The details regarding to the experimental system is given in Section 6.3.2, Table 12. All SZ group catalysts, including calcined and extracted ones, are tested in methanol dehydration reaction.

7.2.1. Activity Results of Calcined SZ Group Catalysts

Calcined SZ catalysts are tested in DME synthesis via methanol dehydration in a temperature range of 250-450°C. The results regarding to the conversion of methanol and selectivities towards DME are given in Figure 52 and Figure 53, respectively.

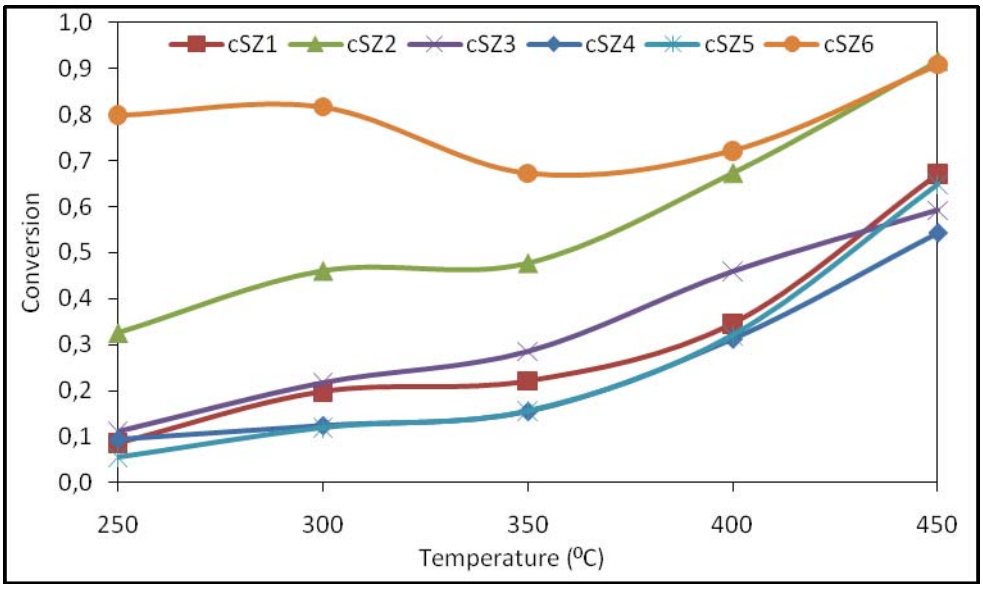

Figure 52: Conversion of methanol with calcined SZ catalysts

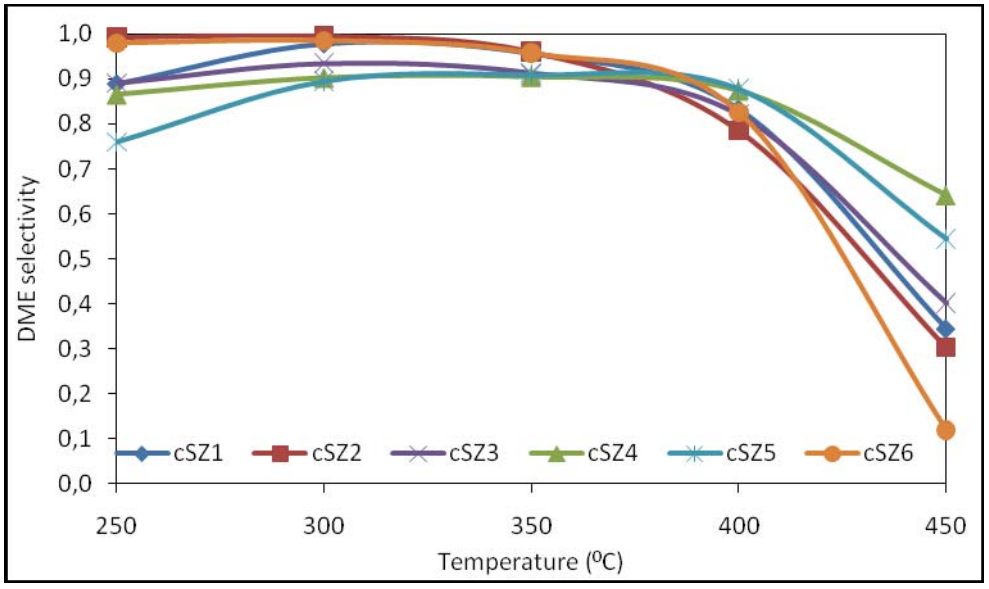

Figure 53: Selectivity of calcined SZ catalysts towards DME

Analyzing the results to investigate the effect of temperature, shows that methanol conversion is directly affected with increase in temperature. However, it is clear in Figure 53 that, DME production is not possible at higher temperatures due to coke formation since the catalysts are calcined at 350°C, and the main product at these ranges, is CH_4 and CO, through coke formed on the surface of the catalysts. In Figure 54, product distribution for cSZ6 catalyst is given.

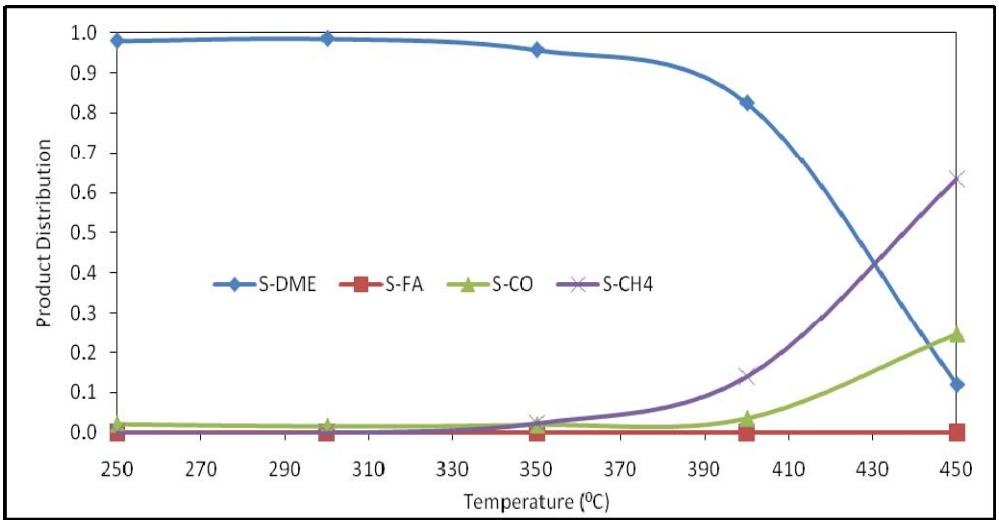

Figure 54: Product distribution in presence of cSZ6 catalyst in methanol dehydration

Comparing the activities with those of non-Zr-added STA incorporated MCM-41, reveals that, with the same W/Si ratio of 0.4, the activities observed with SZ catalysis are lower. This is mainly due to weaker acidities. Although Zr addition also improves the acidity of the material, the additional basic sites coming from ZrO_2 blocks the active sites for methanol dehydration [89].

For other catalysis, product distribution and yields of DME are presented in tabular form in Appendix F.1. At lower temperatures, DME formation is dominant

together with formaldehyde formation via dehydrogenation of methanol as given in Equation (9).

$$CH_3OH \rightleftharpoons CH_2O + H_2 \quad (9)$$

The effect of HPA loading and metal loading can also be seen in the results. Catalysts cSZ1-4, has the same STA loading with a value of 0.4, whereas Zr loading decreases from 0.24 to 0.06 from SZ1 to SZ4. Effect of Zr loading, does not directly affect the activities of the catalysts. However, the results indicate that, sequence of the materials in terms of acidities defined by DRIFTS, is similar to the resulting methanol conversions such that, the ones possessing the highest relative acidity (cSZ2 and cSZ3), lead in higher activity.

On the other hand, effect of HPA loading is also apparent in the results. Among the other catalysts, SZ6 has the highest STA content with W/Si ratio of 0.6, whereas SZ4 and SZ5 are 0.4 and 0.3 respectively. As seen in the DRIFTS analysis, the peaks corresponding to the Brönsted and Lewis acid sites are sharper for cSZ6. This resulted to higher conversion of methanol in the temperature range in consideration.

Comparing the selectivities of the catalysts towards DME, reveal that, all the catalysts are DME selective at lower temperatures with no significant difference in performance. In addition, as stated above, increasing the temperature further (more than calcination temperature) lead to formation of coke and decrease in DME selectivity.

7.2.2. Activity Results of Extracted SZ Group Catalysts

All extracted samples of the catalysts are tested in methanol dehydration reaction within the temperature range of 350-500°C. The results are included in Figure 55 and Figure 56 (conversion of methanol and selectivity towards DME accordingly).

As can be seen in Figure 55, the temperature rise also activates catalyst activity. Contrary to the calcined samples, the extracted samples give conversion at temperatures higher than 350°C.

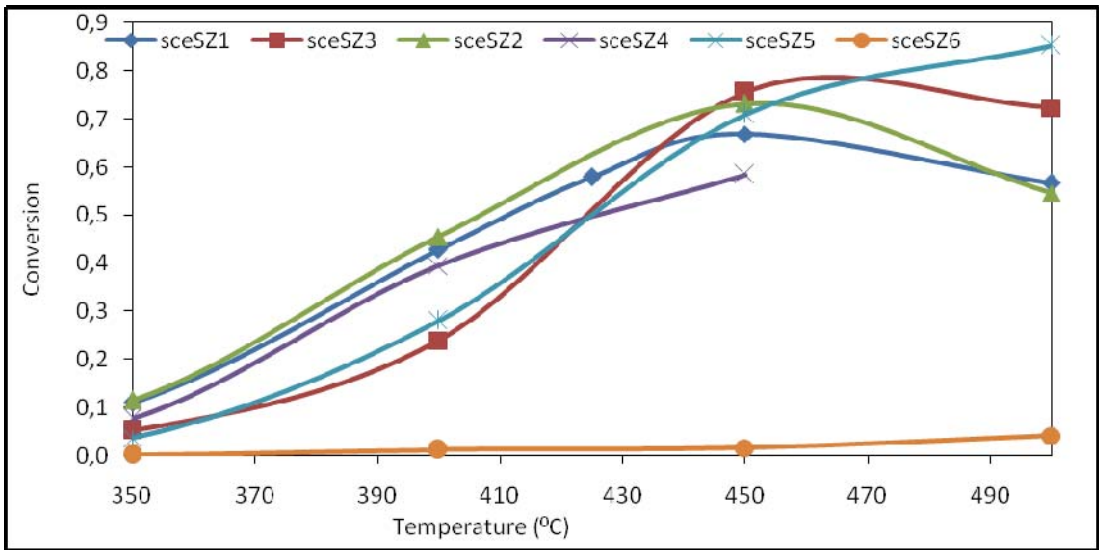

Figure 55: Conversion of methanol with extracted SZ catalysts

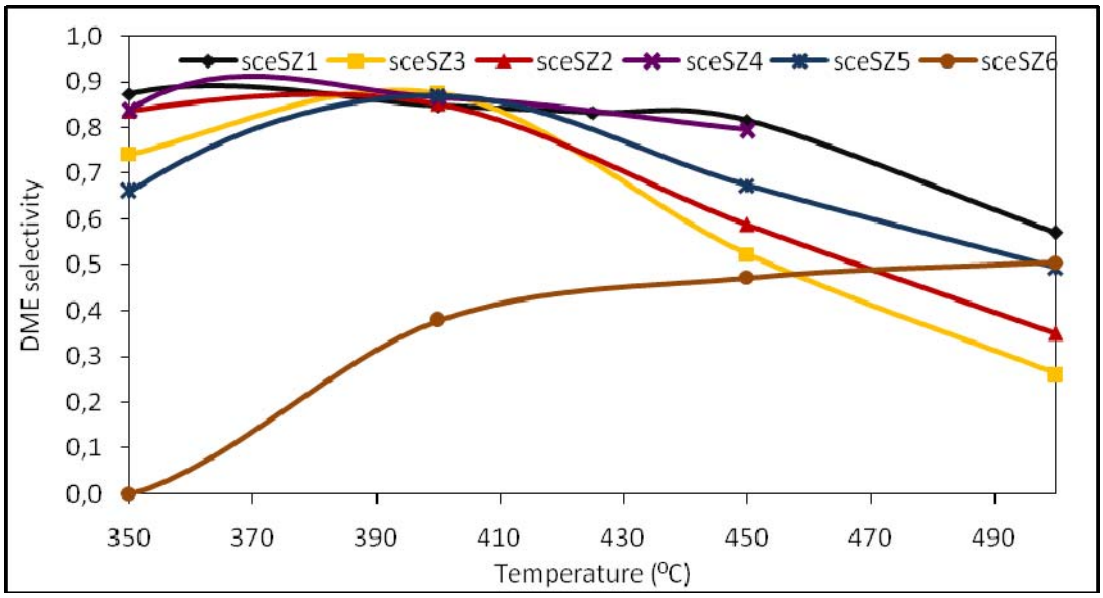

Figure 56: Selectivity of extracted SZ catalysts towards DME

Despite the fact that the normal calcination temperature is 350°C for these catalysts, methanol conversion is still present at higher temperature resulting with a yield of DME. This can be attributed to increased temperature resistivity with extraction process. If these catalysts were treated with calcination, higher temperature should have resulted lower selectivities towards DME.

The catalysts are still selective to DME at even higher temperatures. Enhancing temperature resistivity resulted as less coke formation. In addition, at temperatures between 350-400°C, the side product is formaldehyde, and for the rest is methane and carbonmonoxide. The product distribution for sceSZ1 catalyst is given in Figure 57, and the details related to the product distribution of other catalysis are given in Appendix F.2.

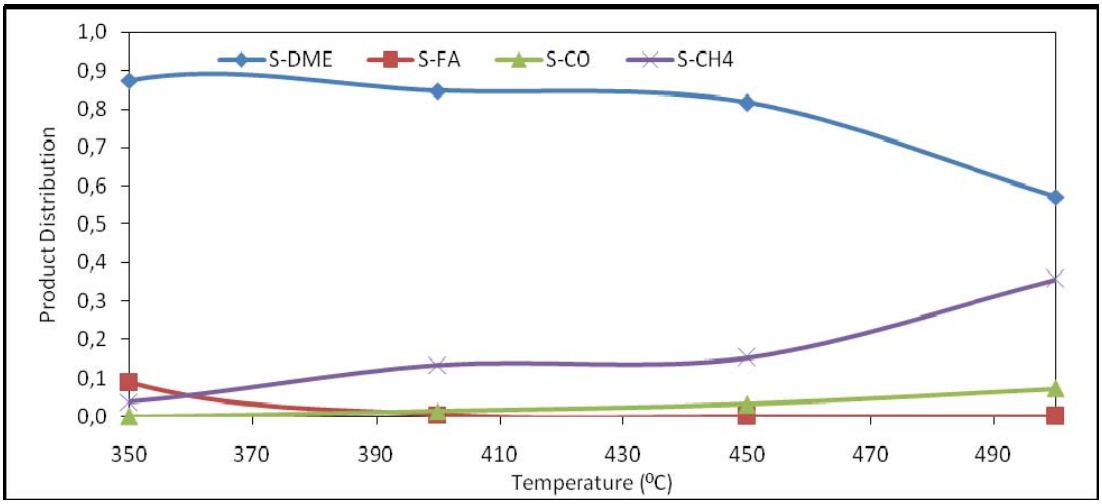

Figure 57: Product distribution in presence of sceSZ1 catalyst in methanol dehydration

The lower activity of the catalysts at lower temperatures can be based on to the DRIFTS results. The extracted samples do not show considerable peaks of acidic

sites in pyridine adsorption. Among the extracted samples, sceSZ3 has the highest acidity as given in Figure 30. However, comparing the yields of DME, of each material show that, sceSZ1 catalyst is the leading one with a value of 0.54 at 450°C. Increasing the temperature also increases the activities of the extracted samples towards both DME and side products as given in Appendix F.2.

CHAPTER 8

CONCLUSIONS AND RECOMMENDATIONS

In this study, DME is synthesized through methanol dehydration in a fixed bed integral reactor at atmospheric pressure at various temperatures at a constant space time of 0.27 s.g.cm^{-3}. DME synthesis is performed with newly prepared materials comprising of silicotungstic acid and zirconium as the metal supported on MCM-41 core structure by direct hydrothermal synthesis method. The surfactant used during the synthesis is removed by calcination and supercritical fluid extraction. The methanol and CO_2 flow rate are kept constant.

SZ1-3 catalysts are treated with CO_2 of 450 bar pressure for 3 hours and SZ4-6 group is extracted at 350 bar for 6 hours. XRD patterns of the calcined group catalysts show a well-distributed structure and the peaks belonging to $W_{20}O_{58}$ and ZrO_2 structures are observed in the catalysts in cSZ4-6. This dispersion behavior is attributed to high content of Zr in first three catalysts. cSZ6 is synthesized with the highest W/Si ratio with increasing the STA content against TEOS. The XRD pattern of that material shows relatively sharp peaks corresponding to core STA structure. On the other hand, XRD patterns of extracted samples at 450 bar (sceSZ1, sceSZ2 and sceSZ3) indicate the mesoporous structure within the catalyst. Compared with the 350 bar extracted samples, these patterns have relatively sharp peaks of mesoporous structure at 2θ between 1-10°. Contrary to the calcined group, the peaks of $W_{20}O_{58}$ and ZrO_2 are rather broad in this group. Therefore, it is concluded that, the formation of both mesoporous structure and the catalytic structures are rather disturbed at lower pressures of SFE.

Nitrogen physisorption analysis revealed that, the extracted materials have comparable properties to calcined one. Especially, the ones extracted at 450 bar, has reached surface areas of 200-240 $m^2.g^{-1}$ whereas the equivalent ones in calcined group has values of 260-280 $m^2.g^{-1}$. The extraction performance can be discussed with the pore volumes as well. The extracted samples have a pore volume between 0.38-0.56 $cm^3.g^{-1}$. On the other hand, the corresponding values are 0.26-0.32 $cm^3.g^{-1}$ for the calcined ones. For the extracted samples at 350 bar, 6 hours, the efficiency of extraction process is rather low when the surface areas and pore volumes are considered. This shows the importance of operating parameters on catalytic properties. The nitrogen isotherms of the materials show similar behaviors in extracted and calcined group. The main factor affecting the isotherms is the W/Si and Metal /Si ratios within the catalyst.

The extracted and calcined samples are characterized with FT-IR. Compared with untreated STA, it is shown that by calcination process there exists some distortions in the structure, since not all the characteristic peaks are obtained. In the calcined samples the W-O_{corner}-W bond is not observed. On the other hand depending on the extraction conditions, there exist similar distortions in STA structure.

It is shown by FT-IR that, although it is obvious that, surfactant removal is carried out successfully with extraction, there still remains additional amount of surfactant that should be removed due to presence of C-H stretching in FT-IR results. Both extracted and calcined catalysts show similar characteristics in finger-print region (500-1500 cm^{-1}), at values of 2800-3000 cm^{-1}, the peaks of C-H bonds are present. These C-H stretching belongs to CTMABR still existing in the catalyst. In addition, when thermogravimetric analysis is conducted with calcined SZ1 (cSZ1) and extracted SZ2 (sceSZ2) catalysts, it is revealed that, although there exists a weight loss in the extracted sample, sceSZ2 (with a value of 16.5% wt/wt), the calcined sample is stable during thermal treatment between 30-400°C. This shows that, although extraction is a promising candidate in surfactant removal, the technique should be developed in terms of application of optimum conditions.

To test the effect of operating parameters of SFE on catalyst properties, SZ3 catalyst (with W/Si=0.4, Zr/Si=0.12) is treated at three pressures, 300-450-600 bar

for 3 hours. Compared with the calcined sample, which is totally amorphous, all three extracted samples show peaks corresponding to mesoporous range and to $W_{20}O_{58}$ and ZrO_2 structures. However the one extracted at 450 bar (called sceSZ3), has rather sharp peaks. By nitrogen physisorption, the surface areas of the materials are ordered as cSZ3 > sceSZ3 > sceSZ3-300 bar > sceSZ3- 600 bar. The reverse ordering is present in weight losses during thermal treatment. During thermal treatment, the weight is lost as follows; sceSZ3 (21.1 %) < sceSZ3-300 bar (27.1 %) < sceSZ3- 600 bar (28.5 %). Therefore it can easily be concluded that there exists an optimum value to carry out the extraction with the highest efficiency. It is revealed that maximum surfactant removal is reached at 450 bar with minimum weight loss during thermal treatment. In present study, the surfactant is dissolved in methanol and CO_2 is used to carry the mixture consisting of methanol and surfactant.

In addition samples of SZ4 catalyst (with W/Si=0.4, Zr/Sİ=0.06) are extracted at 350 bar for 3 hours and 6 hours. Keeping the process for a longer time, improved the catalytic properties; surface area, pore size.

These SZ catalysts are tested in methanol dehydration reaction and selectivities are monitored towards DME. The calcined samples are tested in a range of 250-450°C whereas the extracted ones are in 350-500°C. The effect of HPA loading and metal loading can be seen in the results of calcined samples. The activities in methanol dehydration reaction are parallel with the DRIFTS results of pyridine adsorbed samples. As can be seen in DRIFTS results, cSZ2 and cSZ3 are leading in terms of acidic properties and the highest yield is obtained with cSZ2 catalyst among the others having the same W/Si ratio. On the other hand, increasing the HPA content, also improved the catalytic activity. As the DRIFTS results revealed, cSZ6 has the highest acid sites yielding the maximum DME with a value of 0.80. The activities of catalysts increased with rise in temperature. However in this case, selectivity of DME is suppressed (therefore the yield is) due to formation of side products at higher temperatures. At lower temperatures of 250°C, the selectivity of cSZ6 and cSZ2 reached to values of 1.0. The temperatures higher than calcination temperature of the material, lead to formation of coke.

The activity results of extracted samples are rather low compared with the calcined samples which can also be concluded from DRIFTS analysis of pyridine adsorbed samples. The main difference with the calcined materials is that, these extracted materials have still activity at higher temperatures also with considerable yields of DME at higher temperatures. Application of SFE, improved the temperature resistivity of the materials. At lower temperatures, the main side product is formaldehyde and at higher temperatures methane and carbon monoxide are formed. The acidity of sceSZ3 is the dominant one compared to other extracted samples and sceSZ3 is also successful in DME synthesis. The extracted sample of SZ6 (sceSZ6), having the highest HPA content, is not as active as expected. The result can be attributed to unsuccessful extraction process. The catalytic properties of sceSZ6 are not also promising with low surface area (123.8 $m^2.g^{-1}$).

In addition to zirconium; nickel and copper are also incorporated to MCM-41 structure (with a metal/Si ratio: 0.06) with STA (W/Si= 0.04) and characterized after calcined and extracted. Although the metal incorporations are successful, the final properties of materials are not comparable to Zr added ones. The surface areas are rather low (in the order of 60-90 m^2g^{-1} for both calcined and extracted samples). Nitrogen physisorption analysis showed that, the synthesized materials are no mesoporous but microporous and show Type III isotherms.

To sum up, the synthesis of metal and STA incorporated MCM-41 structures are successfully performed with calcination and by SFE. The resultant materials have comparable physical properties. The synthesized catalysts are active in methanol dehydration and to further improve the activity and selectivity towards DME, the surfactant removal step, extraction, should be developed in terms of operating conditions.

REFERENCES

[1] Marion J., Nsakala N., Griffin T., Bill A., 'Controlling Power Plant CO_2 Emissions: a long Range View', ALSTOM Power Technology Center

[2] Arcoumanis, C., Bae, C., Crookes, R., Kinoshita, E., 'The potential of di-methyl ether (DME) as an alternative fuel for compression ignition engines: A review', 2008, Fuel, 87, 1014-1030

[3] Wikipedia the Free Encylopedia, http://en.wikipedia.org/mainpage http://en.wikipedia.org/wiki/Dimethyl_ether, Last Access Date: 01.04.2011

[4] Galvita, V. V., Semin, G. L., Belyaev, V. D., Yurieva, T. M., Sobyanin, V. A., 'Production of hydrogen from dimethyl ether', 2001, Applied Catalysis A, 216, 85-90.

[5] Tartamella, T., L., Lee, S., 'Development of specialty chemicals from dimethyl ether', 1997, Fuel Processing Technology 38, 4, 228.

[6] Jia, G. X., Ma, H. B., Tan, Y. S., Han, Y. Z., 'Effect of particle size on the hybrid catalyst activity for slurry phase dimethyl ether synthesis', 2005, Industrial and Engineering Chemistry Research, 44, 2011-2015.

[7] DOE topical report, 'Liquid-phase dimethyl ether demonstration in the LaPorte Alternative Fuels Development Unit', Cooperative Agreement No. DE-FC22-92PC90543; January, 2001.

[8] Cai, G. Y., Liu, Z. M., Shi, R. M., He, C. Q., Yang, L. X., Sun, C. L., Chang, Y. J., 'Light alkenes from syngas via dimethyl ether', 1995, Applied Catalysis A, 125, 29-38.

[9] Jiang, T., Liu, C. J., Rao, M. F., Yao, C. D., Fan, G. L., 'A novel synthesis of diesel fuel additives from dimethyl ether using dielectric barrier discharges', 2001, Fuel Processing Technology, 73, 143-152.

[10] Gas Encylopedia, http://encyclopedia.airliquide.com/encyclopedia.asp http://encyclopedia.airliquide.com/Encyclopedia.asp?GasID=80, Last Access Date, 01.09.2010

[11] Kowalewicz, A., Wojtymiak, M., 'New alternative fuels for I.C. engines – A review', 2004, Journal of Kones Internal Combustion Engines, 11, 358-368

[12] Ogawa, T., Inoue, N., Shikada, T., Ohno, Y., 'Direct dimethyl ether synthesis', 2003, Journal of Natural Gas Chemistry, 12, 219-227

[13] Dogu, T., Varisli, D., 'Alcohols as alternatives to petroleum for environmentally clean fuels and petrochemicals', 2007, Turkish Journal of Chemistry, 31, 551-567

[14] Yineg, W., Genbao, L., Wei, Z., Zhou, L., 'Study on the application of DME/diesel blends in a diesel engine', 2007, Fuel Processing Technology, 89, 1272-1280

[15] Semelsberger, T. A., Borup, R. L., Greene, H. L., 'Dimethly ether (DME) as an alternative fuel, 2006, Journal of Power Source, 497-511

[16] Shu, H. K., Lee, C. S., 'Experimental and analytical study on the spray characteristics of dimethyl ether (DME) and diesel fuels within a common-rail injection system in a diesel engine', 2008, Fuel, 87, 925-932

[17] Park, s. H., Kim, H. J., Lee, C. S., 'Effects of dimethyl-ether (DME) spray behavior in the cylinder on the combustion and exhaust emissions characteristics of a high speed diesel engine', 2010, Fuel Processing Technology, 91, 504-513

[18]http://pse.che.ntu.edu.tw/ccyu/Process_Des_Project/Problem_2007/direct%20dimethyl%20ether%20synthesis.pdf, Last Access Date, 01.02.2011

[19] Preparation of Fuel Grade Dimethyl Ether, International Application Published Under the Patent Cooperation Treaty, Haldor Topsoe, 1996

[20] Lei, Z., Zou, Z., Dai, C., Li, Q., Chen, B., "Synthesis of dimethyl ether (DME) by catalytic distillation", 2011, Chemical Engineering Science, 66, 3195-3203

[21] Stanislao, M. D., Malandrino, A., Patrini, R., Pirovana, C., Viva, A., Brunazzi, E., 'DME synthesis via catalytic distillation: experiments and simulation', 17th European Symposium on Computer Aided Process Engineering, 1077-1082

[22] Yoo, K. S., Kim, J. H., Park, M. J., Kim, S. J., Joo, O. S., Jung, K. D., 'Influence of solid acid catalyst on DME production directly from synthesis gas over the admixed catalyst of $Cu/ZnO/Al_2O_3$ and various SAPO catalysts', 2007, Applied Catalysis A: General, 330, 57-62

[23] Xu, M., Lunsford, J. H., Goodman, D. W., Bhattacharyya, D. W., 'Synthesis of dimethyl ther (DME) from methanol over solid-acid catalysts', 1997, Applied Catalysis A: General, 149, 289-301

[24] Varisli, D., "Kinetic Studies for Dimethyl ether and Diethyl ether Production", Ph.D. Thesis, Middle East Technical University, Ankara, Turkey, September 2007.

[25] Vakili, R., Pourazadi, E., Setoodeh, P., Eslamloueyan, R., Rahimpour, M. R., 'Direct dimethyl ether (DME) synthesis through a thermally coupled heat exhanger', 2011, Applied Energy, 88, 1211-1223

[26] Naik, S. P., Ryu, T., Bui, V., Miller, J. D., Drinnan N. B., Zmierczak, W., 'Synthesis of DME from CO_2/H_2 gas mixture', 2011, Chemical Engineering Journal, 167, 362-368

[27] Qi, G. X., Zheng, X. M., Fei, J. H., Hou, Z. Y., 'A novel catalyst for DME synthesis from CO hydrogenation 1. Activity, structure and surface properties', 2001, Journal of Molecular Catalysis A: Chemical, 176, 195-203

[28] Wikipedia the Free Encylopedia, http://en.wikipedia.org/mainpage http://en.wikipedia.org/wiki/Zeolite, Last Access Date, 01.10.2010

[29] Davis, M. E., Lobo, R. F., "Zeolite and molecular sieve synthesis", 1992, Chemistry of Materials, 4, 756-768

[30] Dogan, A. U., "Zeolite mineralogy and Cappadocian erionite", 2003, Indoor and Built Environment, 12, 337-342

[31] Perry, R., H., "Perry's Chemical Engineers' Handbook", Mc-Graw Hill, 1997

[32] Bekkum, H., Flanigen, E. M, Jansen, J. C., "Introduction to zeolite and science and practice", Elsevier, 1991, Amsterdam

[33] Vartuli, Kresge, C. T., Roth, W. J., McCullen, S. B., J. C., Beck, J. S., Schmitt, K. D., Leonowicz, M. E, Lutner, J. D., Sheppard, E. W., "Advanced Catalysts and Nanostructured Materials", Academic Press, 1996, New Jersey

[34] Clark, J. H., Macquarrie, D. J., Tavener, S. J., "The application of modified mesoporous silicas in liquid phase catalysis", 2006, Dalton Transactions, 36, 4297-4309

[35] Kresge, C. T., Vartuli, J. C., Roth, W. J., Leonowicz, M. E., "The discovery of ExxonMobil's M41S family of mesoporous molecular sieves", 2004, Studies in Surface Science and Catalysis, 148, 53-72

[36] Ciesla, U., Schüth, F., "Ordered mesoporous materials", 1999, Microporous and Mesoporous Materials, 27, 131-149

[37] Beck, J. S., Vartuli, J. C., Roth, W. J., Leonowicz, M. E, Kresge, C. T., Schmitt, K. D., Chu, C. T-W., Olson, D. H., Sheppard, E. W., McCullen, S. B., Higgins, J. B., Schlenker, J. L., "A new family of mesoporous molecular sieves prepared with liquid crystal templates", 1992, Journal of American Chemical Society, 27, 10834-10843

[38] Sener, C., Dogu, T., Dogu, G., "Direct hydrothermal synthesis of palladium-incorporated silicate-structured mesoporous catalysts", 2007, Turkish Journal of Chemistry, 31, 473-478

[39] Oye, G., Sjöblom, J., Stöcker, M., "Synthesis, characterization and potential applications of new materials in the mesoporous range", 2001, Advances in Colloid and Interface Science, 89-90, 436-466

[40] Roth, W. J., Vartuli, J. C., "Synthesis of mesoporous molecular sieves", 2005, Studies in Surface Science and Catalysis, 157, 91-110

[41] Sener, C., "Synthesis and characterizatıon of Pd-MCM-type mesoporous nanocomposıte materials", M.S. Thesis, Middle East Technical University, Ankara, Turkey, January 2006.

[42] Zhao, X. S., Lu, G. Q. M., Millar, G. J., "Advances in mesoporous molecular sieves", 1996, Industrial and Engineering Chemistry Research, 35, 2075-2090

[43] Huo, Q., Margolese, D. I., Stucky, G. D., "Surfactant control of phases in the synthesis of mesoporous silica based materials", 1996, Chemistry of Materials, 8, 1147-1160

[44] Romanow, S. G., Sotomayor-Torres, C. M., "Three dimensional lattices of nanostructures: The template approach", 2000, Handbook of Nanostructured Materials and Nanotechnology, 4, 231-323, Academic Press, San Diego

[45] MCM41 and catalyst preparation

[46] Vartuli, J. C., Shih, S. S., Kresge, C. T., Beck, J. S., "Potential applications of M41S type mesoporous molecular sieves", 1998, Mesoporous Molecular Sieves, 117, 13-21

[47] Corma, A., "From microporous to mesoporous molecular sieve materials and their use in catalysis", 1997, Chemical Reviews, 97, 2373-2419

[48] Kozhevnikov, I. V., "Catalysis by heteropolyacids and multicomponent polyoxometalates in liquid phase reactions", 1998, Chemical Reviews, 98, 171-198

[49] Neel, I., "Polyoxometalates, why are they unique?", PhD Seminar,

[50] Lefebvre, F., Liu-Cai, F. X., ,Auroux, A., "Microcalorimetric study of the acidity of tungstic heteropolyanions", 1994, Journal of Materials Chemistry, 4, 125-131

[51] Anderson Ma, H., Wu, L., Pang, H., Meng, X., Peng, J., "Hydrothermal synthesis of two Anderson POM-supported transition metal organic-inorganic compounds", 2010, Journal of Molecular Structure, 967, 15-19

[52] Misono, M., "Recent progress in practical applications of heteropolyacid and perovskite catalysts: Catalytic technology for the sustainable society", 2009, Catalysis Today, 144, 285-291

[53] Okuhara, T., Mizuno, N., Misono, M., "Catalysis by heteropoly compounds-recent developments", 2001, Applied Catalysis A: General, 222, 63-77

[54] Ahmad, M. I., Zaidi, S. M. J., Ahmed, S., "Proton containing composites of heteropolyacids loaded onto MCM-41", 2006, Journal of Power Sources, 157, 35-44

[55] Li, G., Ding, Y., Wang, J., Wang, X., Suo, J., "New progress of Keggin and Wells-Dawson type polyoxometalates catalyze acid and oxidative reactions", 2007, Journal of Molecular Catalysis A: Chemical, 262, 67-76

[56] Kozhevnikov, I. V., "Sustainable heterogeneous catalysis by heteropoly acids", 2007, Journal of Molecular Catalysis A: Chemical, 262, 86-92

[57] Kozhevnikov, I. V., "Heterogeneous acid catalysis by heteropoly acids: Approaches to catalyst deactivation", 2009, Journal of Molecular Catalysis A: Chemical, 305, 104-111

[58] Liu, Q., Wu, W., Wang, J., Ren, X., Wang, Y., "Characterization of 12-tungstophosphoric acid impregnated on mesoporous silica SBA-15 and its catalytic performance in isopropylation of naphthalene with isopropanol", 2004, Microporous and Mesoporous Materials, 76, 51-60

[59] Mizuno, N., Misono, M., "Heterogeneous catalysis", 1998, Chemical Reviews, 98, 199-217

[60] Popa, A., Sasca, V., Halasz, J., "Catalytic properties of molecular sieves MCM41 type doped with heteropolyacids for ethanol oxidation", 2008, Applied Surface Science, 225, 1830-1835

[61] Xia, Q. H., Wee, C. H., Hidajat, K., Kawi, S., "$H_3PW_{12}O_{40}$-Supported MCM-41 acid catalyst for the gas phase synthesis of MTBE", 2004, Studies in Surface Science and Catalysis, 154, 2915-2922

[62] Mizuno, N., Misono, M., "Heteropolyacids catalysts", 1997, Current Opinion in Solid State and Materials Science, 2, 84-89

[63] Herrero, M., Mendiola, J. A., Cifuentes, A., Ibanez, E., "Supercritical fluid extraction: Recent advances and applications", 2010, Journal of Chromatography A, 1217, 2495-2511

[64] Edward, R., Quibai, S., Zhiqiang, Z., Chongmin, Z., Wei, G., "Mini-review: Green sustainable processes using supercritical fluid carbondioxide", 2009, Journal of Environmental Sciences, 21, 720-726

[65] Sahena, F., Zaidul, I. S. M., Jinap, S., Karim, A. A, Abbas, K. A., Norulaini, N. A. N., Omar, A. K. M., "Application of supercritical CO_2 in lipid extraction – A review", 2009, Journal of Food Engineering, 95, 240-253

[66] Pinero, R., Garcia, J., Sokolova, M., Cocero, M. J., "Modelling of the phase behavior for the direct synthesis of dimethyl carbonate from CO_2 and methanol at supercritical or near supercritical conditions", 2007, Journal of Chemical Thermodynamics, 39, 536-549

[67] http://stevengoddard.wordpress.com/2010/09/05/the-freezing-point-and-the-dew%C2%A0point-part-2/, Last Access Date, 01.07.2010

[68] Cansell, F., Aymonier, C., "Design of functional nanostructrues materials using supercritical fluids", 2009, Journal of Supercritical Fluids, 47, 508-516

[69] Erkey, C., "Preparation of metallic supported nanoparticles and films using supercritical fluid deposition", 2009, Journal of Supercritical Fluids, 47,517-522

[70] Chatterjee, M., Hayashi, H., Saito, N., "Role and effect of supercritical fluid extraction of template on the Ti(IV) active sites of Ti-MCM-41", 2003, Microporous and Mesoporous Materials, 57, 143-155

[71] Huang, Z., Luan, D. Y., Shen, S. C., Hidajat, K., Kawi, S., "Supercritical fluid extraction of the organic template from synthesized porous materials: effect of pore size", 2005, Journal of Supercritical Fluids, 35, 40-48

[72] Huang, L., Kawi, S., Poh, C., Hidajat, K., Ng, S. C., "Extraction of cationic surfactant templates from mesoporous materials by CH_3OH-modified CO_2 supercritical fluid", 2005, Talanta, 66, 943-951

[73] Kawi, S., Lai, M. W., "Supercritical fluid extraction and surfactant template from MCM-41", 1998, Chemical Communications, 1407-1408

[74] Scintag, Inc., Basics of X-Ray Diffraction, Chapter 7, 1999

[75] Rouquérol, F. , Rouquérol, J., Sing, K. S. W. "Adsorption by powders & porous solids: principles, methodology and applications", Academic Press, 1999

[76] Wikipedia the Free Encyclopedia, http://en.wikipedia.org/mainpage http://en.wikipedia.org/wiki/Capillary_condensation, Last Access Date, 01.12.2010

[77] Herguth, W. R., "Applications of Scanning Electron Microscopy and Energy Dispersive Spectroscopy (SEM/EDS) to Practical Tribology Problems", Herguth Laboratories, Inc.

[78] Hafner, B., "Scanning Electron Microscopy Primer", 2007, Characterization Facility, University of Minnesota

[79] Thermonicolet, Introduction to Fourier Transform Infrared Spectrometry, 2001

[80] Hsu, C. P. S., "Infrared Spectroscopy", Handbook of Instrumental Techniques for Analytical Chemistry, Separation Sciences Research and Product Development, Mallinckrodt, Inc.

[81] Applied Separations Spe-ed SFE Operations Manual, version 4.1

[82] Varisli, D., Dogu, T., Dogu, G. "Novel mesoporous nanocomposite WO_x-Silicate acidic catalysts: Ethylene and Diethylether from ethanol", 2009, Industrial and Engineering Chemistry Research ,48 (21), 9394–9401

[83] Xu, B., Yamaguchi, T., Tanabe, K., "Acid-base functional behavior of ZrO_2 in dual absorption of CO_2 and NH_3", 1988, Chemistry Letters, 1663-1666

[84] Tomishige, K., Sakaihori, T., Ikeda, Y., Fujimoto, K., "A novel method of direct synthesis of dimethyl carbonate from methanol and carbon dioxide catalyzed by zirconia", 1999, Catalysis Letters, 58, 225-229

[85] Langenfeld, J. J., Hawthorne, S. B., Miller, D. J., Pawliszyn, J., "Effects of temperature and pressure on supercritical fluid extraction efficiencies of polycyclic aromatic hydrocarbons and polychlorinated biphenyls", 1993, Analytic Chemistry, 65, 338-344

[86] Machmudah, S., Kondo, M., Sasaki, M., Goto, M., Munemasa, J., Yamagata, M., "Pressure effect in supercritical CO2 extraction of plant seeds", 2008, Journal of Supercritical Fluids, 44, 301-307

[87] NIST Chemistry WebBook, http://webbook.nist.gov/ http://webbook.nist.gov/cgi/cbook.cgi?ID=C12035368&Units=SI&Mask=800, Last Acces Date, June, 2010

[88] Lu, W. Z., Teng, L. H., Theoretical Analysis of Fluidized-Bed Reactor for Dimethyl Ether Synthesis from Syngas, International Journal of Chemical Reactor Engineering, 2003, 1, 123-136.

APPENDIX A

EQUILIBRIUM CURVE CALCULATION DETAILS

A.1. Methanol dehydration reaction

Methanol dehydration reaction is expressed as follows;

$$2CH_3OH \leftrightarrow CH_3OCH_3 + H_2O$$

By conducting mass balance around the reactor; at any point in the reactor

$F_{MeOH} = F_{MeOH\text{-}in} - F_{DME}$

$F_{water} = F_{DME}$

$$K_p = \frac{P_{DME} \times P_{water}}{(P_{MeOH})^2}$$

where $P_i = \frac{F_i}{F_t} P_t$ assuming and ideal behavior in the gas phase and fugacities are equal to 1. After substituting the latter expression for P_i in K_p equations results as;

$$K_p = \frac{F_{DME} \times F_{water}}{(F_{MeOH})^2}$$

Where equilibrium constant is expressed as [88];

$$\ln K_{P2}^0 = 4019/T + 3.707 \ln T - 2.783 \times 10^{-3} T + 3.8 \times 10^{-7} T^2 - 6.561 \times 10^4 / T^3 - 26.64$$

Substituting these equations into Polymath non-linear program solver, results the equilibrium distribution throughout the reactor. The input and output of the program are given as follows;

Polymath Program used in Equilibrium Analyses of methanol dehydration reaction

```
f(f_DME) = Kp - f_water * f_DME / f_meoh ^ 2
Kp = exp(4019 / T + 3707 / 1000 * ln(T) - 2783 * 10 ^ (-6) * T + 38 * 10 ^ (-8) * T ^ 2 - 65610 / T ^ 3 - 2664 / 100)
P = 1
T = 400
f_water = f_DME
f_meoh = f_meoh_in - 2 * f_DME
f_meoh_in = 100
conv_meoh = (f_meoh_in - f_meoh) / f_meoh_in * 100
f_DME(0) = 20
f_DME(max) = 100
f_DME(min) = 0
```

As can be seen in the results, the change in the pressure does not affect the overall conversion of methanol;

Calculated values of NLE variables

	Variable	Value	f(x)	Initial Guess
P=1	f_DME	47.57309	-0.0544634	50. (0 < f_DME < 100.)
P=50	f_DME	47.57309	-0.0544634	50. (0 < f_DME < 100.)

	Variable	Value	Variable	Value
1	T	400.	T	400.
2	**P**	**50.**	**P**	**1.**
3	Kp	96.00823	Kp	96.00823
4	f_water	47.57309	f_water	47.57309
5	f_meoh_in	100.	f_meoh_in	100.
6	f_meoh	4.853823	f_meoh	4.853823
7	**conv_meoh**	**95.14618**	**conv_meoh**	**95.14618**

A.2. Syn-Gas conversion reactions

In making equilibrium analysis, mass balance is conducted for the species assuming the syn-gas conversion follows these steps,

(1) Methanol Synthesis Reaction: $CO + 2H_2 \leftrightarrow CH_3OH$

(2) DME Synthesis Reaction: $2CH_3OH \leftrightarrow CH_3OCH_3 + H_2O$

(3) Water Gas Shifting Reaction: $CO + H_2O \leftrightarrow CO_2 + H_2$

There are six components that the equilibrium condition should be determined, CO (A), H_2 (B), methanol (C), water (D), CO_2 (E) DME (P). To find the equilibrium distribution, equilibrium constants of three reactions are coupled with mass balances for C, H and O. The equilibrium constants are defined as [88];

$$\log K_{P1}^0 = 3748.7/T - 9.2833\log T + 3.1475\times10^{-3}T - 4.2613\times10^{-7}T^2 + 13.8144$$
$$\ln K_{P2}^0 = 4019/T + 3.707\ln T - 2.783\times10^{-3}T + 3.8\times10^{-7}T^2 - 6.561\times10^{4}/T^3 - 26.64$$
$$\log K_{P3}^0 = 2167/T - 0.5194\log T + 1.037\times10^{-3}T - 2.311\times10^{-7}T^2 - 1.2777$$

Relating equilibrium constants with partial pressures;

$$K_{P1} = \frac{P_{Ce}}{P_{Be}^2 P_{Ae}}$$

$$K_{P2} = \frac{P_{De}P_{Pe}}{P_{Ce}^2}$$

$$K_{P3} = \frac{P_{Ee}P_{Be}}{P_{Ae}P_{De}}$$

where $P_i = \frac{F_i}{F_t} P_t$ (subscript t denotes total whereas e is for equilibrium) assuming and ideal behavior in the gas phase and fugacities are equal to 1. After substituting the latter expression for P_i in K_p equations results as;

$$K_{P1} = \frac{F_{Ce}}{F_{Be}^2 F_{Ae}} \times \left(\frac{F_{te}}{P_{te}} \right)^2$$

$$K_{P2} = \frac{F_{De} F_{Pe}}{F_{Ce}^2}$$

$$K_{P3} = \frac{F_{Ee} F_{Be}}{F_{Ae} F_{De}}$$

The inlet ratio of CO to H_2 is $CO/H_2=m$ (For the results shown in Figure 6, m=1). Making the mass balance;

H balance: $2F_{Bi} = 2F_B + 4F_C + 2F_D + 6F_P$

C balance: $mF_{Bi} = F_A + F_C + F_E + 2F_P$

O balance: $mF_{Bi} = F_A + F_C + F_D + 2F_E + F_P$

Where "i" refers to inlet conditions

Rearranging Equations for F_{De}, F_{Ae} and F_{Be} results

$$F_{De} = F_{Pe} - F_{Ee}$$

$$F_{Ae} = mF_{Bi} - F_{Ce} - F_{Ee} - 2F_{Pe}$$

$$F_{Be} = F_{Bi} - 2F_{Ce} - 4F_{Pe} + F_{Ee}$$

Coupling these equations with equilibrium constants and solving with Polymath program given below, results as the equilibrium flows of each species.

Polymath Program used in Equilibrium Analyses of Syn-Gas Conversion

```
f(fc) = Kp1 - fc / fb ^ 2 / fa * (ft / P) ^ 2 # methanol
f(fp) = Kp2 - fd * fp / fc ^ 2 # DME
f(fe) = Kp3 - fe * fb / fa / fd # CO2
Kp1 = 10 ^ (37487 / 10 / T - 92833 / 10000 * log(T) + 31475 * 10 ^ (-7) * T - 42613 * 10 ^ (-11) * T ^ 2 +
138144 * 10 ^ (-4)) # Equilibrium constant for the first reaction
```

Kp2 = *exp*(4019 / T + 3707 / 1000 * *ln*(T) - 2783 * 10 ^ (-6) * T + 38 * 10 ^ (-8) * T ^ 2 - 65610 / T ^ 3 - 2664 / 100) **# Equilibrium constant for the second reaction**
Kp3 = 10 ^ (2167 / T - 5194 / 10 ^ 4 * *log*(T) + 1037 * 10 ^ (-6) * T - 2331 * 10 ^ (-10) * T ^ 2 - 12777 * 10 ^ (-4)) **#** Equilibrium constant for the third reaction
m = 13 / 10 **# feed ratio (CO/H2)**
ft = (m + 1) * fbin - 2 * fc - 4 * fp **# total flow rate at equilibrium**
P = 450 / 10 **# pressure_bar**
T = 510 **# temperature_K**
fa = m * fbin - fc - fe - 2 * fp **# CO**
fd = fp - fe **# H2O**
fb = fbin - 2 * fc - 4 * fp + fe **# H2**
fbin = 100 **# inlet flow rate of H2**
conv_b = (fbin - fb) / fbin * 100 **# percentage conversion of H2**
conv_a = (m * fbin - fa) / m / fbin * 100 **# percentage conversion of CO**
fc(0) = 1
fp(0) = 28
fe(0) = 25

For different values of m, the output of the program is given as follows

Calculated values of NLE variables

	CO/H_2	M=1	M=1.5	M=2
1	fc	0.5972101	0.14777	0.096552
2	fp	30.26599	32.41505	32.59949
3	fe	30.02201	32.40111	32.59358

	CO/H_2	m=1	m=1.5	m=2
1	T	510.	510.	510.
2	Kp1	0.0033419	0.0033419	0.0033419
3	Kp2	20.70481	20.70481	20.70481
4	m	1.	1.5	2.
5	fbin	100.	100.	100.
6	P	45.	45.	45.
7	Kp3	107.9564	107.9564	107.9564
8	ft	77.74163	120.0443	169.4089
9	fd	0.2439793	0.0139375	0.0059108
10	fa	8.848808	52.62103	102.1109
11	fb	7.76364	2.445383	2.002503
21	conv_b	92.23636	97.55462	97.9975
22	conv_a	91.15119	64.91931	48.94456

APPENDIX B

EVALUATION OF GC RESULTS

The results from GC are analyzed with the specific retention times and calibration factors of each species. These are given in Table 26.

Table 26: Calculation parameters for effluent species from GC

Component	Retention time	Calibration Factor
CO	0.21	2.76
CH4	0.28	2.76
DME	5.1	0.76
Formaldehyde	7.4	1.33
Methanol	7.7	1

Total conversion of methanol is calculated as follows;

$$x_{EtOh} = \frac{\text{number of moles reacted}}{\text{total number of moles MeOh entering}} = \frac{n_r}{n_t}$$

where $n_t = 2 \times n_{DME} + n_{CO} + n_{CH4} + n_{FA} + n_{MeOH}$ and $n_r = n_t - n_{MeOH}$

Selectivity and yield towards DME is calculated as follows;

$$S_{DME} = \frac{2 \times n_{DME}}{n_r} \qquad \text{and} \quad Y_{DME} = x_{MeOH} \times S_{DME}$$

and n_t denotes the total number of moles exiting from reactor and is calculated by the area found from GC analysis and corresponding calibration factor. A sample calculation is made for randomly selected sceSZ3 catalyst at 500°C.

Sample calculation for GC calculations

T=500°C, catalyst sceSZ3

$$\text{Area of CO} = 11.8 \rightarrow n_{CO} = 11.8 \times 2.76 = 32.56$$

$$\text{Area of } CH_4 = 74.4 \rightarrow n_{CH4} = 74.4 \times 2.76 = 205.34$$

$$\text{Area of DME} = 46.8 \rightarrow n_{DME} = 46.8 \times 0.76 = 35.57$$

$$\text{Area of formaldehyde} = 0 \rightarrow n_{FA} = 0 \times 1.33 = 0$$

$$\text{Area of MeOH} = 91 \rightarrow n_{MeOH} = 91 \times 1 = 91$$

$$n_t = 32.56 + 205.34 + 35.57 \times 2 + 0 + 91 = 400.05$$

$$n_r = 400.05 - 91 = 309.05$$

$$\text{Conversion of MeOH} = \frac{309.05}{400.05} = 0.77$$

$$\text{Selectivity of CO} = \frac{32.56}{309.05} = 0.1 \rightarrow \text{Yield of DME} = 0.1 \times 0.77 = 0.077$$

$$\text{Selectivity of } CH_4 = \frac{205.34}{309.05} = 0.66 \rightarrow \text{Yield of DME} = 0.66 \times 0.77 = 0.51$$

$$\text{Selectivity of DME} = \frac{35.57 \times 2}{309.05} = 0.23 \rightarrow \text{Yield of DME} = 0.11 \times 0.77 = 0.18$$

$$\text{Selectivity of formaldehyde} = \frac{0}{309.05} = 0 \rightarrow \text{Yield of DME} = 0.0 \times 0.77 = 0.0$$

APPENDIX C

PORE DIAMETER CALCULATION

In calculation of pore diameters of the materials indicated in this study, BJH desorption raw data are used. A sample calculation is given below for the sample cSZ1.

$$d_p = \frac{\int d \times dV}{V_p}$$

Diameter (Å)	Pore Vol (cc/g)	d average	dV	d dV	
16.7	2.27E-03	17.945	0.003936	0.070632	
19.19	6.20E-03	20.45	0.004556	0.09317	
21.71	1.08E-02	23.05	0.00569	0.131155	
24.39	1.65E-02	25.835	0.00706	0.182395	
27.28	2.35E-02	28.79	0.00837	0.240972	
30.3	3.19E-02	32.045	0.02288	0.73319	
33.79	5.48E-02	35.88	0.04954	1.777495	
37.97	1.04E-01	40.39	0.0476	1.922564	Average pore diameter
42.81	1.52E-01	45.86	0.0673	3.086378	
48.91	2.19E-01	52.53	0.0363	1.906839	
56.15	2.56E-01	60.205	0.0124	0.746542	
64.26	2.68E-01	70.615	0.0165	1.165148	
76.97	2.84E-01	85.755	0.014	1.20057	
94.54	2.98E-01	106.88	0.0068	0.726784	
119.22	3.05E-01	142.06	0.0055	0.78133	
164.9	3.11E-01	218.225	0.0053	1.156593	
271.55	3.16E-01	786.135	0.014	11.00589	
1300.72	3.30E-01	--	--	--	
total		last data included	0.327732	26.92765	82.16361
		last data excluded	0.309796	15.85112	51.16633

The calculation methadology for the first data is as follows

$$d = \frac{16.7 + 19.19}{2} = 17.945$$

$$dV = 6.2 \times 10^{-3} - 2.27 \times 10^{-3} = 3.93 \times 10^{-3} = 0.00393$$

$$d \times dV = 17.945 \times 0.00393 = 0.071$$

All data is examined as above and the integral term is evaluated as given in the table.

Total volume is evaluated by summation of dV terms

Average pore diameter is then calculated as volume average diameter. Both integral term and volume calculation are performed depending on whether last data is included or not.

$$d_p = \frac{\int d \times dV}{V_p} = \frac{26.92}{0.33} = 82.16\ A = 8.2\ nm\ with\ last\ data\ included$$

$$d_p = \frac{\int d \times dV}{V_p} = \frac{15.85}{0.31} = 51.2\ A = 5.1\ nm\ with\ last\ data\ excluded$$

APPENDIX D

SEM IMAGES OF CATALYSIS

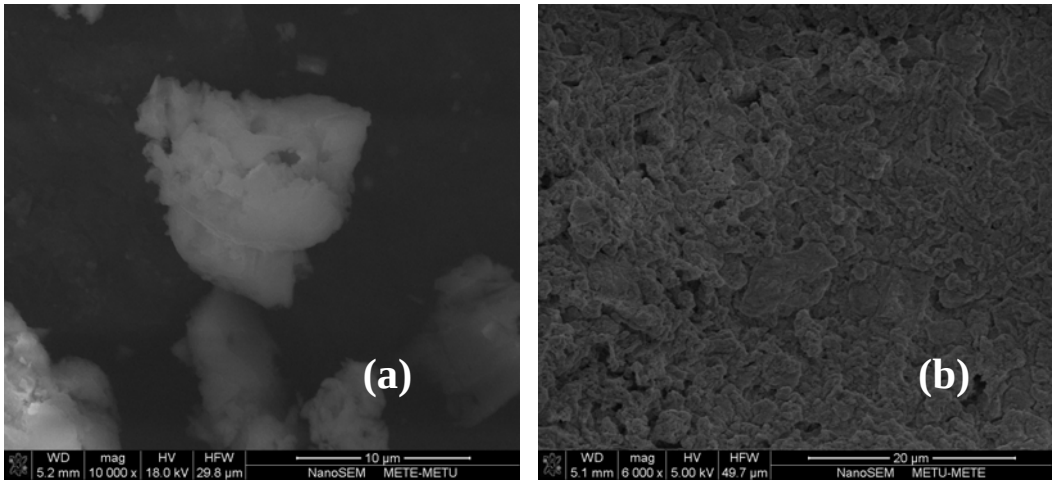

Figure 58: SEM images of (a) cSZ1 and (b) cSZ2

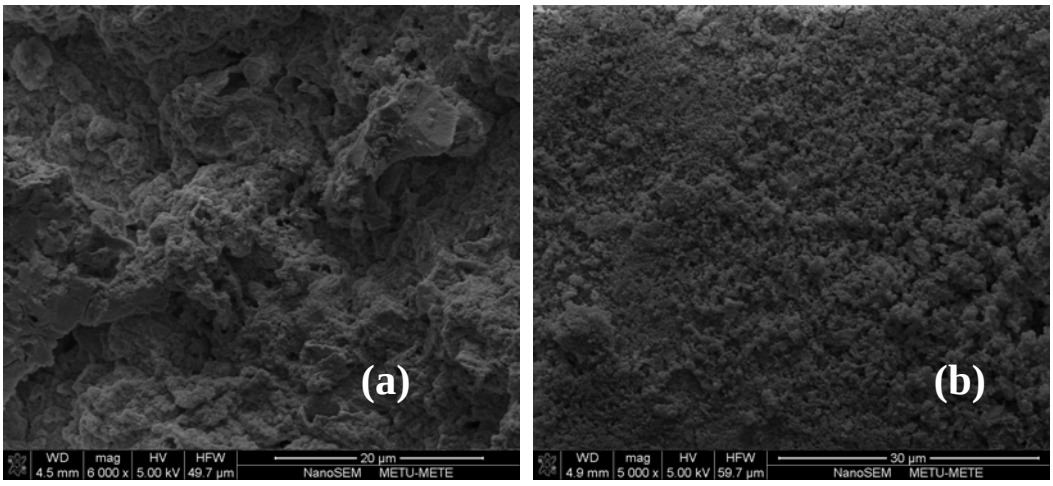

Figure 59: SEM images of (a) cSZ3 and (b) cSZ4

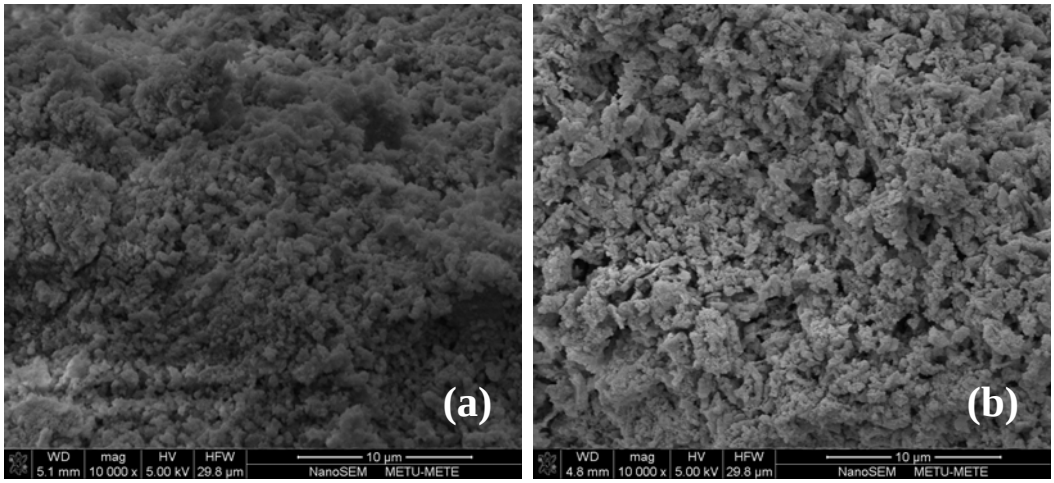

Figure 60: SEM images of (a) cSZ5 and (b) cSZ6

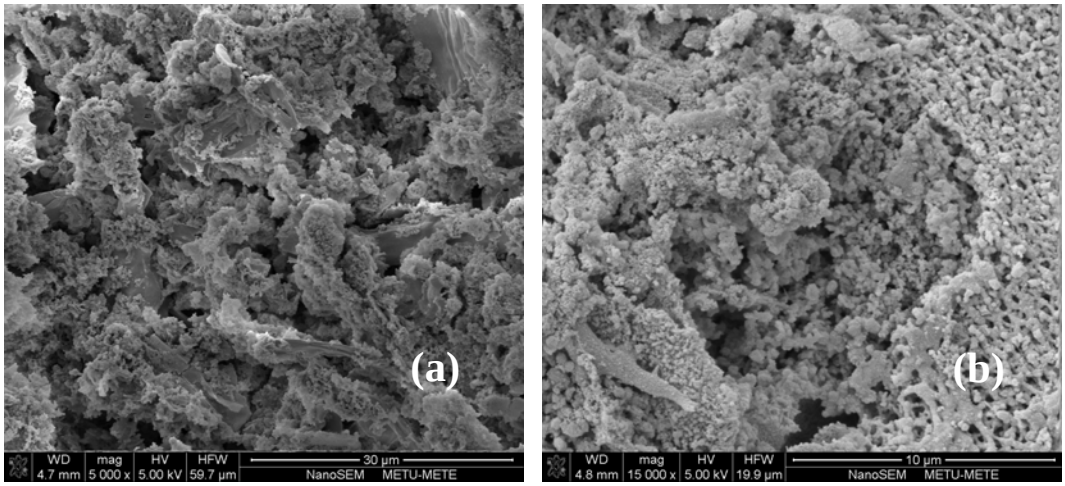

Figure 61: SEM images of (a) cSC and (b) cSN

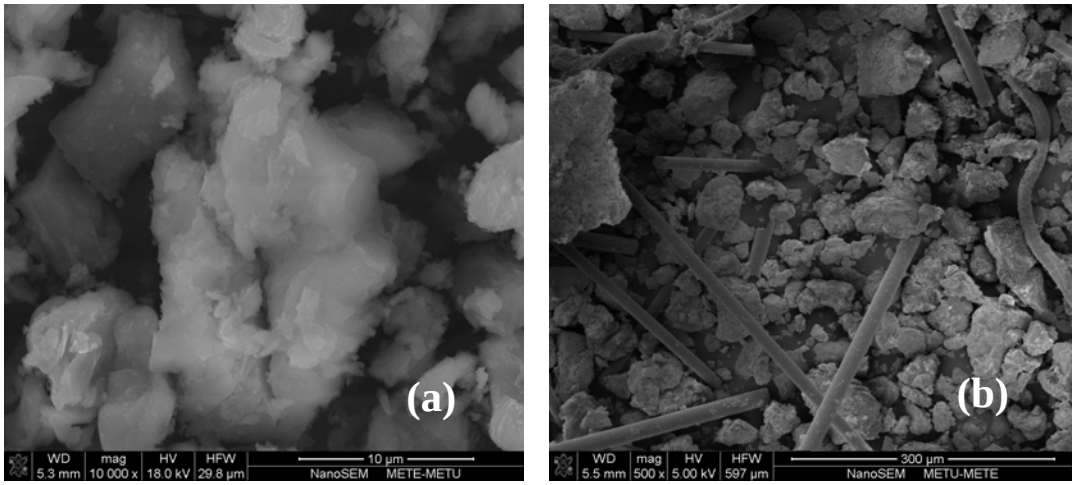

Figure 62: SEM images of (a) sceSZ1 and (b) sceSZ2

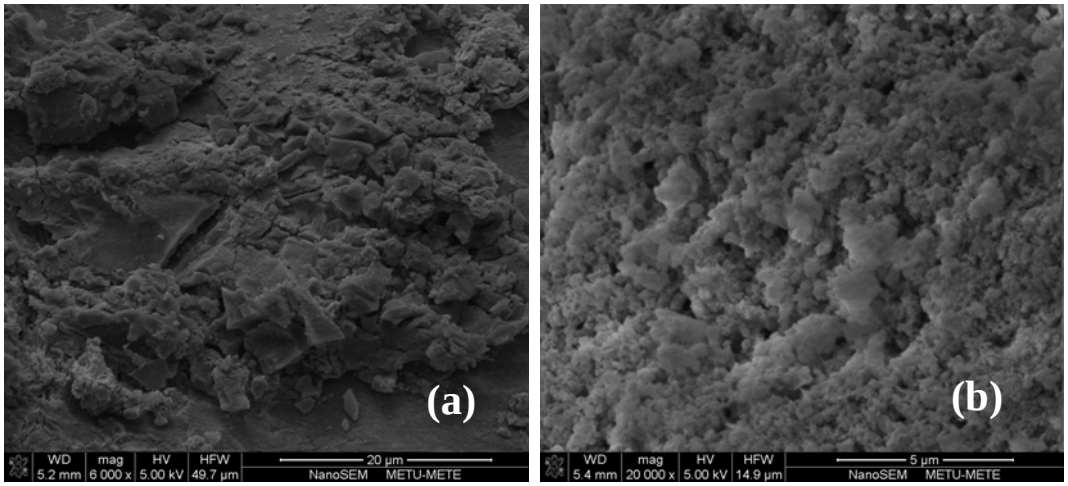

Figure 63: SEM images of (a) sceSZ3 and (b) sceSZ4

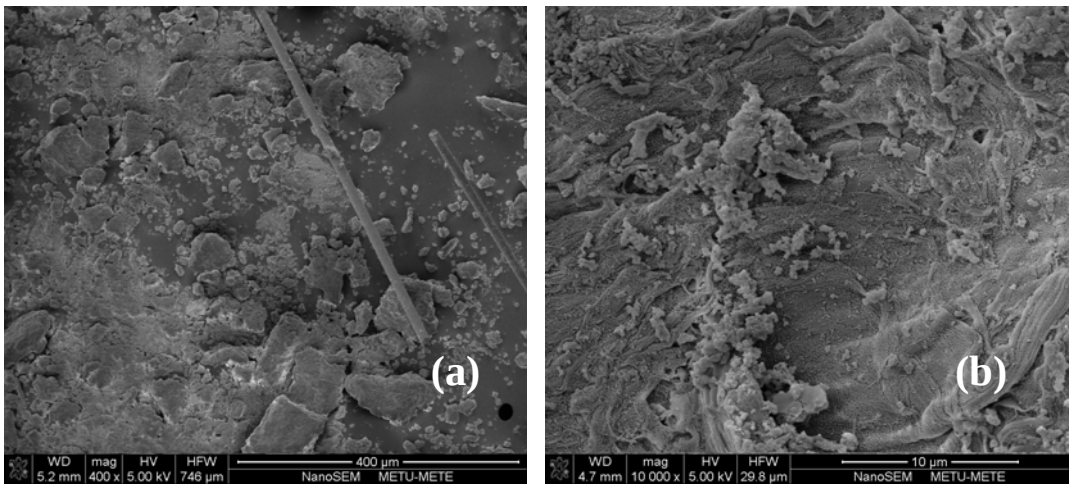

Figure 64: SEM images of (a) sceSZ5 and (b) sceSZ6

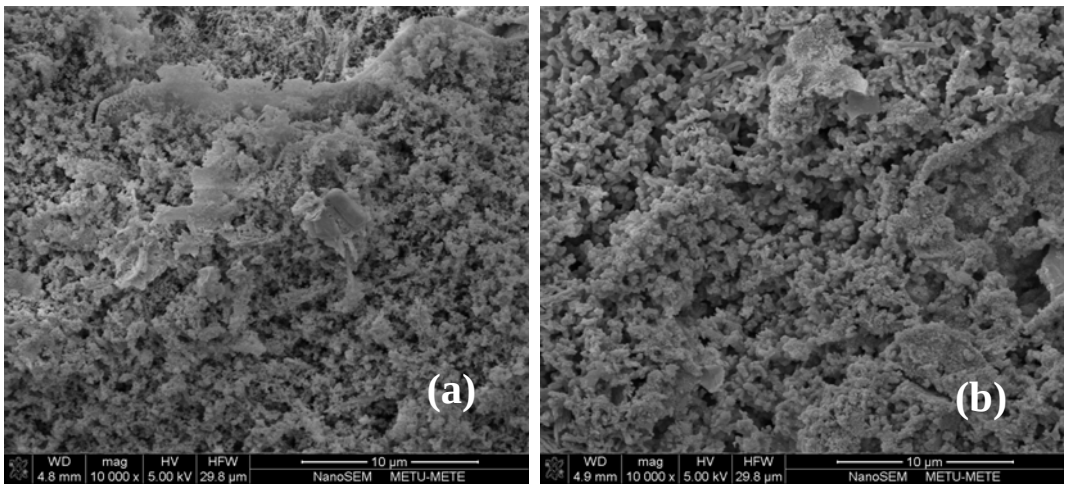

Figure 65: SEM images of (a) sceSC and (b) sceSN

APPENDIX E

TGA CURVES OF SELECTED SAMPLES

E.1. TGA Curves of Catalyst Used in Comparison of Extraction and Calcination

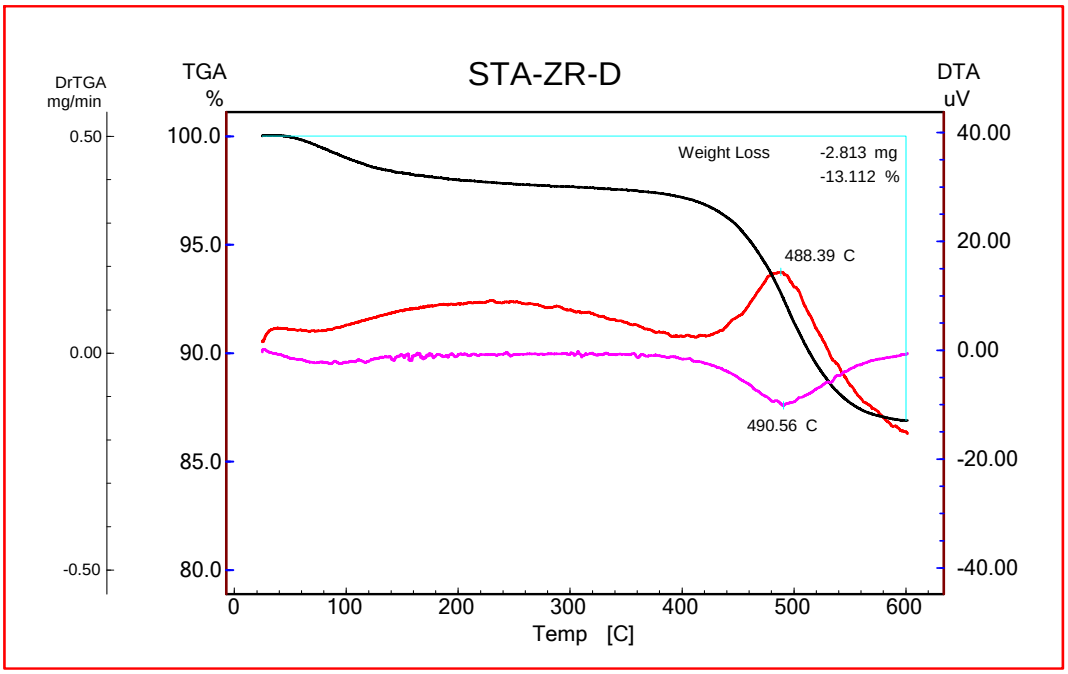

Figure 66: TGA curve of cSZ1

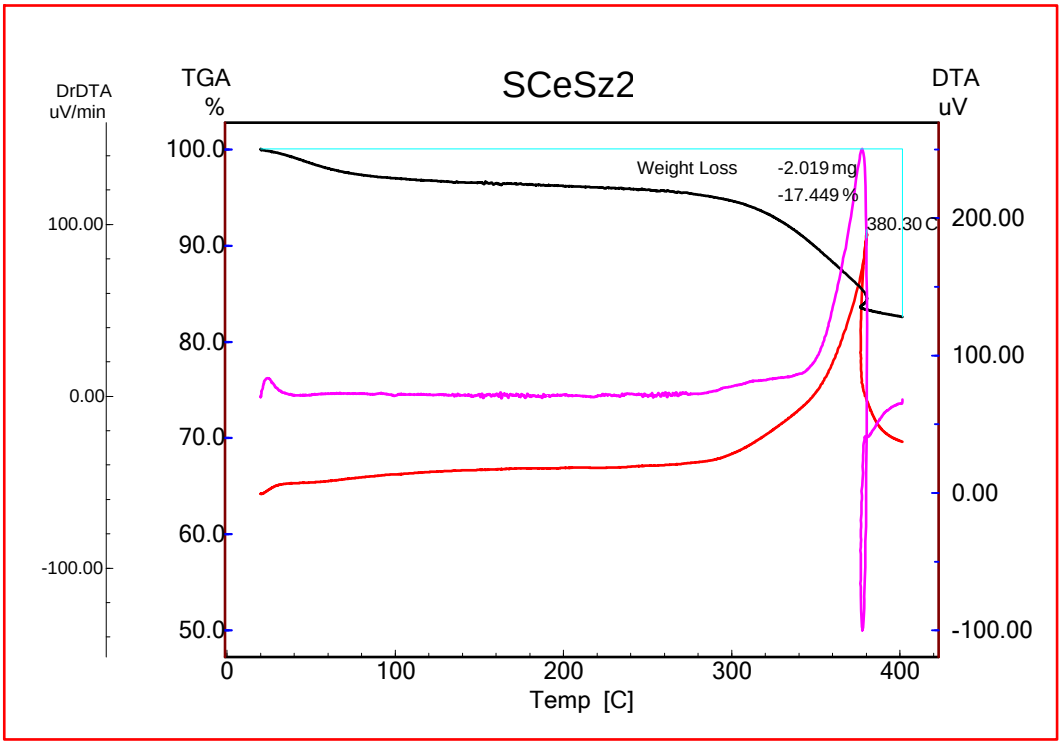

Figure 67: TGA curve of sceSZ2

E.2. TGA Curves of Catalyst Used in Effect of Pressure in Extraction

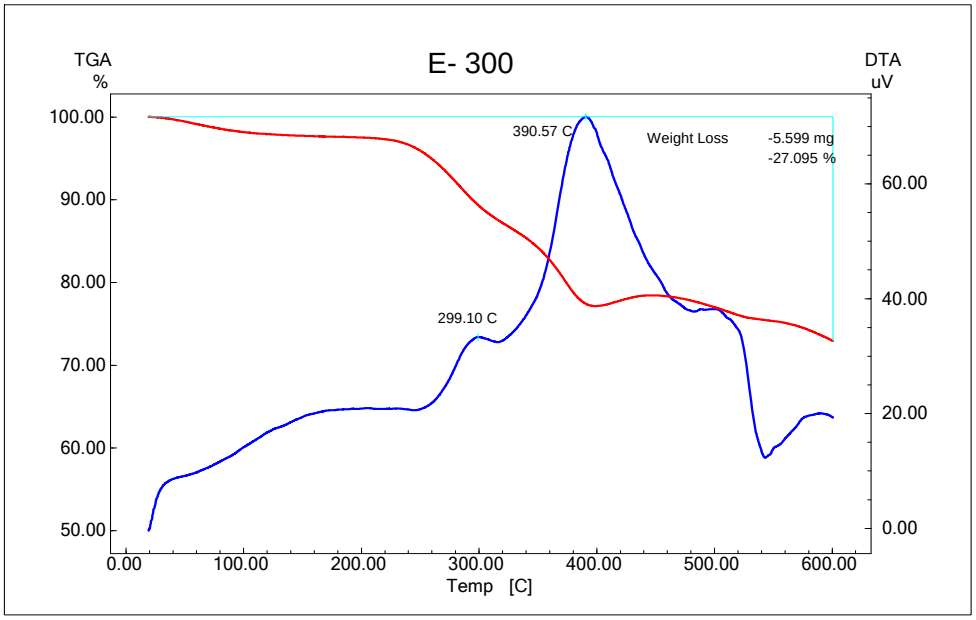

Figure 68: TGA curve of sceSZ3-300

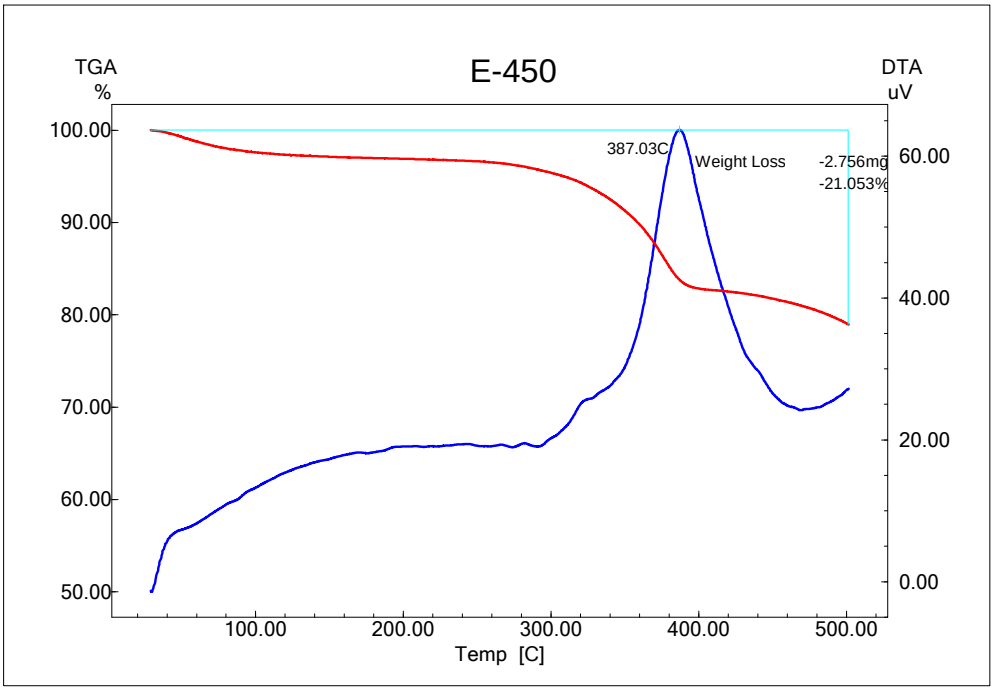

Figure 69: TGACurve of sceSZ3

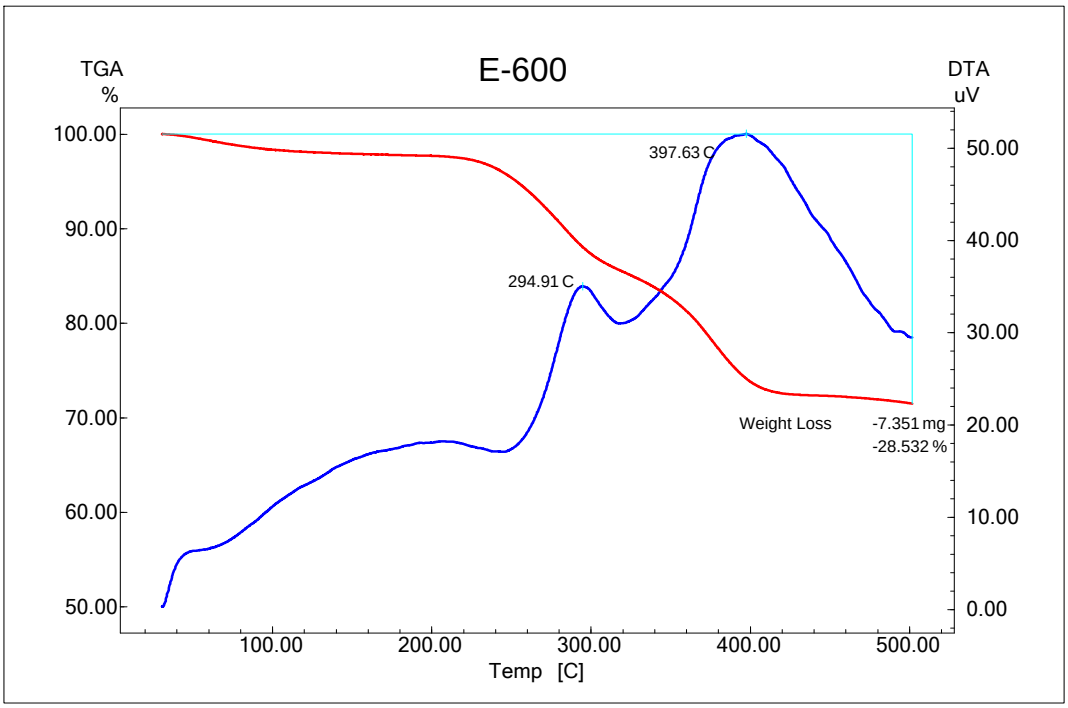

Figure 70: TGA curve of sceSZ3-600

APPENDIX F

PRODUCT DISTRIBUTIONS IN METHANOL DEHYDRATION REACTIONS

F.1. Product Distribution in methanol dehydration reaction performed with calcined samples

Table 27: Product distribution in presence of calcined catalysis (τ= 0.27 s.g/cm^3)

Catalyts	Temperature	X_{MeOH}	S_{DME}	Y_{DME}	S_{FA}	S_{CO}	S_{CH4}
cSZ1	250	0.085	0.889	0.076	0.111	0	0
	300	0.198	0.978	0.193	0.022	0	0
	350	0.221	0.956	0.211	0.011	0	0.033
	400	0.346	0.832	0.288	0.006	0.008	0.154
	450	0.670	0.345	0.231	0.000	0.055	0.600
cSZ2	250	0.325	0.992	0.322	0.008	0	0
	300	0.460	0.995	0.458	0.005	0	0
	350	0.477	0.960	0.458	0.003	0	0.036
	400	0.673	0.785	0.528	0	0.020	0.195
	450	0.916	0.303	0.278	0	0.080	0.617
cSZ3	250	0.111	0.891	0.099	0.109	0	0
	300	0.217	0.934	0.203	0.066	0	0
	350	0.285	0.914	0.260	0.044	0	0.042
	400	0.458	0.820	0.376	0.005	0.006	0.169
	450	0.592	0.401	0.238	0.001	0.068	0.530
cSZ4	250	0.094	0.865	0.082	0.135	0	0
	300	0.124	0.902	0.112	0.098	0	0
	350	0.155	0.904	0.140	0.076	0	0.020
	400	0.312	0.873	0.272	0.007	0	0.119
	450	0.542	0.642	0.348	0.002	0.030	0.327
cSZ5	250	0.055	0.760	0.042	0.240	0	0
	300	0.119	0.895	0.107	0.105	0	0
	350	0.156	0.909	0.141	0.072	0	0.019
	400	0.321	0.877	0.281	0.007	0	0.115
	450	0.648	0.544	0.353	0	0.035	0.420

F.2. Product Distribution in methanol dehydration reaction performed with extracted samples

Table 28: Product distribution in presence of extracted catalysis (τ= 0.27 s.g/cm^3)

Catalyts	Temperature	X_{MeOH}	S_{DME}	Y_{DME}	S_{FA}	S_{CO}	S_{CH4}
sceSZ2	350	0.115	0.836	0.097	0.088	0	0.076
	400	0.455	0.852	0.388	0.003	0	0.145
	450	0.732	0.587	0.430	0	0.045	0.367
	500	0.546	0.350	0.191	0.003	0.132	0.516
sceSZ3	350	0.053	0.742	0.039	0.182	0	0.075
	400	0.239	0.876	0.210	0.022	0	0.102
	450	0.755	0.523	0.395	0	0.031	0.446
	500	0.723	0.262	0.189	0	0.096	0.642
sceSZ4	350	0.078	0.839	0.065	0.106	0	0.055
	400	0.395	0.867	0.342	0.005	0	0.128
	450	0.584	0.795	0.465	0	0.017	0.188
sceSZ5	350	0.037	0.661	0.024	0.307	0	0.032
	400	0.282	0.870	0.245	0.019	0	0.111
	450	0.709	0.673	0.477	0	0.033	0.294
	500	0.853	0.494	0.421	0	0.093	0.413
sceSZ6	350	0.003	0	0	1	0	0
	400	0.013	0.379	0.005	0.621	0	0
	450	0.017	0.473	0.008	0.527	0	0
	500	0.042	0.505	0.021	0.223	0.215	0.057